J. Fluid Mech. (1984), *vol.* 145, *pp.* 11–70
Printed in Great Britain

Interfacial shapes between two superimposed rotating simple fluids

By H. A. TIEU†, D. D. JOSEPH AND G. S. BEAVERS
Department of Aerospace Engineering and Mechanics, University of Minnesota, Minneapolis, Minnesota 55455

(Received 7 June 1983 and in revised form 6 February 1984)

The interfacial shape of two immiscible simple fluids in a vertical cylinder which oscillates about its axis is investigated using the theory of domain perturbations. The perturbation stresses are expressed by integrals over the history of the deformation. At first order the azimuthal velocity field satisfies the requirements of continuity in velocity and shear stresses across the interface. At second order the solution consists of a mean part and a time-periodic part varying at twice the frequency of the cylinder. The mean problem is inverted for the mean secondary flow, pressure and interfacial shape. Experimental data for two polymeric oils (TLA227 and STP) show qualitative agreement with theoretical predictions for the mean interfacial shapes.

1. Introduction

The interfacial shape between two immiscible fluids at rest is governed by capillarity (i.e. the balance between interfacial tension and hydrostatic pressures). When fluids are set in motion, the interface changes its shape. The dependence of the interfacial shape on the states of stress can be used to determine some rheological properties of the fluids.

The free surface on a simple fluid between cylinders rotating at different speeds has been studied by Joseph & Fosdick (1973), using the method of domain perturbations. Assuming a rest state with a flat free surface, the authors carried out the analysis through the fourth order. Their solution exhibits the following features. A primary Couette flow field exists at first order. At second order the first deviations of pressure and free-surface shape from the hydrostatic pressure and the flat position are observed. Alteration to the azimuthal velocity field occurs next at third order. And at fourth order the first secondary motion appears, together with alterations in the pressure field and the free-surface shape.

A comparison between the second-order theoretical free-surface shapes and experimental data for rods rotating in STP (a solution of polyisobutylene in oil) was made by Joseph, Beavers & Fosdick (1973). They got good agreements for small angular velocities. More-extensive rotating-rod experiments, with efforts to control the wetting angle and to establish the dependence of the climb on temperature, were reported later by Beavers & Joseph (1975).

The free surface on a simple fluid between cylinders undergoing torsional oscillations has also been studied through the second order by Joseph & Beavers (1976) with particular reference to a rod oscillating in an infinite fluid. The first-order solution gives a time-periodic azimuthal velocity field varying with the forcing frequency. The

† Present address: Goodyear Tire and Rubber Company, Akron, Ohio.

solution at second order consists of a mean part and a time-periodic part varying at twice the frequency of the rod. When the angular velocity ω of the rod approaches zero, the solution for the mean part reduces to the second-order solution of the steady problem mentioned above. The predicted mean rise at the rod was compared with experimental data for TLA227 (a solution of a methacrylate copolymer in oil). For some small range of ω, there is a good agreement between theory and experiment. The range of agreement can be increased by appropriate choices for the decay constants in the material relaxation functions $G(s)$ and $\gamma(s_1, s_2)$. Additional experimental measurements with Paratone 715 fluid were reported by Kolpin, Beavers & Joseph (1980).

A distinction between the first-order solutions of the two problems above is that the azimuthal velocity distribution in the steady case is a Couette flow, and therefore independent of the fluid properties, whereas the velocity distribution in the unsteady case depends on fluid properties. This special feature in the steady case is convenient for analyses of rotating rods in superimposed immiscible fluids, in the sense that the second-order solutions for such analyses are much the same as the one with a single fluid. Then, the only minor distinction between a free surface and an interface is that the fluid density in the surface-shape equation is to be replaced by the difference in the densities of the two neighbouring fluids. This fact is fully exploited in the work of Beavers & Joseph (1977) to magnify the Weissenberg effects.

The present work deals with the interfacial shape in rotating simple fluids. Our analysis falls in the framework of the papers mentioned above. The current study involves two simple fluids contained in a vertical oscillating cylinder. The boundary conditions on the interface are such that the interface is a streamline, the velocities and shear stresses are continuous across the interface, and the normal stresses are balanced by the interfacial tension.

The plan and findings of this paper are as follows. The mathematical formulation and the corresponding perturbed problems at first and second orders are described in §2. We next give the first-order solution, and its asymptotic form when the angular velocity of the cylinder ω approaches zero. At small ω the azimuthal velocity in a fluid consists of a solid-body oscillation and a deviation whose magnitude is proportional to the Reynolds number of the fluid. The z-dependent part of this deviation is important only in the neighbourhood of the interface, and in fact vanishes if the kinematic viscosities of the fluids are the same. We then derive the problem for the mean motion at second order, and give its solution in §§4 and 5. In contrast with the earlier works (Joseph *et al.* 1973; Joseph & Beavers 1976), there is a second-order mean motion in our problem. The stream function for the mean motion is decomposed into particular and homogeneous parts. The former is obtained using the appropriate Green function, whereas the latter is expressed in terms of biorthogonal series. Formulae for the mean pressure and interfacial shape are presented in §§5.2 and 5.3. In the limit $\omega \to 0$ the asymptotic interfacial shape is parabolic (i.e. as in solid-body oscillations). Experiments with the two simple fluids TLA227 and STP are described in §6. The mean distortion of the interface is much larger than the time-periodic distortion. Comparison between theoretical results and experimental data (in §7) show a good qualitative agreement for some range of small ω.

2. Mathematical formulation

2.1. *Description of the full problem*

Two immiscible, incompressible, simple fluids fill the interior of an infinitely tall, vertical cylinder of inside radius a. When the cylinder is stationary, the fluids are at rest with fluid (1) above fluid (2), and the rest configuration is determined by capillarity. If the boundary condition for the interface at the cylinder wall is properly chosen (see Tieu 1983), or if the interfacial tension parameter is negligibly small, then the interface between the two fluids at rest is horizontally flat. We choose cylindrical coordinates at the centre of the flat interface, and the z-axis coincides with the axis of the cylinder. The interior of the stationary cylinder is partitioned into

$$\mathscr{V}_{(1)} = \{(R,\theta,z): R\in[0,a], \theta\in[0,2\pi), z\geqslant 0\},$$

$$\mathscr{V}_{(2)} = \{(R,\theta,z): R\in[0,a], \theta\in[0,2\pi), z\leqslant 0\}.$$

When the cylinder is in sinusoidal motion in the θ-direction, $\boldsymbol{U} = \boldsymbol{e}_\theta \epsilon a \sin\omega t$ the interface is symmetrically deformed about the z-axis. The position of the interface is then described by

$$z = h(r,t;\epsilon,\omega) \equiv h(r,t;\epsilon),$$

where ϵ is the perturbation parameter, and the implicit dependence on ω is understood in $h(r,t;\epsilon)$. The upper fluid (1) is then confined to a new domain

$$\mathscr{V}_{(1,\epsilon)} \equiv \{(r,\theta,z): r\in[0,a], \theta\in[0,2\pi), z\geqslant h\},$$

and the bottom fluid (2) to

$$\mathscr{V}_{(2,\epsilon)} \equiv \{(r,\theta,z): r\in[0,a], \theta\in[0,2\pi), z\leqslant h\}.$$

Figure 1 depicts the deformed spatial configuration of the fluids. We are interested in the mean interfacial shape $\mathring{h}(r;\epsilon)$, up to second order in ϵ. The mean of a periodic function $g(\boldsymbol{x},t;\epsilon) = g(\boldsymbol{x},t+T;\epsilon)$ is defined as follows:

$$\mathring{g}(\boldsymbol{x};\epsilon) = \frac{1}{T}\int_0^T g(\boldsymbol{x},t;\epsilon)\,\mathrm{d}t.$$

Equations governing the motion in $\mathscr{V}_{(\cdot,\epsilon)}$ are

$$\rho\left[\frac{\partial \boldsymbol{U}}{\partial t} + \boldsymbol{U}\cdot\boldsymbol{\nabla}\boldsymbol{U}\right] = -\boldsymbol{\nabla}\Phi + \boldsymbol{\nabla}\cdot\boldsymbol{S}, \tag{2.1}$$

$$\boldsymbol{\nabla}\cdot\boldsymbol{U} = 0 \tag{2.2}$$

where $\boldsymbol{U}, \Phi$ and $\boldsymbol{S}$ are the velocity vector, reduced pressure and extra stress tensor respectively. Subscripts j ($j = 1,2$) are used to indicate fluids (1) and (2) respectively. There is no slip between the cylinder wall and the fluids:

$$\boldsymbol{U}_{(j)}(a,\theta,z,t;\epsilon) = \boldsymbol{e}_\theta \epsilon a \sin\omega t \quad (j = 1,2). \tag{2.3}$$

The velocity along the centreline is bounded, i.e.

$$\boldsymbol{U}_{(j)}(0,\theta,z,t;\epsilon) \quad \text{is finite.} \tag{2.4}$$

On the interface $z = h(r,t;\epsilon)$ we require that the shear stresses and velocities are continuous. We introduce the notation

$$[\![(\cdot)]\!] \equiv (\cdot)_{(2)} - (\cdot)_{(1)}.$$

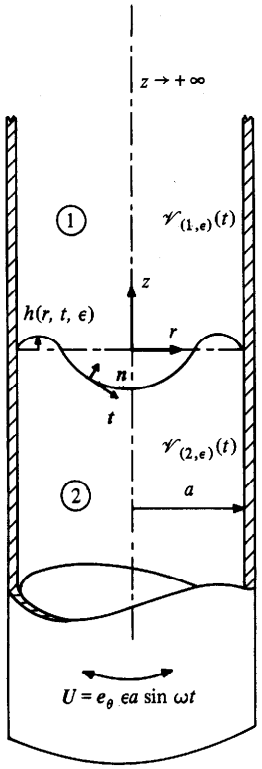

FIGURE 1. Interfacial shape between two immiscible fluids in an oscillating cylinder.

Then the shear component in the θ-direction satisfies

$$[\![\boldsymbol{S}_{z\theta}]\!] - \frac{\partial h}{\partial r}[\![\boldsymbol{S}_{r\theta}]\!] = 0, \tag{2.5}$$

and the shear component in the tangential direction satisfies

$$\frac{\partial h}{\partial r}[\![\boldsymbol{S}_{zz} - \boldsymbol{S}_{rr}]\!] + \left[1 - \left(\frac{\partial h}{\partial r}\right)^2\right][\![\boldsymbol{S}_{rz}]\!] = 0. \tag{2.6}$$

The velocity vector $\boldsymbol{U}(r, \theta, h, t; \epsilon)$ is continuous across $z = h$:

$$[\![\boldsymbol{U}]\!] = \boldsymbol{0}. \tag{2.7}$$

The kinematic condition at the interface requires that

$$u_{(j)} = \frac{\partial h}{\partial t} + \frac{\partial h}{\partial r} w_{(j)}, \tag{2.8}$$

where w, u are radial and axial components of $\boldsymbol{U}$. Finally, the normal stress along the interface must be balanced by the interfacial tension σ multiplied by the mean curvature:

$$-[\![\Phi]\!] + [\![\boldsymbol{S}_{nn}]\!] + [\![\rho]\!] gh - \frac{\sigma}{r}\frac{\partial}{\partial r}\left\{\frac{r\,\partial h/\partial r}{(1 + (\partial h/\partial r)^2)^{\frac{1}{2}}}\right\} = 0, \tag{2.9}$$

where

$$\boldsymbol{S}_{nn} = \frac{\boldsymbol{S}_{zz} + \boldsymbol{S}_{rr}(\partial h/\partial r)^2 - 2\,\partial h/\partial r\, \boldsymbol{S}_{zr}}{1 + (\partial h/\partial r)^2}. \tag{2.10}$$

Equation (2.9) is a differential equation for $h(r,t;\epsilon)$, whose boundary conditions may be taken as

$$\left.\begin{aligned} &\text{(i)} \quad \left.\frac{\partial h}{\partial r}\right|_{r=0} = 0, \quad \left.\frac{\partial h}{\partial r}\right|_{r=a} = \alpha(t;\epsilon), \\ \text{or} \qquad &\\ &\text{(ii)} \quad \left.\frac{\partial h}{\partial r}\right|_{r=0} = 0, \quad h(a,t;\epsilon) = 0. \end{aligned}\right\} \tag{2.11}$$

The first condition of (i) and (ii) above expresses the requirement that the interface be smooth at $r = 0$. The second condition of (i) expresses that the interface wets the cylinder wall at an angle $\frac{1}{2}\pi - \kappa$, where $\kappa = \tan^{-1}\alpha$. (The convention adopted here is that a liquid wets a solid surface when $\kappa > 0$, a liquid does not wet a solid surface when $\kappa < 0$. Neutral wetting corresponds to $\kappa = 0$.) The second condition of (ii) holds whenever the contact line is fixed. When either the set of boundary conditions (i) with $\alpha(t;0) = 0$, or the set (ii) holds, the static interface is horizontally flat $h(r,t;0) = 0$ (see Tieu 1983).

As $|z| \to 0$ we require that the solutions

$$\boldsymbol{\Phi}_{(j)}, \quad \boldsymbol{U}_{(j)} \tag{2.12}$$

are independent of z.

Since the flows are incompressible, the volumes are conserved; therefore allowable interfacial shapes must satisfy the constraint

$$\int_0^a r h(r,t;\epsilon)\,\mathrm{d}r = 0. \tag{2.13}$$

This constraint determines the pressure difference across the interface.

2.2. *Domain perturbation of the rest state*

We expand the extra stress $\boldsymbol{S}$ around the rest state and take the expansion up to terms of order two. For this second-order approximation (Joseph 1976) we have

$$\boldsymbol{S} \simeq \int_0^\infty G(s)\,\boldsymbol{\Pi}(t-s,\epsilon)\,\mathrm{d}s + \int_0^\infty \int_0^\infty \boldsymbol{\gamma}(s_1,s_2)\,\boldsymbol{\Pi}(t-s_1,\epsilon)\,\boldsymbol{\Pi}(t-s_2,\epsilon)\,\mathrm{d}s_1\,\mathrm{d}s_2, \tag{2.14}$$

where $G(s), \boldsymbol{\gamma}(s_1,s_2)$ are the linear and quadratic relaxation functions of the fluid, and $\boldsymbol{\Pi}$ is the time derivative of relative strain tensor at some past time $\tau = t-s$. The three material constants which appear in the constitutive expression for the extra stress of a second-grade fluid, are defined in terms of $G(s)$ and $\boldsymbol{\gamma}(s_1,s_2)$ as follows:

$$\mu = \int_0^\infty G(s)\,\mathrm{d}s, \quad \alpha_1 = -\int_0^\infty sG(s)\,\mathrm{d}s, \quad \alpha_2 = \int_0^\infty \int_0^\infty \boldsymbol{\gamma}(s_1,s_2)\,\mathrm{d}s_1\,\mathrm{d}s_2. \tag{2.15a,b,c}$$

The components of the tensor $\boldsymbol{\Pi}$ are given by

$$\boldsymbol{\Pi}(t-s,\epsilon)_{ij} = \frac{\partial \boldsymbol{\chi}_t}{\partial x_i}\cdot\frac{\partial \boldsymbol{U}(\tau)}{\partial x_j} + \frac{\partial \boldsymbol{\chi}_t}{\partial x_j}\cdot\frac{\partial \boldsymbol{U}(\tau)}{\partial x_i}, \tag{2.15d}$$

in which $\boldsymbol{\chi}_t(\boldsymbol{x},\tau;\epsilon)$ is the relative position vector

$$\boldsymbol{\chi}_t(\boldsymbol{x},\tau,\epsilon) = \boldsymbol{x} + \sum_{n=1}^{\infty} \epsilon^n \boldsymbol{\chi}_t^{\langle n\rangle}(\boldsymbol{x},\tau), \tag{2.16a}$$

such that $\chi_t^{\langle n\rangle}(\boldsymbol{x},t)=0$ for $\forall n\in\mathbb{N}^+$. The velocity vector $\boldsymbol{U}(\boldsymbol{x},\tau;\epsilon)$ of a particle at $\boldsymbol{\chi}_t(\boldsymbol{x},\tau;\epsilon)$ can also be expanded into a series:

$$\boldsymbol{U}(\boldsymbol{x},\tau;\epsilon)=\sum_{n=1}^{\infty}\epsilon^n\boldsymbol{U}^{\langle n\rangle}(\boldsymbol{x},\tau). \tag{2.16b}$$

And the relation between $\chi_t^{\langle n\rangle}(\boldsymbol{x},\tau)$ and $\boldsymbol{U}^{\langle n\rangle}(\boldsymbol{x},\tau)$ is as follows:

$$\chi_t^{\langle n\rangle}(\boldsymbol{x},\tau)=\int_t^{\tau}\boldsymbol{U}^{\langle n\rangle}(\boldsymbol{x},\tau')\,\mathrm{d}\tau'. \tag{2.17}$$

Joseph (1976) formed expressions for the extra stress $\boldsymbol{S}$, up to second order in ϵ, by expanding (2.15d), using (2.16a,b) and then substituting the resulting expression into (2.14). He found

$$\boldsymbol{S}=\epsilon\boldsymbol{S}_1[\boldsymbol{U}^{\langle 1\rangle}]+\epsilon^2(\boldsymbol{S}_1[\boldsymbol{U}^{\langle 2\rangle}]+\boldsymbol{S}_2[\boldsymbol{U}^{\langle 1\rangle}])+o(\epsilon^2), \tag{2.18}$$

where

$$\boldsymbol{S}_1[\boldsymbol{U}]\equiv\int_0^{\infty}G(s)\boldsymbol{A}_1[\boldsymbol{U}(s)]\,\mathrm{d}s, \tag{2.19a}$$

$$\begin{aligned}\boldsymbol{S}_2[\boldsymbol{U}^{\langle 1\rangle}]\equiv\int_0^{\infty}G(s)\{&\boldsymbol{\chi}_t^{\langle 1\rangle}(s)\cdot\boldsymbol{\nabla}\boldsymbol{A}_1[\boldsymbol{U}^{\langle 1\rangle}(s)]+\boldsymbol{A}_1[\boldsymbol{U}^{\langle 1\rangle}(s)]\boldsymbol{\nabla}\boldsymbol{\chi}_t^{\langle 1\rangle}(s)\\&+[\boldsymbol{A}_1[\boldsymbol{U}^{\langle 1\rangle}(s)]\boldsymbol{\nabla}\boldsymbol{\chi}_t^{\langle 1\rangle}(s)]^T\}\,\mathrm{d}s\\&+\int_0^{\infty}\int_0^{\infty}\gamma(s_1,s_2)\boldsymbol{A}_1[\boldsymbol{U}^{\langle 1\rangle}(s_1)]\boldsymbol{A}_1[\boldsymbol{U}^{\langle 1\rangle}(s_2)]\,\mathrm{d}s_1\,\mathrm{d}s_2,\end{aligned} \tag{2.19b}$$

and the first Rivlin–Ericksen tensor $\boldsymbol{A}_1[\boldsymbol{U}]$ is defined as

$$\boldsymbol{A}_1[\boldsymbol{U}(\boldsymbol{x},s)]\equiv\boldsymbol{\nabla}\boldsymbol{U}+[\boldsymbol{\nabla}\boldsymbol{U}]^{\mathrm{T}}. \tag{2.20}$$

Since the above problem, defined by (2.1)–(2.13), is posed in domains symmetric with respect to θ, and the boundary data are independent of θ, we may look for axisymmetric solutions:

$$\begin{aligned}&\boldsymbol{U}_{(j)}(\boldsymbol{x},t;\epsilon)=\boldsymbol{U}_{(j)}(r,z,t;\epsilon)=w_{(j)}\boldsymbol{e}_r+v_{(j)}\boldsymbol{e}_\theta+u_{(j)}\boldsymbol{e}_z,\\&\boldsymbol{\Phi}_{(j)}(\boldsymbol{x},t;\epsilon)=\boldsymbol{\Phi}_{(j)}(r,z,t;\epsilon)\quad(j=1,2).\end{aligned}$$

Furthermore, when we change ϵ to $-\epsilon$ we reverse the direction of the azimuthal velocity component, but leave the velocity components in the radial and axial directions, the reduced pressure, and the interface deformation $h(r,t;\epsilon)$ unaltered. In other words, the functions $v_{(j)}(\boldsymbol{x},t;\epsilon)$ are odd in ϵ, while $w_{(j)}$, $u_{(j)}$, $\boldsymbol{\Phi}_{(j)}$ and $h(r,t;\epsilon)$ are even functions in ϵ.

We will resolve the above problem by the method of domain perturbations. Details of this method can be found elsewhere (Joseph & Fosdick 1973; Joseph & Beavers 1977). Here we shall assume that there is a solution of the form:

$$\begin{bmatrix}\boldsymbol{U}_{(j)}(\boldsymbol{x},t;\epsilon)\\\boldsymbol{\Phi}_{(j)}(\boldsymbol{x},t;\epsilon)\\h(r,t;\epsilon)\end{bmatrix}=\sum_{n=0}^{2}\begin{bmatrix}\boldsymbol{U}_{(j)}^{[n]}(\boldsymbol{X},t)\\\boldsymbol{\Phi}_{(j)}^{[n]}(\boldsymbol{X},t)\\h^{[n]}(R,t)\end{bmatrix}\epsilon^n+o(\epsilon^2), \tag{2.21}$$

where $\boldsymbol{x}\in\mathscr{V}_{(j,\epsilon)}$ and $\boldsymbol{X}\in\mathscr{V}_{(j)}\equiv\mathscr{V}_{(j,0)}$, for every $j=1,2$. The shift map which carries $\mathscr{V}_{(j)}$ into $\mathscr{V}_{(j,\epsilon)}$ is defined as follows:

$$r=R,\quad\theta=\theta,\quad z=Z+h(r,t;\epsilon). \tag{2.22}$$

The total and partial 'derivatives' of a function $f(\boldsymbol{x}(\boldsymbol{X}, t, \epsilon), t; \epsilon)$ are defined as follows:

$$f^{[n]}(\boldsymbol{X}, t) \equiv \frac{1}{n!}\frac{\mathrm{d}^n}{\mathrm{d}\epsilon^n} f(\boldsymbol{x}, t; \epsilon)\Big|_{\epsilon=0}, \quad \text{keeping } \boldsymbol{X} \text{ fixed}, \tag{2.23a}$$

whereas

$$f^{\langle n\rangle}(\boldsymbol{X}, t) \equiv \frac{1}{n!}\frac{\partial^n}{\partial\epsilon^n} f(\boldsymbol{x}, t; \epsilon)\Big|_{\epsilon=0}, \quad \text{keeping } \boldsymbol{x} \text{ fixed}. \tag{2.23b}$$

These derivatives are related by (2.22).

We will restrict our analysis to the following cases: (*a*) neutral wetting; (2.11)(i) with $\alpha^{[0]} = 0$; (*b*) fixed contact line; (2.11)(ii); (*c*) zero interfacial tension, $\sigma = 0$.

When any one of these three cases holds, the interface shape at the rest state is flat. We then have

$$\boldsymbol{U}_{(j)}^{[0]} = \boldsymbol{\Phi}_{(j)}^{[0]} - \text{constant } \boldsymbol{\Phi}_0 = 0,$$

and $h^{[0]} = 0$. An important consequence of $h^{[0]} = 0$ and $h(r, t; \epsilon)$ being an even function of ϵ, is that the total and partial derivatives (2.23*a*, *b*) are interchangeable up to second order ($n = 2$). Sine $\boldsymbol{\Phi}_{(j)}$ and h are even in ϵ, (2.21) becomes

$$\begin{bmatrix} \boldsymbol{U}_{(j)}(\boldsymbol{x}, t; \epsilon) \\ \boldsymbol{\Phi}_{(j)}(\boldsymbol{x}, t; \epsilon) - \boldsymbol{\Phi}_0 \\ h(r, t; \epsilon) \end{bmatrix} = \epsilon \begin{bmatrix} \boldsymbol{U}_{(j)1}(\boldsymbol{X}, t) \\ 0 \\ 0 \end{bmatrix} + \epsilon^2 \begin{bmatrix} \boldsymbol{U}_{(j)2}(\boldsymbol{X}, t) \\ \boldsymbol{\Phi}_{(j)2}(\boldsymbol{X}, t) \\ h_2(R, t) \end{bmatrix} + o(\epsilon^2), \tag{2.24}$$

where

$$\boldsymbol{U}_{(j)1} = \boldsymbol{U}_{(j)}^{[1]} = \boldsymbol{U}_{(j)}^{\langle 1\rangle} \equiv V_{(j)}(R, Z, t)\, \boldsymbol{e}_\theta,$$
$$\boldsymbol{U}_{(j)2} = \boldsymbol{U}_{(j)}^{[2]} = \boldsymbol{U}_{(j)}^{\langle 2\rangle} \equiv W_{(j)}(R, Z, t)\, \boldsymbol{e}_R + U_{(j)}(R, Z, t)\, \boldsymbol{e}_Z$$

for $j = 1, 2$; and $h_2 = h^{[2]} = h^{\langle 2\rangle}$.

2.3. *Governing equations at first and second orders*

The governing equations for the coefficients of ϵ are as follows:

$$\rho_{(j)} \frac{\partial}{\partial t} \boldsymbol{U}_{(j)1} = \boldsymbol{\nabla}\cdot\boldsymbol{S}_1[\boldsymbol{U}_{(j)1}], \tag{2.25a}$$

$$\boldsymbol{\nabla}\cdot\boldsymbol{U}_{(j)1} = 0 \quad \text{in } \mathscr{V}_{(j)}, \tag{2.25b}$$

$$\boldsymbol{U}_{(j)1}(a, Z, t) = \boldsymbol{e}_\theta\, a \sin\omega t, \tag{2.25c}$$

$$\boldsymbol{U}_{(j)1}(0, Z, t) \text{ is finite}, \tag{2.25d}$$

$$[\![\boldsymbol{S}_{1Z\theta}[\boldsymbol{U}_1]]\!] = 0, \tag{2.25e}$$

$$[\![\boldsymbol{U}_1]\!] = 0 \quad \text{along} \quad Z = 0, \tag{2.25f}$$

$$\frac{\partial}{\partial Z} \boldsymbol{U}_{(j)1}\Big|_{|Z|\to\infty} = 0. \tag{2.25g}$$

Equations (2.25*a–d*) come from (2.1)–(2.4), while (2.25*e–g*) come from (2.5), (2.7) and (2.12). Other boundary conditions, e.g. (2.6) and (2.8) and the balance of normal stress (2.9) are identically satisfied at first order in ϵ because the radial and axial velocity components and the interface shape are even functions in ϵ.

The governing equations for the coefficients of ϵ^2 in (2.24) are as follows:

$$\rho_{(j)}\frac{\partial}{\partial t}\boldsymbol{U}_{(j)2}+\nabla\Phi_{(j)2}-\nabla\cdot\boldsymbol{S}_1[\boldsymbol{U}_{(j)2}]=\nabla\cdot\boldsymbol{S}_2[\boldsymbol{U}_{(j)1}]-\rho_{(j)}\,\boldsymbol{U}_{(j)1}\cdot\nabla\boldsymbol{U}_{(j)1}, \tag{2.26a}$$

$$\nabla\cdot\boldsymbol{U}_{(j)2}=0 \quad \text{in } \mathscr{V}_{(j)}; \tag{2.26b}$$

$$\boldsymbol{U}_{(j)2}(a,Z,t)=\boldsymbol{0}, \tag{2.26c}$$

$$\boldsymbol{U}_{(j)2}(0,Z,t) \text{ is bounded}, \tag{2.26d}$$

$$[\![\boldsymbol{S}_{1RZ}[\boldsymbol{U}_2]]\!]=-[\![\boldsymbol{S}_{2RZ}[\boldsymbol{U}_1]]\!], \tag{2.26e}$$

$$[\![\boldsymbol{U}_2]\!]=\boldsymbol{0}, \tag{2.26f}$$

$$\boldsymbol{U}_{(j)}=\frac{\partial}{\partial t}h_2 \quad \text{along } Z=0 \quad (j=1,2), \tag{2.26g}$$

$$\frac{\partial}{\partial Z}\boldsymbol{U}_{(j)2}\Big|_{|Z|\to\infty}=\boldsymbol{0}, \tag{2.26h}$$

$$\frac{\partial}{\partial Z}\Phi_{(j)2}\Big|_{|Z|\to\infty}=0. \tag{2.26i}$$

Equations (2.26*a–d*) come from (2.1)–(2.4), while (2.26*e–g*) and (2.26*h*, *i*) come from (2.6)–(2.8) and (2.12). The boundary condition (2.5) is identically satisfied at second order because $\boldsymbol{U}_{(j)2}$ are independent of θ, and the azimuthal velocity components are odd functions in ϵ. The interfacial shape correction $h_2(R,t)$ satisfies

$$-[\![\Phi_2]\!]+[\![\boldsymbol{S}_{1ZZ}[\boldsymbol{U}_2]+\boldsymbol{S}_{2ZZ}[\boldsymbol{U}_1]]\!]+[\![\rho]\!]\rho h_2=\frac{\sigma}{R}\frac{\partial}{\partial R}\left[R\frac{\partial}{\partial R}h_2\right] \tag{2.27}$$

at $Z=0$, such that

(i)

$$\frac{\partial h_2}{\partial R}\Big|_{R=0}=\frac{\partial h_2}{\partial R}\Big|_{R=a}-\alpha^{[2]}(t)=0, \tag{2.28a}$$

or

(ii)

$$\frac{\partial}{\partial R}h_2\Big|_{R=0}=h_2\Big|_{R=a}=0, \tag{2.28b}$$

where

$$\int_0^a Rh_2(R,t)\,\mathrm{d}R=0. \tag{2.29}$$

Equations (2.27)–(2.29) come from (2.3), (2.11) and (2.13) respectively.

When the interfacial tension σ is zero, h_2 must satisfy (2.27) with vanishing right-hand side, and the constraint (2.29).

We first solve the first-order problem (2.25). When $\boldsymbol{U}_{(j)1}(\boldsymbol{X},t)$ is known, the pathline $\boldsymbol{\chi}_t^{\langle 1\rangle}(\boldsymbol{X},t)$ can be found using (2.17). Then the right-hand side of (2.26*a*) is completely determined. The next step is to solve the problem (2.26) for $\boldsymbol{U}_{(j)2}$, $\Phi_{(j)2}$, and a problem of the type (2.27)–(2.29) for h_2.

Generally speaking, when perturbation data are periodic with frequency $\omega/2\pi$ then the first-order solution is also periodic with the same frequency, and the second-order solution consists of a mean part and a periodic part varying at twice the frequency (i.e. ω/π). This observation can be verified by examining the forcing functions on the

right-hand sides of (2.26). However, in our experiments, the mean part dominates the interface shape, with only a small ω/π-periodic deviation from the mean. We shall derive the solution for the mean part to compare with experiments.

3. The solution at first order

3.1. *Form of the first-order solution*

The only non-vanishing, azimuthal component $V_{(j)}(R,Z,t)$ $(j=1,2)$ of the velocity vector at first order satisfies the following system of equations:

$$\rho_{(j)}\frac{\partial}{\partial t}V_{(j)}(R,Z,t)=\int_0^\infty G_{(j)}(s)\left[\frac{1}{R}\frac{\partial}{\partial R}\left(R\frac{\partial}{\partial R}\right)-\frac{1}{R^2}+\frac{\partial^2}{\partial Z^2}\right]V_{(j)}(R,Z,t-s)\,\mathrm{d}s \quad \text{in } \mathscr{V}_{(j)}, \tag{3.1}$$

$$V_{(j)}(a,Z,t)=a\sin\omega t, \tag{3.2}$$

$$V_{(j)}(0,Z,t) \text{ is finite}, \tag{3.3}$$

$$\left[\!\left[\int_0^\infty G(s)\frac{\partial V}{\partial Z}(R,Z,t-s)\,\mathrm{d}s\right]\!\right]=[\![V(R,Z,t)]\!]=0 \quad \text{along} \quad z=0, \tag{3.4),(3.5}$$

$$\frac{\partial}{\partial Z}V_{(j)}(R,Z,t)\Big|_{|Z|\to\infty}=0. \tag{3.6}$$

We construct a solution of the form

$$V_{(j)}(R,Z,t)=P_{(j)}(R)\,\mathrm{e}^{\beta_{(j)}Z}\,\mathrm{e}^{\mathrm{i}\omega t}+\text{conjugate}, \tag{3.7}$$

in which $P_{(j)}(R)$ and $\beta_{(j)}$ can be complex or real, and $\mathrm{i}=\sqrt{-1}$. Substituting (3.7) into (3.1), we obtain

$$\begin{aligned}&[\rho_{(j)}\,\mathrm{i}\omega P_{(j)}\,\mathrm{e}^{\beta_{(j)}Z}\,\mathrm{e}^{\mathrm{i}\omega t}+\text{conjugate}]\\&=\int_0^\infty G_{(j)}(s)\left[\left(P''_{(j)}+\frac{P'_{(j)}}{R}-\frac{P_{(j)}}{R^2}+\beta_{(j)}^2P_{(j)}\right)\mathrm{e}^{\beta_{(j)}Z}\,\mathrm{e}^{\mathrm{i}\omega(t-s)}+\text{conjugate}\right]\mathrm{d}s,\end{aligned} \tag{3.8}$$

where $(\cdot)'(R)\equiv \mathrm{d}(\cdot)/\mathrm{d}R$. We further define the following complex numbers:

$$\eta_{(j)}(\omega)\equiv\int_0^\infty G_{(j)}(s)\,\mathrm{e}^{-\mathrm{i}\omega s}\,\mathrm{d}s, \tag{3.9}$$

and

$$\mathbb{A}_{(j)}^2(\omega)\equiv\frac{\mathrm{i}\omega\rho_{(j)}}{\eta_{(j)}}. \tag{3.10}$$

Equation (3.8) may be written in the form

$$\mathrm{e}^{\mathrm{i}\omega t}\,\mathrm{e}^{\beta_{(j)}Z}\left[\rho_{(j)}\,\mathrm{i}\omega P_{(j)}-\eta_{(j)}\left(P''_{(j)}+\frac{P'_{(j)}}{R}-\frac{P_{(j)}}{R^2}+\beta_{(j)}^2P_{(j)}\right)\right]+\text{conjugate}=0,$$

which implies that

$$P''_{(j)}+\frac{1}{R}P'_{(j)}+\left(\beta_{(j)}^2-\mathbb{A}_{(j)}^2-\frac{1}{R^2}\right)P_{(j)}=0. \tag{3.11}$$

Since $P_{(j)}(0)$ is finite, the solution $P_{(j)}(R)$ is given in terms of Bessel functions of the first kind $J_1(\mathbb{B}_{(j)}R)$, where $\mathbb{B}_{(j)}^2=\beta_{(j)}^2-\mathbb{A}_{(j)}^2$.

If there were only one fluid in the cylinder, we would have the following solution:

$$V(R,Z,t)=\frac{a}{2\mathrm{i}}\frac{J_1(\mathrm{i}\mathbb{A}R)}{J_1(\mathrm{i}\mathbb{A}a)}\,\mathrm{e}^{\mathrm{i}\omega t}+\text{conjugate}. \tag{3.12}$$

When there are two fluids, the solutions will attain the form (3.12) asymptotically at large $|Z|$. At small $|Z|$ the parts of the solutions which depend on Z become important, and in fact are crucial in satisfying the interfacial conditions (2.4) and (2.5). We find solutions in the form:

$$V_{(1)} = \left[\frac{a}{2\mathrm{i}}\frac{J_1(\mathrm{i}\mathbb{A}_{(1)}R)}{J_1(\mathrm{i}\mathbb{A}_{(1)}a)} + \sum_{n=1}^{\infty} C_n J_1\left(\sigma_n \frac{R}{a}\right) \mathrm{e}^{\beta_{(1)n}Z}\right] \mathrm{e}^{\mathrm{i}\omega t} + \text{conjugate} \quad \text{for} \quad Z \geqslant 0, \tag{3.13a}$$

and

$$V_{(2)} = \left[\frac{a}{2i}\frac{J_1(\mathrm{i}\mathbb{A}_{(2)}R)}{J_1(\mathrm{i}\mathbb{A}_{(2)}a)} + \sum_{n=1}^{\infty} D_n J_1\left(\sigma_n \frac{R}{a}\right) e^{\beta_{(2)n}Z}\right] \mathrm{e}^{\mathrm{i}\omega t} + \text{conjugate} \quad \text{for} \quad Z \leqslant 0, \tag{3.13b}$$

where σ_n is the nth root of the equation $J_1(\sigma_n) = 0$,

$$\beta_{(1)n} = \left(\frac{\sigma_n^2}{a^2} + \mathbb{A}_{(1)}^2\right)^{\frac{1}{2}} \quad \text{with negative real part,} \tag{3.14a}$$

$$\beta_{(2)n} = \left(\frac{\sigma_n^2}{a^2} + \mathbb{A}_{(2)}^2\right)^{\frac{1}{2}} \quad \text{with positive real part.} \tag{3.14b}$$

The real roots σ_n are tabulated in Abramowitz & Stegun (1970). The coefficients C_n and D_n are chosen such that conditions (3.4) and (3.5) are fulfilled.

Application of (3.13) to (3.4) yields

$$\sum_{n=1}^{\infty} [D_n \beta_{(2)n}\eta_{(2)} - C_n \beta_{(1)n}\eta_{(1)}] J_1\left(\sigma_n \frac{R}{a}\right) = 0 \tag{3.15}$$

$\forall R \in [0, a]$. Using the orthogonality property of Bessel functions

$$\int_0^a J_\nu(q_n Z) J_\nu(q_m Z)\, Z\,\mathrm{d}Z = \begin{cases} 0 & \text{if} \quad q_n \neq q_m, \\ \dfrac{a^2}{2} J_{\nu-1}^2(q_n a) & \text{if} \quad q_n = q_m, \end{cases}$$

for q_n such that $J_\nu(q_n a) = 0$ and $\mathrm{Re}\,(\nu) > -1$, we find that

$$C_n = D_n \frac{\beta_{(2)n}\eta_{(2)}}{\beta_{(1)n}\eta_{(1)}}. \tag{3.16}$$

The condition (3.5) requires that

$$\sum_{n=1}^{\infty} [D_n - C_n] J_1\left(\sigma_n \frac{R}{a}\right) = \frac{a}{2\mathrm{i}}\left[\frac{J_1(\mathrm{i}\mathbb{A}_{(1)}R)}{J_1(\mathrm{i}\mathbb{A}_{(2)}R)} - \frac{J_1(\mathrm{i}\mathbb{A}_{(2)}R)}{J_1(\mathrm{i}\mathbb{A}_{(1)}a)}\right]. \tag{3.17}$$

Multiplying both sides of the preceding equation by $J_1(\sigma_n R/a)\,R$, and integrating from 0 to a, we find that

$$[D_n - C_n] \int_0^a J_1\left(\sigma_n \frac{R}{a}\right)^2 R\,\mathrm{d}R = \frac{a}{2\mathrm{i}} \int_0^a \left[\frac{J_1(\mathrm{i}\mathbb{A}_{(1)}R)}{J_1(\mathrm{i}\mathbb{A}_{(1)}a)} - \frac{J_1(\mathrm{i}\mathbb{A}_{(2)}R)}{J_1(\mathrm{i}\mathbb{A}_{(2)}a)}\right] J_1\left(\sigma_n \frac{R}{a}\right) R\,\mathrm{d}R.$$

Computation of these definite integrals (see Tieu 1983) and elimination of C_n from (3.16) leads us to the following expression:

$$D_n = \frac{\mathrm{i}\sigma_n(\mathbb{A}_{(2)}^2 - \mathbb{A}_{(1)}^2)}{aJ_0(\sigma_n)\beta_{(1)n}^2\beta_{(2)n}^2}\left[1 - \frac{\beta_{(2)n}\eta_{(2)}}{\beta_{(1)n}\eta_{(1)}}\right]^{-1}. \tag{3.18}$$

We have thus determined completely the expressions (3.13) for the first-order azimuthal velocity components $V_{(j)}$. The series in (3.13a, b) converge. The convergence of these series can be shown by the following arguments. The left-hand side of (3.17) is the Fourier–Bessel series of the function

$$f(R) = \frac{a}{2\mathrm{i}}\left[\frac{J_1(\mathrm{i}\mathbb{A}_{(1)}R)}{J_1(\mathrm{i}\mathbb{A}_{(1)}a)} - \frac{J_1(\mathrm{i}\mathbb{A}_{(2)}R)}{J_1(\mathrm{i}\mathbb{A}_{(2)}a)}\right],$$

which vanishes at $R = 0$ and a. Moreover the integral

$$\int_0^a f(R)\, R^{\frac{1}{2}}\, \mathrm{d}R$$

is finite. It is known that the Fourier-Bessel expansion of a continuous function which has finite fluctuation in the interval $[0, a]$ and vanishes at end points, converges uniformly to that function (Watson 1958). Extending this result to the complex function, then the series on the left-hand side of (3.17) must converge uniformly in the interval $[0, a]$.

We further observe that, as $\sigma_n \to \infty$, $\beta_{(2)n}/\beta_{(1)}n \to -1$, which in turn implies, by (3.16), that $D_n - C_n \to D_n[1 + \eta_{(2)}/\eta_{(1)}]$. Since $|1 + \eta_{(2)}/\eta_{(1)}| > 1$, uniform convergence of the series $\Sigma_{n=1}^{\infty}(D_n - C_n)J_1(\sigma_n R/a)$ in the interval $[0, a]$ implies uniform convergence of $\Sigma_{n=1}^{\infty} D_n J_1(\sigma_n R/a)$. Likewise, since $|1 + \eta_{(2)}/\eta_{(1)}| > |\eta_{(2)}/\eta_{(1)}|$, the series $\Sigma_{n=1}^{\infty} C_n J_1(\sigma_n R/a)$ also converges uniformly in the interval $[0, a]$. These results assure that the series in (3.13) converge uniformly.

We have shown that the first-order azimuthal velocity components $V_{(j)}(R, Z, t)$ $(j = 1, 2)$ are expressible as follows:

$$V_{(j)}(R, Z, t) = v_{(j)}(R, Z)\, \mathrm{e}^{\mathrm{i}\omega t} + \text{conjugate} \tag{3.19a}$$

$$= R[\omega^*_{(j)}(R, Z)\, \mathrm{e}^{\mathrm{i}\omega t} + \text{conjugate}], \tag{3.19b}$$

where

$$v_{(1)}(R, Z) = \lim_{N\to\infty}\left\{\frac{a}{2\mathrm{i}}\frac{J_1(\mathrm{i}\mathbb{A}_{(1)}R)}{J_1(\mathrm{i}\mathbb{A}_{(1)}a)} + \sum_{n=1}^{N} C_n J_1\left(\sigma_n \frac{R}{a}\right)\mathrm{e}^{\beta_{(1)n}Z}\right\}, \tag{3.20a}$$

$$v_{(2)}(R, Z) = \lim_{N\to\infty}\left\{\frac{a}{2\mathrm{i}}\frac{J_1(\mathrm{i}\mathbb{A}_{(2)}R)}{J_1(\mathrm{i}\mathbb{A}_{(2)}a)} + \sum_{n=1}^{N} D_n J_1\left(\sigma_n \frac{R}{a}\right)\mathrm{e}^{\beta_{(2)n}Z}\right\} \tag{3.20b}$$

and

$$\omega^*_{(j)}(R, Z) = \frac{v_{(j)}(R, Z)}{R}. \tag{3.21}$$

The polar representation of $\omega^*_{(j)}(R, Z)$ is

$$\omega^*_{(j)}(R, Z) = |\omega^*_{(j)}|\,(\cos[\mathrm{Arg}\,(\omega^*_{(j)})] + \mathrm{i}\sin[\mathrm{Arg}\,(\omega^*_{(j)})]),$$

where $|\omega^*_{(j)}|$ and $\mathrm{Arg}\,(\omega^*_{(j)})$ are respectively the modulus and the argument of $\omega^*_{(j)}(R, Z)$. The azimuthal velocity components $V_{(j)}(R, Z, t)$ may be rewritten in the form

$$V_{(j)}(R, Z, t) = 2R\,|\omega^*_{(j)}|\cos(\omega t + \mathrm{Arg}\,(\omega^*_{(j)})), \tag{3.22a}$$

$$= 2R\,|\omega^*_{(j)}|\sin(\omega t - \delta_{(j)}(R, Z)), \tag{3.22b}$$

where $\delta_{(j)}(R, Z)$ are the phase lags. The relation between the phase lags $\delta_{(j)}(R, Z)$ and the arguments of $\omega^*_{(j)}(R, Z)$ is

$$\delta_{(j)}(R, Z) = \tfrac{3}{2}\pi - \mathrm{Arg}\,(\omega^*_{(j)}(R, Z)). \tag{3.23}$$

When $2|\omega^*_{(j)}(R,Z)|$ is equal to 1 and the phase lag $\delta_{(j)}$ is zero, (3.22b) represents the velocity distribution in a solid body undergoing sinusoidal oscillation.

3.2. *Asymptotic expressions of the first-order solution as* $\omega \to 0$

When $\omega \to 0$ we observe that

$$\eta_{(j)} = \mu_{(j)} + O(\omega), \tag{3.24}$$

where the viscosity $\mu_{(j)}$ is defined by (2.15a). Expression (3.10) in turn gives

$$\mathbb{A}^2_{(j)} = \frac{\mathrm{i}\omega\rho_{(j)}}{\mu_{(j)}} + o(\omega). \tag{3.25}$$

Using (3.14b,c), (3.24) and (3.25) in (3.16) and (3.18), we find that

$$D_n = -\frac{a}{J_0(\sigma_n)\,\sigma_n^3}[\![Re]\!]\frac{\mu_{(1)}}{\mu_{(1)}+\mu_{(2)}} + o(\omega), \tag{3.26a}$$

$$C_n = \frac{a}{J_0(\sigma_n)\,\sigma_n^3}[\![Re]\!]\frac{\mu_{(2)}}{\mu_{(1)}+\mu_{(2)}} + o(\omega), \tag{3.26b}$$

where the dimensionless group, $Re_{(j)} \equiv a^2\omega\rho_{(j)}/\mu_{(j)}$ is the Reynolds number for each fluid. Furthermore, replacing the numerator and denominator by their Taylor series about zero in the following quotient gives:

$$\frac{J_1(\mathrm{i}\mathbb{A}_{(j)}R)}{J_1(\mathrm{i}\mathbb{A}_{(j)}a)} = \frac{J_1'(0)\,(\mathrm{i}\mathbb{A}_{(j)}R) + \frac{1}{2}J_1''(0)\,(\mathrm{i}\mathbb{A}_{(j)}R)^2 + \frac{1}{6}J_1'''(0)\,(\mathrm{i}\mathbb{A}_{(j)}R)^3 + \ldots}{J_1'(0)\,(\mathrm{i}\mathbb{A}_{(j)}a) + \frac{1}{2}J_1''(0)\,(\mathrm{i}\mathbb{A}_{(j)}a)^2 + \frac{1}{6}J_1'''(0)\,(\mathrm{i}\mathbb{A}_{(j)}a)^3 + \ldots}.$$

Since $J_1'(0) = \frac{1}{2}$, $J_1'''(0) = -\frac{3}{8}$ and $J_1''(0) = 0$, the preceding expression can be reduced to

$$\begin{aligned}\frac{J_1(\mathrm{i}\mathbb{A}_{(j)}R)}{J_1(\mathrm{i}\mathbb{A}_{(j)}a)} &= \frac{R}{a} + \frac{1}{6}\frac{J_1'''(0)}{J_1'(0)}\mathbb{A}^2_{(j)}a^2\left[\frac{R}{a} - \left(\frac{R}{a}\right)^3\right] + o(|\mathbb{A}_{(j)}|^2)\\ &= \frac{R}{a}\left(1 - \frac{\mathrm{i}Re_{(j)}}{8}\left[1 - \left(\frac{R}{a}\right)^2\right]\right) + o(\omega).\end{aligned} \tag{3.27}$$

Substituting (3.25) and (3.27) into (3.20), we finally get

$$\begin{aligned}v_{(j)}(R,Z) = R\left(-\tfrac{1}{2}\mathrm{i} - \tfrac{1}{16}Re_{(j)}\left[1 - \left(\frac{R}{a}\right)^2\right]\right)\\ + ka[\![Re]\!]\frac{\mu_{(j+k)}}{\mu_{(1)}+\mu_{(2)}}\lim_{N\to\infty}\left\{\sum_{n=1}^{N}\frac{J_1\left(\sigma_n\frac{R}{a}\right)e^{\beta_{(j)n}Z}}{J_0(\sigma_n)\,\sigma_n^3}\right\} + o(\omega)\end{aligned} \tag{3.28}$$

where $k = (-1)^{j+1}$.

The above expression (3.28) implies the following properties of the solution at first order.

(a) When $\omega \to 0$, $Re_{(j)} = 0$ we have

$$v_{(j)}(R,Z) + \tfrac{1}{2}\mathrm{i}R = 2|\omega^*_{(j)}(R,Z)| - 1 = \delta_{(j)}(R,Z) = 0,$$

and

$$V_{(j)}(R,Z,t) = R\sin\omega t. \tag{3.29}$$

The fluids inside the cylinder thus oscillate as a solid body with the cylinder.

(b) When ω is small, the motion of a fluid inside the cylinder deviates from the oscillation of a solid body (3.29). The deviation is proportional to the Reynolds number $Re_{(j)}$ of the fluid. Two fluids inside an oscillating cylinder are distinguished

from one another, at first order, solely by their Reynolds numbers, or more specifically by the inverses of their kinematic viscosities

$$\frac{1}{\nu_{(j)}} = \frac{\rho_{(j)}}{\mu_{(j)}}.$$

If the kinematic viscosities, and therefore the Reynolds numbers, of the two fluids are different, the azimuthal velocity components $V_{(j)}(R, Z, t)$ will have Z-dependent parts which satisfy the continuity requirements of velocity and shear stress across the interface. The Z-dependent part of the azimuthal velocity of a fluid is important only in the proximity of the interface, and is proportional to the ratio of the dynamic viscosity of the other fluid to the sum of the dynamic viscosities of the two fluids.

4. The mean motion at second order

4.1. *Expressions for the inhomogeneous terms at second order*

Having obtained the solution at first order, we now derive the expressions for $\boldsymbol{S}_{2RZ}[\boldsymbol{U}_{(j)1}]$, $\boldsymbol{S}_{2ZZ}[\boldsymbol{U}_{(j)1}]$ and

$$\mathscr{G}_{(j)} \equiv \boldsymbol{\nabla}\cdot\boldsymbol{S}_2[\boldsymbol{U}_{(j)1}] - \rho_{(j)}\,\boldsymbol{U}_{(j)1}\cdot\boldsymbol{\nabla}\boldsymbol{U}_{(j)1}, \tag{4.1}$$

which appear in the second-order problem (2.26)–(2.29). Since

$$\boldsymbol{U}^{\langle 1\rangle}_{(j)} = \boldsymbol{U}_{(j)1} = V_{(j)}(\boldsymbol{X}, t)\,\boldsymbol{e}_\theta,$$

where $V_{(j)}(\boldsymbol{X}, t)$ are given by (2.13a, b), the history $\boldsymbol{\chi}^{\langle 1\rangle}_{t(j)}(\boldsymbol{X}, t-s)$ is determined by (2.17) with $n = 1$:

$$\begin{aligned}\boldsymbol{\chi}^{\langle 1\rangle}_{t(j)}(\boldsymbol{X}, t-s) &= \int_t^{t-s} V_{(j)}(\boldsymbol{X}, \tau')\,\boldsymbol{e}_\theta\,\mathrm{d}\tau' \\ &= \boldsymbol{e}_\theta \int_t^{t-s} [R\omega^*_{(j)}\,\mathrm{e}^{\mathrm{i}\omega\tau'} + \text{conjugate}]\,\mathrm{d}\tau' \\ &= \boldsymbol{e}_\theta R\left[\frac{\omega^*_{(j)}}{\mathrm{i}\omega}\mathrm{e}^{\mathrm{i}\omega t}(\mathrm{e}^{-\mathrm{i}\omega s} - 1) + \text{conjugate}\right].\end{aligned}$$

We define

$$((\theta))_{(j)} \equiv \left[\frac{\omega^*_{(j)}}{\mathrm{i}\omega}\mathrm{e}^{\mathrm{i}\omega t}(\mathrm{e}^{-\mathrm{i}\omega s} - 1) + \text{conjugate}\right] \tag{4.2}$$

and

$$\Omega_{(j)}(R, Z, t-s) \equiv \frac{V_{(j)}}{R}(R, Z, t-s) = [\omega^*_{(j)}(R, Z)\,\mathrm{e}^{\mathrm{i}\omega(t-s)} + \text{conjugate}], \tag{4.3a, b}$$

then

$$\boldsymbol{\chi}^{\langle 1\rangle}_{t(j)} = \boldsymbol{e}_\theta R((\theta))_{(j)} \tag{4.4a}$$

and

$$\boldsymbol{A}_1[\boldsymbol{U}_{(j)1}] = R\Omega_{(j),R}(\boldsymbol{e}_R\boldsymbol{e}_\theta + \boldsymbol{e}_\theta\boldsymbol{e}_R) + R\Omega_{(j),Z}(\boldsymbol{e}_Z\boldsymbol{e}_\theta + \boldsymbol{e}_\theta\boldsymbol{e}_Z), \tag{4.4b}$$

where the comma subscript denotes partial differentiation with respect to the variables that follow.

Using (4.4a, b) in (2.19b), we find the following expressions:

$$\begin{aligned}&\boldsymbol{S}_{2RZ}[\boldsymbol{U}_{(j)1}] \equiv \boldsymbol{e}_R\cdot\boldsymbol{S}_2[\boldsymbol{U}_{(j)1}]\cdot\boldsymbol{e}_Z \\ &= \int_0^\infty G(s)\,R^2[((\theta))_{,Z}\,\Omega_{,R} + ((\theta))_{,R}\,\Omega_{,Z}]\,\mathrm{d}s + \int_0^\infty\int_0^\infty \gamma(s_1, s_2)\,R^2\,\Omega_{,R}(s_1)\,\Omega_{,Z}(s_2)\,\mathrm{d}s_1\,\mathrm{d}s_2,\end{aligned} \tag{4.5a}$$

$$\boldsymbol{S}_{2zz}[\boldsymbol{U}_{(j)1}] \equiv \boldsymbol{e}_Z \cdot \boldsymbol{S}_2[\boldsymbol{U}_{(j)1}] \cdot \boldsymbol{e}_Z$$
$$= 2\int_0^\infty G(s)\, R^2((\theta))_{,Z}\, \Omega_{,Z}\, \mathrm{d}s + \int_0^\infty \int_0^\infty \gamma(s_1, s_2)\, R^2 \Omega_{,Z}(s_1)\, \Omega_{,Z}(s_2)\, \mathrm{d}s_1\, \mathrm{d}s_2, \tag{4.5b}$$

where subscript (j), with $j = 1$ or 2, is omitted from $G(s)$, $\gamma(s_1, s_2)$, $((\theta))$ and Ω for the sake of clarity. In the rest of our analysis, subscript (j) will be included only where it is necessary to avoid ambiguity. Similar computations give the following:

$$\nabla \cdot \int_0^\infty G(s)\, [\chi_t^{\langle 1\rangle} \cdot \nabla \boldsymbol{A}_1 + \boldsymbol{A}_1 \nabla \chi_t^{\langle 1\rangle} + [\boldsymbol{A}_1 \nabla \chi_t^{\langle 1\rangle}]^{\mathrm{T}}]\, \mathrm{d}s$$
$$= \int_0^\infty G(s)\, \{([R^2 \Omega_{,R}((\theta))_{,Z} + R^2 \Omega_{,Z}((\theta))_{,R}]_{,R} + [2R^2 \Omega_{,Z}((\theta))_{,Z}]_{,Z}$$
$$+ R[\Omega_{,R}((\theta))_{,Z} + \Omega_{,Z}((\theta))_{,R}])\, \boldsymbol{e}_Z$$
$$+ ([2R^2 \Omega_{,R}((\theta))_{,R}]_{,R} + 2R\Omega_{,R}((\theta))_{,R} + R^2[\Omega_{,R}((\theta))_{,Z} + \Omega_{,Z}((\theta))_{,R}]_{,Z})\, \boldsymbol{e}_R\}\, \mathrm{d}s, \tag{4.6a}$$

$$\nabla \cdot \int_0^\infty \int_0^\infty \gamma(s_1, s_2)\, \boldsymbol{A}_1(s_1)\, \boldsymbol{A}_1(s_2)\, \mathrm{d}s_1\, \mathrm{d}s_2$$
$$= \int_0^\infty \int_0^\infty \gamma(s_1, s_2)\, \{([R^2 \Omega_{,R}(s_1)\, \Omega_{,R}(s_2)]_{,R} + [R^2 \Omega_{,R}(s_1)\, \Omega_{,Z}(s_2)]_{,Z}$$
$$- R\Omega_{,Z}(s_1)\, \Omega_{,Z}(s_2))\, \boldsymbol{e}_R + ([R^2 \Omega_{,R}(s_2)\, \Omega_{,Z}(s_1)]_{,R}$$
$$+ [R^2 \Omega_{,Z}(s_1)\, \Omega_{,Z}(s_2)]_{,Z} + R\Omega_{,R}(s_2)\, \Omega_{,Z}(s_1))\, \boldsymbol{e}_z\}\, \mathrm{d}s_1\, \mathrm{d}s_2, \tag{4.6b}$$

and

$$\rho \boldsymbol{U}_1 \cdot \nabla \boldsymbol{U}_1 = -R\Omega^2 \boldsymbol{e}_R. \tag{4.6c}$$

The forcing function $\mathscr{G}_{(j)}$ defined by (4.1) is therefore completely determined by (2.19b) and (4.6). If we now put (4.2) and (4.3b) into (4.6), expand products of sums into sum of products, carry out the integrations with respect to s and finally group terms, we will get results in terms of $\omega^*_{(j)}(R, z)$ and related material functions. The work involved is tedious, and will not be shown here.

To present the above results in manageable forms we introduce the following functions:

$$\left.\begin{aligned}
r_1 &= \frac{4}{R}[R^3 |\omega^*_{,R}|^2]_{,R} + 2R^2[\bar{\omega}^*_{,R}\omega^*_{,Z} + \omega^*_{,R}\bar{\omega}^*_{,Z}]_{,Z},\\
s_1 &= \frac{2}{R}[R^3(\omega^*_{,R})^2]_{,R} + 2R^2[\omega^*_{,Z}\omega^*_{,R}]_{,Z},\\
r_3 &= 2[R^2|\omega^*_{,R}|^2]_{,R} + R^2[\omega^*_{,R}\bar{\omega}^*_{,Z} + \bar{\omega}^*_{,R}\omega^*_{,Z}]_{,Z} - 2R|\omega^*_{,Z}|^2,\\
s_3 &= [R^2(\omega^*_{,R})^2]_{,R} + R^2[\omega^*_{,R}\omega^*_{,Z}]_{,Z} - R(\omega^*_{,Z})^2,\\
r_4 &= \frac{1}{R}[R^3(\omega^*_{,R}\bar{\omega}^*_{,Z} + \bar{\omega}^*_{,R}\omega^*_{,Z})]_{,R} + 2R^2[|\omega^*_{,Z}|^2]_{,Z},\\
s_4 &= \frac{1}{R}[R^3\omega^*_{,R}\omega^*_{,Z}]_{,R} + R^2[(\omega^*_{,Z})^2]_{,Z},\\
r_5 &= 2R|\omega^*|^2, \quad s_5 = R(\omega^*)^2,
\end{aligned}\right\} \tag{4.7}$$

where $|(\cdot)|$ and $\overline{(\cdot)}$ denote respectively the modulus and complex conjugate of $(\cdot)$. Material-related functions, arising from our analysis at second order, are listed below:

$$\left.\begin{aligned}
\eta_1(\omega) &\equiv \int_0^\infty G(s)\frac{\sin\omega s}{\omega}\,\mathrm{d}s,\\
\not\eta(\omega) &\equiv \int_0^\infty\int_0^\infty \gamma(s_1,s_2)\cos\omega(s_1-s_2)\,\mathrm{d}s_1\,\mathrm{d}s_2,\\
\eta^*(\omega) &\equiv \int_0^\infty G(s)\frac{\mathrm{e}^{-\mathrm{i}\omega s}(1-\mathrm{e}^{-\mathrm{i}\omega s})}{\mathrm{i}\omega}\,\mathrm{d}s,\\
\not\eta^*(\omega) &\equiv \int_0^\infty\int_0^\infty \gamma(s_1,s_2)\,\mathrm{e}^{-\mathrm{i}\omega(s_1+s_2)}\,\mathrm{d}s_1\,\mathrm{d}s_2,\\
\Sigma_1(\omega) &\equiv \not\eta-2\eta_1,\quad \Sigma_1^*(\omega)\equiv\not\eta^*-2\eta^*.
\end{aligned}\right\} \tag{4.8}$$

These functions are not material functions, because they depend also on external factors that induce the motion. In this problem such a factor is the angular velocity ω. When $\omega\to 0$ the limits of the above functions are

$$\eta_1(0)=\eta^*(0)=-\alpha_1,\quad \not\eta(0)=\not\eta^*(0)=\alpha_2,\quad \Sigma_1(0)=\Sigma_1^*(0)=\alpha_2+2\alpha_1, \tag{4.9}$$

where α_1 and α_2 are defined in (2.15b,c). We remark that since $\gamma(s_1,s_2)=\gamma(s_2,s_1)$,

$$\int_0^\infty\int_0^\infty \gamma(s_1,s_2)\sin\omega\,(s_1-s_2)\,\mathrm{d}s_1\,\mathrm{d}s_2=0.$$

The forcing function $\mathscr{G}_{(j)}$ can then be expressed in terms of the functions defined in (4.7) and (4.8) as follows:

$$\begin{aligned}
\mathscr{G}(R,Z,t) = {}& (-\eta_1 r_1+\not\eta r_3+\rho r_5)\,\boldsymbol{e}_R+\Sigma_1 r_4\,\boldsymbol{e}_Z\\
&+\{\mathrm{e}^{2\mathrm{i}\omega t}[(-\eta^* s_1+\not\eta^* s_3+\rho s_5)\,\boldsymbol{e}_R+\Sigma_1^* s_4\,\boldsymbol{e}_Z].+\text{conjugate}\}.
\end{aligned} \tag{4.10}$$

Similarly, we find that

$$\boldsymbol{S}_{2RZ}[\boldsymbol{U}_1]=R^2(\omega^*_{,Z}\,\bar\omega^*_{,R}+\bar\omega^*_{,Z}\,\omega^*_{,R})\,\Sigma_1+\{\mathrm{e}^{2\mathrm{i}\omega t}R^2\omega^*_{,Z}\,\omega^*_{,R}\,\Sigma_1^*+\text{conjugate}\} \tag{4.11a}$$

and

$$\boldsymbol{S}_{2ZZ}[\boldsymbol{U}_1]=2R^2|\omega^*_{,Z}|^2\,\Sigma_1+\{\mathrm{e}^{2\mathrm{i}\omega t}\,R^2(\omega^*_{,Z})^2\,\Sigma_1^*+\text{conjugate}\}. \tag{4.11b}$$

Expressions (4.10), and (4.11) are of the form

$$f(R,Z,t)=\mathring{f}(R,Z)+\hat{f}(R,Z,t), \tag{4.12a}$$

where $\hat{f}(R,Z,t)$ is a time-periodic function about zero mean level with period π/ω:

$$\hat{f}(R,Z,t)=\hat{f}\left(R,Z,t+\frac{\pi}{\omega}\right)\quad\text{for all time } t.$$

The time-independent parts of $\mathscr{G}(R,Z,t)$, $\boldsymbol{S}_{2RZ}[\boldsymbol{U}_1]$ and $\boldsymbol{S}_{2ZZ}[\boldsymbol{U}_1]$ are

$$\mathring{\mathscr{G}}(R,Z)=(-\eta_1 r_1+\not\eta r_3+\rho r_5)\,\boldsymbol{e}_R+\Sigma_1 r_4\,\boldsymbol{e}_Z, \tag{4.13a}$$

$$\mathring{\boldsymbol{S}}_{2RZ}[\boldsymbol{U}_1]=R^2(\omega^*_{,Z}\,\bar\omega^*_{,R}+\bar\omega^*_{,Z}\,\omega^*_{,R})\,\Sigma_1 \tag{4.13b}$$

and

$$\mathring{\boldsymbol{S}}_{2ZZ}[\boldsymbol{U}_1]=2R^2|\omega^*_{,Z}|^2\,\Sigma_1. \tag{4.13c}$$

The time-periodic parts $\hat{\mathscr{G}}(R,Z,t)$, $\hat{\boldsymbol{S}}_{2RZ}(R,Z,t)$ and $\hat{\boldsymbol{S}}_{2ZZ}(R,Z,t)$ are the terms in curly brackets of (4.10) and (4.11a,b) respectively.

Since the inhomogeneous terms $\mathscr{G}_{(j)}(R,Z,t)$, $\boldsymbol{S}_{(j)2RZ}[\boldsymbol{U}_1]$ and $\boldsymbol{S}_{(j)2ZZ}[\boldsymbol{U}_1]$, of the second-order problem defined by (2.26)–(2.29), are periodic, the solution $\boldsymbol{U}_{(j)2}$, $\boldsymbol{\Phi}_{(j)2}$ and h_2 can be decomposed into a mean part and periodic part of the same period π/ω.

$$\left.\begin{aligned} \boldsymbol{U}_{(j)2} &= \tfrac{1}{2}\bar{\bar{\boldsymbol{U}}}_{(j)} + \tfrac{1}{4}[\mathrm{e}^{2\mathrm{i}\omega t}\,\tilde{\boldsymbol{U}}_{(j)} + \text{conjugate}], \\ \boldsymbol{\Phi}_{(j)2} &= \tfrac{1}{2}\bar{\bar{\boldsymbol{\Phi}}}_{(j)} + \tfrac{1}{4}[\mathrm{e}^{2\mathrm{i}\omega t}\,\tilde{\boldsymbol{\Phi}}_{(j)} + \text{conjugate}], \\ h_2 &= \tfrac{1}{2}\bar{\bar{h}} + \tfrac{1}{4}[\mathrm{e}^{2\mathrm{i}\omega t}\,\tilde{h} + \text{conjugate}]. \end{aligned}\right\} \tag{4.14}$$

We can view the $\bar{\bar{(\cdot)}}$ as mean values of second derivatives with respect to ϵ of the original function $(\cdot)$.

4.2. *The problem for the mean motion*

The governing equations for the mean motion at second order can be derived by substituting (4.10), (4.11) and (4.14) in (2.26) and collecting terms which are time-independent. In this way we find

$$\boldsymbol{\nabla}\bar{\bar{\boldsymbol{\Phi}}}_{(j)} - \mu_{(j)}\nabla^2\bar{\bar{\boldsymbol{U}}}_{(j)} = 2\mathring{\mathscr{G}}_{(j)}(R,Z), \tag{4.15a}$$

$$\boldsymbol{\nabla}\cdot\bar{\bar{\boldsymbol{U}}}_{(j)} = 0 \quad \text{in } \mathscr{V}_{(j)}; \tag{4.15b}$$

$$\bar{\bar{\boldsymbol{U}}}_{(j)}(a,Z) = 0, \quad \bar{\bar{\boldsymbol{U}}}_{(j)}(0,Z) \text{ is bounded}; \tag{4.15c,d}$$

$$\left[\!\left[\mu\frac{\partial\bar{\bar{w}}}{\partial Z}\right]\!\right] = -2\,[\![\mathring{\boldsymbol{S}}_{2RZ}[\boldsymbol{U}_1]]\!], \tag{4.15e}$$

$$[\![\bar{\bar{w}}]\!] = \bar{\bar{w}}_{(j)} = 0 \quad \text{along} \quad Z = 0; \tag{4.15f,g}$$

$$\frac{\partial}{\partial Z}\bar{\bar{\boldsymbol{U}}}_{(j)}\bigg|_{|Z|\to\infty} = \frac{\partial\bar{\bar{\boldsymbol{\Phi}}}_{(j)}}{\partial Z}\bigg|_{|Z|\to\infty} = 0. \tag{4.15h,k}$$

And $\bar{\bar{h}}$ satisfies

$$\sigma\left[\bar{\bar{h}}'' + \frac{1}{R}\bar{\bar{h}}'\right] - [\![\rho]\!]g\bar{\bar{h}} = -[\![\bar{\bar{\Phi}}]\!] + \left[\!\left[2\mu\frac{\partial\bar{\bar{u}}}{\partial Z} + 2\mathring{\boldsymbol{S}}_{2ZZ}[\boldsymbol{U}_1]\right]\!\right] \tag{4.16}$$

at $z = 0$ and for $R \in [0,a]$, such that

$$\text{(i)} \quad \bar{\bar{h}}'(0) = \bar{\bar{h}}'(a) - \bar{\bar{\alpha}} = 0, \tag{4.17a}$$

or

$$\text{(ii)} \quad \bar{\bar{h}}'(0) = \bar{\bar{h}}(a) = 0, \tag{4.17b}$$

where

$$\int_0^a R\bar{\bar{h}}\,\mathrm{d}R = 0. \tag{4.18}$$

The mean motion $\bar{\bar{\boldsymbol{U}}} = \bar{\bar{w}}\boldsymbol{e}_R + \bar{\bar{u}}\boldsymbol{e}_z$ and reduced pressure $\bar{\bar{\Phi}}$ will be obtained by solving problem (4.15). To this end we define a stream function $\psi(R,Z)$ such that

$$\bar{\bar{\boldsymbol{U}}}_{(j)} \equiv \boldsymbol{\nabla}\times\left[\frac{\psi_{(j)}}{R}\boldsymbol{e}_\theta\right]. \tag{4.19}$$

The radial and axial components of (4.19) are

$$\bar{\bar{w}}_{(j)} = -\frac{1}{R}\frac{\partial}{\partial Z}\psi_{(j)}, \quad \bar{\bar{u}}_{(j)} = \frac{1}{R}\frac{\partial}{\partial R}\psi_{(j)}. \tag{4.20a,b}$$

Taking the curl of both sides of (4.15a), we get

$$-\mu_{(j)}\,\boldsymbol{\nabla}\times[\nabla^2\bar{\bar{\boldsymbol{U}}}_{(j)}] = 2\boldsymbol{\nabla}\times\mathring{\mathscr{G}}_{(j)}.$$

We then invoke the vector identity

$$\nabla^2 \boldsymbol{a} = \nabla(\nabla\cdot\boldsymbol{a}) - \nabla\times(\nabla\times\boldsymbol{a}),$$

and note that

$$\nabla\times\overline{\overline{U}} = -\frac{1}{R}\mathscr{L}\psi\boldsymbol{e}_\theta,$$

where

$$\mathscr{L}(\cdot) \equiv \left(\frac{\partial^2}{\partial R^2} - \frac{1}{R}\frac{\partial}{\partial R} + \frac{\partial^2}{\partial Z^2}\right)(\cdot). \tag{4.21}$$

It can be shown that ψ satisfies the equation

$$\mathscr{L}^2\psi = \frac{2R}{\mu}\left\{\frac{\partial}{\partial Z}(-\eta_1 r_1 + \gamma r_3 + \rho r_5) - \Sigma_1\frac{\partial}{\partial R}r_4\right\}. \tag{4.22}$$

Equation (4.22) applies to both fluids. Moreover, the $\psi_{(j)}$ must also satisfy boundary conditions

$$\psi(a, Z) = \psi_{,R}(a, Z) = 0, \tag{4.23a}$$

$$\frac{\psi}{R} \text{ and } \frac{\psi_{,R}}{R} \text{ remain finite as } R\to 0; \tag{4.23b}$$

$$\left[\!\left[\frac{\mu}{R}\psi_{,ZZ}\right]\!\right] = 2[\![\hat{\boldsymbol{S}}_{2RZ}[\boldsymbol{U}_1]]\!], \tag{4.23c}$$

$$[\![\psi_{,Z}]\!] = \psi_{(j)} = 0 \quad \text{at} \quad Z = 0, \tag{4.23d,e}$$

$$\psi_{(j)}\to 0 \quad \text{as } |Z|\to\infty. \tag{4.23f}$$

(Boundary condition (4.23*e*) was derived using (4.15*c*,*g*).) When the $\psi_{(j)}$ are known, we may integrate (4.15*a*) to find $\overline{\overline{\Phi}}_{(j)}$. Finally, we can compute the inhomogeneous terms of (4.16) and solve (4.16)–(4.18) for $\overline{\overline{h}}$.

5. The solution for the problem of the mean motion

5.1. *The stream function*

The stream function $\psi_{(j)}(R, Z)$, defined by (4.19), may be decomposed into two parts

$$\psi_{(j)}(R, Z) = \psi_{\mathrm{P}(j)}(R, Z) + \psi_{\mathrm{H}(j)}(R, Z) \tag{5.1}$$

where $\psi_{\mathrm{P}(j)}$ is a particular solution of the following problem:

$$\mathscr{L}^2\psi_{(j)} = f_{(j)}(R, Z) \quad \text{in } \mathscr{V}_{(j)}, \tag{5.2a}$$

subject to boundary conditions

$$\psi_{(j)}(a, Z) = \frac{\partial}{\partial R}\psi_{(j)}(a, Z) = 0, \tag{5.2b,c}$$

$$\frac{\psi_{(j)}}{R}(R, Z) \text{ and } \frac{1}{R}\frac{\partial}{\partial R}\psi_{(j)}(R, Z) \text{ are finite as } R\to 0, \tag{5.2d,e}$$

and

$$\psi_{(j)}\to 0 \quad \text{as } |Z|\to\infty. \tag{5.2f}$$

The forcing function on the right-hand side of (5.2*a*) is defined below:

$$f_{(j)}(R, Z) \equiv \frac{2R}{\mu_{(j)}}\left\{\frac{\partial}{\partial Z}\left(-\eta_1 r_1 + \gamma r_3 + \rho r_5\right) - \Sigma_1\frac{\partial}{\partial R}r_4\right\}_{(j)}. \tag{5.3}$$

On the other hand, $\psi_{\mathrm{H}(j)}$ satisfies the edge problem defined by (5.2*a–f*) with $f_{(j)} \equiv 0$, and interface conditions at $z = 0$:

$$[\![\mu\psi_{\mathrm{H},zz}]\!] = -[\![\mu\psi_{\mathrm{P},zz}]\!] + 2R[\![\mathring{\boldsymbol{S}}_{2RZ}[\boldsymbol{U}_1]]\!], \tag{5.4a}$$

$$[\![\psi_{H,Z}]\!] = -[\![\psi_{\mathrm{P},Z}]\!], \quad \text{and} \quad \psi_{\mathrm{H}(j)} = -\psi_{\mathrm{P}(j)}. \tag{5.4b,c}$$

5.1.1. *Expressions for particular solutions*

The form of $\psi_{\mathrm{P}(j)}$ depends on the form of the forcing function $f_{(j)}(R, Z)$. We now derive explicit expressions for $f_{(j)}(R, Z)$. We note that since $v_{(j)}(R, Z)$ satisfy

$$\frac{\partial^2}{\partial R^2}v + \frac{1}{R}\frac{\partial}{\partial R}v - \frac{v}{R^2} + \frac{\partial^2 v}{\partial Z^2} = \mathcal{A}^2 v, \tag{5.5a}$$

the function $\omega^*_{(j)}(R, Z) = v_{(j)}(R, Z)/R$ must satisfy

$$\frac{3\omega^*_{,R}}{R} + \omega^*_{,RR} + \omega^*_{,ZZ} = \mathcal{A}^2\omega^*. \tag{5.5b}$$

Equation (5.5*b*) allows us to express high-order derivatives of ω^* in terms of lower-order derivatives. Substituting appropriate expressions from (4.7) into (5.3) and using (5.5*b*) to eliminate high-order derivatives of ω^*, we get

$$f_{(j)}(R, Z) = \left\{\frac{4R^2}{\mu}\left[\frac{\partial}{\partial Z}\left\{\rho|\omega^*|^2 - 2\Sigma_2(|\omega^*_{,R}|^2 + |\omega^*_{,Z}|^2)\right\} - \Sigma_1(\mathcal{A}^2\omega^*\bar{\omega}^*_{,Z} + \bar{\mathcal{A}}^2\bar{\omega}^*\omega^*_{,Z})\right] + \frac{2R^3}{\mu}\Sigma_1(\mathcal{A}^2 - \bar{\mathcal{A}}^2)(\omega^*_{,Z}\bar{\omega}^*_{,R} - \omega^*_{,R}\bar{\omega}^*_{,Z})\right\}_{(j)}, \tag{5.6}$$

where

$$\Sigma_2 \equiv \gamma - \eta_1. \tag{5.7}$$

We then evaluate (5.6), using the first-order solution, and find that

$$\begin{aligned} f_{(1)}(R, Z) = \frac{2}{\mu_{(1)}}\Bigg[& \frac{a}{\mathrm{i}J_1(\mathrm{i}\mathcal{A}_{(1)}a)}\lim_{L\to\infty}\sum_{l=1}^{L} \mathrm{e}^{\bar{\beta}_{(1)l}Z}\bar{C}_l\bar{\beta}_{(1)l} \\ & \times\left\{(\rho_{(1)} - \Sigma_{(1)1}\mathcal{A}^2_{(1)})J_1(\mathrm{i}\mathcal{A}_{(1)}R)J_1\left(\sigma_l\frac{R}{a}\right) - 2\mathrm{i}\Sigma_{(1)2}\mathcal{A}_{(1)}\frac{\sigma_l}{a}J_2(\mathrm{i}\mathcal{A}_{(1)}R)J_1\left(\sigma_l\frac{R}{a}\right)\right. \\ & \left.+\frac{\mathrm{i}}{a}(\mathcal{A}^2_{(1)} - \bar{\mathcal{A}}^2_{(1)})\Sigma_{(1)1}\mathcal{A}_{(1)}RJ_2(\mathrm{i}\mathcal{A}_{(1)}R)J_1\left(\sigma_l\frac{R}{a}\right)\right\} \\ & + \lim_{\substack{N\to\infty \\ M\to\infty}}\sum_{m=1}^{M}\sum_{n=1}^{N} C_m\bar{C}_n\bar{\beta}_{(1)n}\mathrm{e}^{(\beta_{(1)n}+\beta_{(1)m})Z} \\ & \times\left\{2(\rho_{(1)} - 2\Sigma_{(1)2}\beta^2_{(1)m} - \Sigma_{(1)1}\mathcal{A}^2_{(1)})J_1\left(\sigma_n\frac{R}{a}\right)J_1\left(\sigma_m\frac{R}{a}\right)\right. \\ & -4\Sigma_{(1)2}\frac{\sigma_n\sigma_m}{a^2}J_2\left(\sigma_n\frac{R}{a}\right)J_2\left(\sigma_m\frac{R}{a}\right) \\ & \left.+(\mathcal{A}^2_{(1)} - \bar{\mathcal{A}}^2_{(1)})\sum_{(1)}\frac{\sigma_m}{a}RJ_1\left(\sigma_n\frac{R}{a}\right)J_2\left(\sigma_m\frac{R}{a}\right)\right\} + \text{conjugate}\Bigg]. \end{aligned} \tag{5.8}$$

The expression for $f_{(2)}(R, Z)$ can be obtained by replacing subscript (1) and coefficients C by subscript (2) and coefficients D in (5.8). The right-hand side of (5.8) consists of a single sum on subscript l and a double sum on subscripts m and n. We denote the truncated form of $f_{(j)}(R, Z)$ as $f^{\langle L,M,N\rangle}_{(j)}$ when the limits of these summations on subscripts l, m and n are L, M and N respectively.

Expressions of the type (5.8) are computable. Nevertheless they are not in the most

manageable form, especially for the lengthy calculations to follow. We next derive approximate expressions for $f_{(j)}(R, Z)$ valid in the range of parameter of interest. To this end, we first recall that

$$\beta^2_{(j)n} = \left(\frac{\sigma_n}{a}\right)^2 + A^2_{(j)}$$

and

$$A^2_{(j)} = \frac{\mathrm{i}\omega\rho_{(j)}}{\int_0^\infty G_{(j)}\,\mathrm{e}^{-\mathrm{i}\omega s}\,\mathrm{d}s} = \frac{\mathrm{i}\omega\rho_{(j)}}{\mu_{(j)}} + o(\omega).$$

For sufficiently small ω it is possible to approximate the $\beta^2_{(j)n}$ by

$$\beta^2_{(j)n} = \left(\frac{\sigma_n}{a}\right)^2, \tag{5.9a}$$

so that

$$\beta_{(j)n} = (-1)^j \frac{\sigma_n}{a}. \tag{5.9b}$$

Therefore

$$\left.\begin{aligned} \exp\left(\beta_{(j)n} Z\right) &\approx \exp\left[(-1)^j \sigma_n \frac{Z}{a}\right], \\ \exp\left[\bar{\beta}_{(j)n} + \beta_{(j)m}\right) Z] &\approx \exp\left[(-1)^j (\sigma_n + \sigma_m)\frac{Z}{a}\right]. \end{aligned}\right\} \tag{5.10}$$

Using approximations (5.9) and (5.10) in expressions of the type (5.8), we get

$$\begin{aligned} f_{(j)}(R,Z) = \lim_{L\to\infty} \sum_{l=1}^{L} &\left\{\exp\left[(-1)^j \sigma_l \frac{Z}{a}\right]\right\}\left[\nu_{(j)1l} J_1(\mathrm{i}A_{(j)} R)\, J_1\left(\sigma_l \frac{R}{a}\right)\right. \\ &\left. + \nu_{(j)2l} R J_2(\mathrm{i}A_{(j)} R)\, J_1\left(\sigma_l \frac{R}{a}\right) + \nu_{(j)3l} J_2(\mathrm{i}A_{(j)} R)\, J_2\left(\sigma_l \frac{R}{a}\right) + \text{conjugate}\right] \\ + \lim_{\substack{N\to\infty \\ M\to\infty}} \sum_{n=1}^{N} \sum_{m=1}^{M} &\left\{\exp\left[(-1)^j (\sigma_n + \sigma_m)\frac{Z}{a}\right]\right\}\left[i_{(j)1nm} J_1\left(\sigma_n \frac{R}{a}\right) J_1\left(\sigma_m \frac{R}{a}\right)\right. \\ &\left. + i_{(j)2nm} R J_1\left(\sigma_n \frac{R}{a}\right) J_2\left(\sigma_m \frac{R}{a}\right) + i_{(j)3nm} J_2\left(\sigma_n \frac{R}{a}\right) J_2\left(\sigma_m \frac{R}{a}\right) + \text{conjugate}\right], \end{aligned} \tag{5.11}$$

where the coefficients $\nu_{(j)kn}$ and $i_{(j)knm}$, with $k = 1, 2, 3$, are defined below.
For $j = 1$:

$$\left.\begin{aligned} \nu_{(1)1l} &\equiv -\left\{\frac{2}{\mathrm{i}\mu J_1(\mathrm{i}Aa)} \sigma_l (\rho - \Sigma_1 A^2)\right\}_{(1)} \bar{C}_l, \\ \nu_{(1)2l} &\equiv -\left\{\frac{1}{\mu J_1(\mathrm{i}Aa)} \sigma_l (A^2 - \bar{A}^2)\, \Sigma_1 A\right\}_{(1)} \bar{C}_l, \\ \nu_{(1)3l} &\equiv \left\{\frac{4}{\mu J_1(\mathrm{i}Aa)} \sigma_l^2 \Sigma_2 Aa\right\}_{(1)} \bar{C}_l, \\ i_{(1)1nm} &\equiv -\left\{\frac{4}{\mu}\frac{\sigma_n}{a}\left(\rho - 2\Sigma_2 \frac{\sigma_m^2}{a^2} - \Sigma_1 A^2\right)\right\}_{(1)} \bar{C}_n C_m \\ i_{(1)2nm} &\equiv -\left\{\frac{2}{\mu}\frac{\sigma_n \sigma_m}{a^2}(A^2 - \bar{A}^2)\, \Sigma_1\right\}_{(1)} \bar{C}_n C_m, \\ i_{(1)3nm} &\equiv \left\{\frac{8}{\mu}\frac{\sigma_n^2 \sigma_m}{a^3} \Sigma_2\right\}_{(1)} \bar{C}_n C_m. \end{aligned}\right\} \tag{5.12}$$

n	σ_n	$\check{\sigma}_n = \frac{1}{n-1}\sum_{i=1}^{n-1}(\sigma_i+\sigma_{n-i})$
1	3.83171	(not needed)
2	7.01559	7.66342
3	10.17347	10.84730
4	13.32369	14.01385
5	16.47063	17.17223
6	19.61586	20.32604
7	22.76008	23.47698
8	25.90367	26.62601
9	29.04683	29.77367
10	32.18968	32.92034

TABLE 1. The first ten exponential coefficients in (5.17)

For $j = 2$ the coefficients $\nu_{(2)kl}$ and $i_{(2)knm}$ are defined similarly as in (5.12), with all the right-hand sides multiplied by -1, and subscript (1) and coefficients C replaced by subscript (2) and coefficients D respectively.

Expressions (5.11) can be further simplified because of the following property of σ_n. Large zeroes σ_n of $J_1(\sigma_n) = 0$ are given asymptotically (Abramowitz & Stegun 1970) as

$$\sigma_n \approx (n+\tfrac{1}{4})\,\pi, \tag{5.13}$$

which implies that for large n

$$\sigma_n - \sigma_{n-1} = \pi, \tag{5.14}$$

and that given a positive increasing sequence m, n, r, s such that $m+s = n+r$ then

$$\sigma_m + \sigma_s \simeq \sigma_n + \sigma_r. \tag{5.15}$$

The asymptotic property (5.15) gives rise to a further approximation of the double summation in (5.11). We define

$$\check{\sigma}_n = \frac{1}{n-1}\sum_{k=1}^{n-1}(\sigma_k+\sigma_{n-k}) \quad (n \geqslant 2). \tag{5.16}$$

The first ten values of σ_n and nine values of $\check{\sigma}_n$ are displayed in table 1.

It now follows that (5.11) may be approximated by:

$$f_{(j)}(R,Z) = \lim_{N\to\infty}\sum_{n=1}^{N} f_{(j)n}(R)\exp\left[(-1)^j\sigma_n\frac{Z}{a}\right] + \lim_{M\to\infty}\sum_{m=2}^{M}\check{f}_{(j)m}(R)\exp\left[(-1)^j\check{\sigma}_m\frac{Z}{a}\right], \tag{5.17a}$$

where

$$f_{(j)n}(R) \equiv \left[\nu_{(j)1n}J_1(\mathrm{i}\mathbb{A}_{(j)}R)J_1\left(\sigma_n\frac{R}{a}\right) + \nu_{(j)2n}RJ_2(\mathrm{i}\mathbb{A}_{(j)}R)J_1\left(\sigma_n\frac{R}{a}\right) + \nu_{(j)3n}J_2(\mathrm{i}\mathbb{A}_{(j)}R)J_2\left(\sigma_n\frac{R}{a}\right) + \text{conjugate}\right], \tag{5.17b}$$

$$\check{f}_{(j)m}(R) \equiv \sum_{k=1}^{m-1} f_{(j)kl}(R), \quad \text{with} \quad l = m-k, \quad m \geqslant 2, \tag{5.17c}$$

and

$$f_{(j)kl}(R) \equiv \left[i_{(j)1kl} J_1\left(\sigma_k \frac{R}{a}\right) J_1\left(\sigma_l \frac{R}{a}\right) + i_{(j)2kl} R J_1\left(\sigma_k \frac{R}{a}\right) J_2\left(\sigma_l \frac{R}{a}\right) + i_{(j)3kl} J_2\left(\sigma_k \frac{R}{a}\right) J_2\left(\sigma_l \frac{R}{a}\right) + \text{conjugate} \right]. \quad (5.17d)$$

The second single summation in (5.17*a*) is the approximation of the double summation in (5.11). The motivation for this approximation is the property (5.15), the application of which is to replace all $\exp[-(\sigma_k+\sigma_l)Z/a]$ of every k, l such that $k+l=m$, by $\mathrm{e}^{-\check{\sigma}_m Z/a}$, where the exponents $-\check{\sigma}_m$ are defined in (5.16). We then group all the functions $f_{(j)kl}(R)$ which are to be multiplied by $\mathrm{e}^{-\check{\sigma}_m Z/a}$, to form new functions $\check{f}_{(j)m}(R)$ as defined by (5.17*b–d*). This type of reduction not only renders the presentations of the $f_{(j)}(R,Z)$ simple, but also reduces the computational time and storage requirements in computations that involve these functions.

Using (5.17*a*) in (5.2*a*), we find that $\psi_{\mathrm{P}(j)}$, which is a particular solution of (5.2*a–f*) (see Tieu 1983), is given by

$$\psi_{\mathrm{P}(j)}(R,Z) = (\tfrac{1}{2}\pi)^2 R \left[\lim_{N\to\infty} \sum_{n=1}^{N} \left\{ \exp\left[(-1)^j \sigma_n \frac{Z}{a} \right] \right\} \int_0^a G_n(R,\xi)\, \mathscr{H}_{(j)n}(\xi)\, \mathrm{d}\xi + \lim_{M\to\infty} \sum_{m=2}^{M} \left\{ \exp\left[(-1)^j \check{\sigma}_m \frac{Z}{a} \right] \right\} \int_0^a \check{G}_m(R,\xi)\, \check{\mathscr{H}}_{(j)m}(\xi)\, \mathrm{d}\xi \right], \quad (5.18)$$

where

$$G_n(R,\xi) \equiv \begin{cases} Y_1\left(\sigma_n \frac{R}{a}\right) J_1\left(\sigma_n \frac{\xi}{a}\right) & (\xi \leqslant R), \\ J_1\left(\sigma_n \frac{R}{a}\right) Y_1\left(\sigma_n \frac{\xi}{a}\right) & (\xi \geqslant R), \end{cases} \quad (5.19a)$$

$$\mathscr{H}_{(j)n}(\xi) \equiv \xi \left[F_{(j)n}(\xi) - Q_{(j)n} J_1\left(\sigma_n \frac{\xi}{a}\right) \right], \quad (5.19b)$$

$$F_{(j)n}(\xi) \equiv \int_0^a G_n(\xi,\zeta) f_{(j)n}(\zeta)\, \mathrm{d}\zeta, \quad (5.19c)$$

$$Q_{(j)n} \equiv \frac{\int_0^a \xi J_1\left(\sigma_n \frac{\xi}{a}\right) F_{(j)n}(\xi)\, \mathrm{d}\xi}{\int_0^a \xi J_1\left(\sigma_n \frac{\xi}{a}\right)^2 \mathrm{d}\xi}, \quad (5.19d)$$

and $\check{G}_m(R,\xi)$, $\check{\mathscr{H}}_{(j)m}(\xi)$, $\check{F}_{(j)m}(\xi)$, $\check{Q}_{(j)m}$, with $m \geqslant 2$, are defined exactly as their counterparts (5.19*a–d*), with $\check{\sigma}_m, \check{f}_{(j)m}(R)$ replacing $\sigma_n, f_{(j)n}(R)$ respectively.

5.1.2. *Determination of the homogeneous solutions*

The homogeneous parts $\psi_{\mathrm{H}(j)}$ can be expressed by biorthogonal series (Yoo & Joseph 1978):

$$\left.\begin{aligned} \psi_{\mathrm{H}(1)}(R,Z) &= \sum_{-\infty}^{\infty} A_n\, \mathrm{e}^{-p_n Z/a} \frac{a^2}{p_n^2} \phi_1^{(n)}(R), \\ \psi_{\mathrm{H}(2)}(R,Z) &= \sum_{-\infty}^{\infty} B_n\, \mathrm{e}^{p_n Z/a} \frac{a^2}{p_n^2} \phi_1^{(n)}(R), \end{aligned}\right\} \quad (5.20)$$

where $\mathrm{Re}\{p_n\} \geqslant 0$. The eigenfunction $\phi_1^{(n)}(R)$ must satisfy the differential equation

$$\mathrm{L}_n^2 \phi_1^{(n)} \equiv \left[\frac{\mathrm{d}^2}{\mathrm{d}R^2} - \frac{1}{R}\frac{\mathrm{d}}{\mathrm{d}R} + \left(\frac{p_n}{a}\right)^2 \right]^2 \phi_1^{(n)} = 0. \quad (5.21)$$

The general form of $\phi_1^{(n)}$ is therefore given by

$$\phi_1^{(n)} = e_1 R J_1\left(p_n \frac{R}{a}\right) + e_2 R Y_1\left(p_n \frac{R}{a}\right) + e_3 R^2 J_0\left(p_n \frac{R}{a}\right) + e_4 R^2 Y_0\left(p_n \frac{R}{a}\right). \tag{5.22}$$

The coefficients of $e_l, l = 1, \ldots, 4$, are determined by the boundary conditions (5.2b,c) at $R = a$ and $R = 0$. The boundary conditions at $R = 0$ require that

$$\lim_{R\to 0}\left(\frac{\phi_1^{(n)}}{R}\right) \quad \text{and} \quad \lim_{R\to 0}\left(\frac{\phi_{1,R}^{(n)}}{R}\right) \quad \text{remain finite.} \tag{5.23a}$$

Hence

$$e_2 = e_4 = 0. \tag{5.23b}$$

The sidewall boundary conditions (5.2b,c) are fulfilled if

$$\phi_1^{(n)}(a) = \phi_{1,R}^{(n)}(a) = 0. \tag{5.24}$$

Using (5.22) and (5.23b) in (5.24), we get

$$\begin{aligned} e_1 a J_1(p_n) + e_3 a^2 J_0(p_n) &= 0, \\ e_1 p_n J_0(p_n) + e_3[2a J_0(p_n) - p_n a J_1(p_n)] &= 0. \end{aligned} \tag{5.25}$$

The determinant of (5.25) must therefore vanish:

$$p_n J_1^2(p_n) - 2J_1(p_n) J_0(p_n) + p_n J_0^2(p_n) = 0. \tag{5.26}$$

Each root p_n of (5.26) is an eigenvalue, corresponding to the eigenfunction

$$\phi_1^{(n)} = R J_1\left(p_n \frac{R}{a}\right) - \frac{J_1(p_n)}{a J_0(p_n)} R^2 J_0\left(p_n \frac{R}{a}\right). \tag{5.27}$$

The expression (5.27) may be derived from (5.22) using (5.23b), and (5.25a) to eliminate e_3. We have absorbed the unknown constant e_1 into the A_n and B_n.

Eigenfunctions of the form (5.22) have been used in the study of Stokes' flow between concentric cylinders (Yoo 1977). In the limiting case in which the inner cylinder shrinks to zero, the equation (5.26) and eigenfunctions (5.27) are recovered. The eigenfunctions $\phi_1^{(n)}$ have also been used in the study of 'die swell' of Newtonian fluids (Trogdon & Joseph 1980).

The eigenvalues p_n, satisfying (5.26), are symmetrically located in a complex plane, and numbered in increasing order of magnitude. The p_n used in (5.20) are the roots that lie in the right-half complex plane. Let p_n be the roots of (5.26) that lie in the first quadrant of the complex plane, and define

$$p_{-n} \equiv \bar{p}_n. \tag{5.28}$$

Since the edge data (5.4a–c) at $Z = 0$ are real, we have

$$A_{-n} \equiv \bar{A}_n, \quad B_{-n} \equiv \bar{B}_n. \tag{5.29}$$

We note that the zero eigenvalue p_0 is not in the spectrum.

A biorthogonal property for the eigenfunction can be derived as follows. We define

$$\phi_2^{(n)} \equiv \frac{a^2}{p_n^2} R \frac{\mathrm{d}}{\mathrm{d}R}\left[\frac{1}{R}\frac{\mathrm{d}}{\mathrm{d}R}\phi_1^{(n)}\right], \tag{5.30}$$

and

$$\boldsymbol{\phi}^{(n)} \equiv \begin{bmatrix} \phi_1^{(n)} \\ \phi_2^{(n)} \end{bmatrix}. \tag{5.31}$$

Using the definitions (5.30) and (5.31), (5.21) can be rewritten as

$$R\frac{\mathrm{d}}{\mathrm{d}R}\left[\frac{1}{R}\frac{\mathrm{d}}{\mathrm{d}R}\boldsymbol{\phi}^{(n)}\right]+\frac{p_n^2}{a^2}\boldsymbol{A}\cdot\boldsymbol{\phi}^{(n)}=\mathbf{0}, \tag{5.32}$$

where

$$\boldsymbol{A}=\begin{bmatrix}0 & -1\\ 1 & 2\end{bmatrix}.$$

The problem adjoint to (5.32), (5.23a) and (5.24) is defined by

$$\left.\begin{aligned}&\boldsymbol{\psi}^{(n)}(R)=[\psi_1^{(n)}(R),\psi_2^{(n)}(R)],\\ &R\frac{\mathrm{d}}{\mathrm{d}R}\left[\frac{1}{R}\frac{\mathrm{d}}{\mathrm{d}R}\boldsymbol{\psi}^{(n)}\right]+\frac{p_n^2}{a^2}\boldsymbol{\psi}^{(n)}\cdot\boldsymbol{A}=\mathbf{0},\end{aligned}\right\} \tag{5.33}$$

and associated boundary conditions

$$\psi_2^{(n)}(a)=\frac{\mathrm{d}}{\mathrm{d}R}\psi_2^{(n)}(a)=0, \tag{5.34}$$

$$\lim_{R\to 0}\frac{\psi_2^{(n)}}{R}\quad\text{and}\quad\lim_{R\to 0}\frac{1}{R}\frac{\mathrm{d}}{\mathrm{d}R}\psi_2^{(n)}\quad\text{are finite.} \tag{5.35}$$

The functions $\psi_2^{(n)}$ and $\phi_1^{(n)}$ satisfy the same differential equation (5.21) and boundary conditions (5.23a) and (5.24), hence we may take

$$\psi_2^{(n)}=\phi_1^{(n)}. \tag{5.36}$$

Using (5.32), (5.33) and associated boundary conditions, it is possible to show that

$$\int_0^a\frac{1}{R}\boldsymbol{\psi}^{(m)}\cdot\boldsymbol{A}\cdot\boldsymbol{\phi}^{(n)}\,\mathrm{d}R=\delta_{mn}K_n, \tag{5.37}$$

where δ_{mn} is a Kronecker delta:

$$\delta_{mn}=\begin{cases}0 & (m\neq n),\\ 1 & (m=n).\end{cases}$$

Computations (see Tieu 1983) yield

$$K_n=-\frac{2a^2J_1^4(p_n)}{p_n^2J_0^2(p_n)}. \tag{5.38}$$

We also introduce the product

$$\gamma_{ln}=\int_0^a\frac{1}{R}\psi_2^{(l)}\phi_1^{(n)}\,\mathrm{d}R=\int_0^a\frac{1}{R}\phi_1^{(l)}\phi_1^{(n)}\,\mathrm{d}R, \tag{5.39a}$$

and find that

$$\gamma_{ln}=\gamma_{nl}=\frac{8a^2p_np_l}{(p_l^2-p_n^2)^3}\left\{p_l\frac{J_1(p_n)}{J_0(p_n)}-p_n\frac{J_1(p_l)}{J_0(p_l)}\right\}J_1(p_n)J_1(p_l), \tag{5.39b}$$

$$\gamma_{ll}=\int_0^a\frac{1}{R}\phi_1^{(l)2}\,\mathrm{d}R=-\frac{a^2}{3p_l}\frac{J_1(p_l)^3}{J_0(p_l)}\left(1+\frac{1}{p_l}\frac{J_1(p_l)}{J_0(p_l)}\right). \tag{5.39c}$$

The coefficients A_n and B_n in (5.20) can be next determined as follows. Substituting (5.20) into boundary conditions (5.4*a–c*), we get

$$\sum_{-\infty}^{\infty} (\mu_{(2)} B_n - \mu_{(1)} A_n)\, \phi_1^{(n)} = -[\![\mu \psi_{\mathrm{P},ZZ}(R,0)]\!] + 2R\,[\![\mathring{\boldsymbol{S}}_{2RZ}[\boldsymbol{U}_1]]\!], \tag{5.40}$$

$$\sum_{-\infty}^{\infty} (B_n + A_n) \frac{a}{p_n} \phi_1^{(n)} = -[\![\psi_{\mathrm{P},Z}(R,0)]\!], \tag{5.41}$$

$$\sum_{-\infty}^{\infty} A_n \frac{a^2}{{p_n}^2} \phi_1^{(n)} = -\psi_{\mathrm{P}(1)}(R,0), \tag{5.42}$$

and

$$\sum_{-\infty}^{\infty} B_n \frac{a^2}{p_n^2} \phi_1^{(n)} = -\psi_{\mathrm{P}(2)}(R,0), \tag{5.43}$$

where $\psi_{\mathrm{P}(j)}$ and $\mathring{\boldsymbol{S}}_{2RZ}[\boldsymbol{U}_{(j)1}]$ are given by (5.18) and (4.13*b*) respectively. Addition of (5.42) and (5.43) yields

$$\sum_{-\infty}^{\infty} (B_n + A_n) \frac{a^2}{p_n^2} \phi_1^{(n)} = -(\psi_{\mathrm{P}(1)}(R,0) + \psi_{\mathrm{P}(2)}(R,0)). \tag{5.44}$$

Multiplying (4.42) by $-\mu_{(1)}$, and (4.43) by $\mu_{(2)}$, then adding the resulting equations together we get

$$\sum_{-\infty}^{\infty} (\mu_{(2)} B_n - \mu_{(1)} A_n) \frac{a^2}{p_n^2} \phi_1^{(n)} = -[\![\mu \psi_{\mathrm{P}}(R,0)]\!]. \tag{5.45}$$

We define the following differential operator:

$$\Gamma(\cdot) \equiv R \frac{\mathrm{d}}{\mathrm{d}R}\left(\frac{1}{R}\frac{\mathrm{d}}{\mathrm{d}R}\right)(\cdot) \equiv (\cdot)^{\bigstar}.$$

Applying Γ to (5.44) and (5.45), we find

$$\sum_{-\infty}^{\infty} (B_n + A_n)\, \phi_2^{(n)} = -(\psi^{\bigstar}_{\mathrm{P}(1)}(R,0) + \psi^{\bigstar}_{\mathrm{P}(2)}(R,0)), \tag{5.46}$$

and

$$\sum_{-\infty}^{\infty} (\mu_{(2)} B_n - \mu_{(1)} A_n)\, \phi_2^{(n)} = -[\![\mu \psi_{\mathrm{P}}(R,0)^{\bigstar}]\!]. \tag{5.47}$$

Combining (5.40) with (5.47), and (5.41) with (5.46), one gets

$$\sum_{-\infty}^{\infty} (\mu_{(2)} B_n - \mu_{(1)} A_n)\, \boldsymbol{\phi}^{(n)} = \boldsymbol{y}, \tag{5.48a}$$

and

$$\sum_{-\infty}^{\infty} (B_n + A_n)\, \boldsymbol{\phi}^{(n)} + \sum_{-\infty}^{\infty} (B_n + A_n) \begin{pmatrix} a - p_n \\ \hline p_n \end{pmatrix} \begin{bmatrix} \phi_1^{(n)} \\ 0 \end{bmatrix} = \tilde{\boldsymbol{Y}}, \tag{5.48b}$$

where:

$$\boldsymbol{y} = \begin{bmatrix} y_1 \\ y_2 \end{bmatrix} = \begin{bmatrix} -[\![\mu \psi_{\mathrm{P},ZZ}]\!] + 2R[\![\mathring{\boldsymbol{S}}_{2RZ}[\boldsymbol{U}_1]]\!] \\ -[\![\mu \psi^{\bigstar}_{\mathrm{P}}(R,0)]\!] \end{bmatrix}, \tag{5.49a}$$

and

$$\tilde{\boldsymbol{Y}} = \begin{bmatrix} \tilde{Y}_1 \\ \tilde{Y}_2 \end{bmatrix} = \begin{bmatrix} -[\![\psi_{\mathrm{P},Z}]\!] \\ -(\psi^{\bigstar}_{\mathrm{P}(1)} + \psi^{\bigstar}_{\mathrm{P}(2)}) \end{bmatrix}. \tag{5.49b}$$

Expressions for the components y_1, y_2, $\tilde{Y}_1$ and $\tilde{Y}_2$ are listed in the Appendix.

If we put

$$\mu_{(2)}B_n-\mu_{(1)}A_n=a_n,\quad B_n+A_n=b_n, \tag{5.50}$$

then the inverse of (5.50) is given by

$$B_n=\frac{a_n+\mu_{(1)}b_n}{\mu_{(2)}+\mu_{(1)}},\quad A_n=\frac{-a_n+\mu_{(2)}b_n}{\mu_{(2)}+\mu_{(1)}}. \tag{5.51}$$

Equations (5.48a,b) can be rewritten as

$$\lim_{N\to\infty}\sum_{-N}^{N}a_n\boldsymbol{\phi}^{(n)}=\boldsymbol{y} \tag{5.52a}$$

and

$$\lim_{N\to\infty}\sum_{-N}^{N}\left\{b_n\boldsymbol{\phi}^{(n)}+b_n\frac{a-p_n}{p_n}\begin{bmatrix}\phi_1^{(n)}\\0\end{bmatrix}\right\}=\boldsymbol{\Upsilon}. \tag{5.52b}$$

Premultiplying (5.52a,b) by $R^{-1}\boldsymbol{\psi}^{(l)}\cdot\boldsymbol{A}$ and integrating from 0 to a, we get

$$a_l k_l=\int_0^a\frac{1}{R}\boldsymbol{\psi}^{(l)}\cdot\boldsymbol{A}\cdot\boldsymbol{y}\,\mathrm{d}R, \tag{5.53a}$$

$$b_l k_l+\sum_{\substack{(n)\\-\infty}}^{\infty}b_n\frac{a-p_n}{p_n}\gamma_{ln}=\int_0^a\frac{1}{R}\boldsymbol{\psi}^{(l)}\cdot\boldsymbol{A}\cdot\boldsymbol{\Upsilon}\mathrm{d}R. \tag{5.53b}$$

Equation (5.53a) in turn yields

$$a_l=\frac{1}{k_l}\int_0^a\frac{1}{R}\boldsymbol{\psi}^{(l)}\cdot\boldsymbol{A}\cdot\boldsymbol{y}\,\mathrm{d}R; \tag{5.54}$$

and (5.53b) leads us to an infinite system of linear algebraic equations in b_n. We solve the system by truncation (Kantorovich & Krylov 1958). Once a_n and b_n are known, the coefficients A_n and B_n are determined by (5.51).

We finally note that, since the solution $\psi_{\mathrm{P}(j)}$, given by (5.18), and $\psi_{\mathrm{P}(j),R}$ vanish at $R=0$ and $R=a$, the first components in (5.49a,b) satisfy

$$Y_1=Y_{1,R}=0\quad\text{at}\quad R=0\quad\text{and}\quad R=a,$$

$$y_1=y_{1,R}=0\quad\text{at } R=0,$$

$$y_1=0\quad\text{and}\quad y_{1,R}=2a^3[\![|\omega_{,R}|^2{}_{,Z}\,\Sigma_1]\!]\quad\text{at } R=a.$$

It then follows from earlier work of Joseph (1977) that the expansion series in terms of $\boldsymbol{\phi}^{(n)}$ for $\boldsymbol{\Upsilon}$ in the right-hand side of (5.53b) converges uniformly and absolutely for $R\in[0,a]$. And the expansion series for $\boldsymbol{y}$ in (5.53a) converges absolutely.

The stream functions $\psi_{(j)}(R,Z)$ have thus been derived in the form

$$\begin{aligned}\psi_{(j)}(R,Z)=&\sum_{-\infty}^{\infty}E_n\left\{\exp\left[(-1)^j p_n\frac{Z}{a}\right]\right\}\frac{a^2}{p_n^2}\phi_1^{(n)}(R)\\&+\left(\frac{\pi}{2}\right)^2 R\left[\sum_{n=1}^{\infty}\left\{\exp\left[(-1)^j\sigma_n\frac{Z}{a}\right]\right\}\int_0^a G_n(R,\xi)\,\mathscr{H}_{(j)n}(\xi)\,\mathrm{d}\xi\right.\\&\left.+\sum_{m=2}^{\infty}\left\{\exp\left[(-1)^j\check{\sigma}_m\frac{Z}{a}\right]\right\}\int_0^a\check{G}_m(R,\xi)\,\mathscr{H}_{(j)m}(\xi)\,\mathrm{d}\xi\right],\end{aligned} \tag{5.55a}$$

where

$$E_n=\begin{cases}A_n & (j=1),\\ B_n & (j=2).\end{cases} \tag{5.55b}$$

The foregoing expression for $\psi_{(j)}(R, Z)$ is based on approximations of the type (5.9). The problem can be solved without these approximations but the formulas are much bigger.

5.2. *The mean pressure*

The mean components of the vector equation (4.15a) are

$$e_Z\colon \quad \frac{\partial \bar{\bar{\Phi}}}{\partial Z} - \mu \nabla^2 \bar{\bar{u}} = 2\Sigma_1 r_4, \tag{5.56a}$$

$$e_R\colon \quad \frac{\partial \bar{\bar{\Phi}}}{\partial R} - \mu\left(\nabla^2 \bar{\bar{w}} - \frac{\bar{\bar{w}}}{R^2}\right) = 2(-\eta_1 r_1 + \not{\eta} r_3 + \rho r_5). \tag{5.56b}$$

For an arbitrary function $f(R, Z)$, we define the following decomposition

$$f(R, Z) = \mathbb{E}\mathrm{x}(f(R, Z)) + \mathbb{N}\mathbb{E}\mathrm{x}(f(R, Z)),$$

where $\mathbb{E}\mathrm{x}\,(f(R, Z)) \equiv$ part of $f(R, Z)$ that depends on Z, so that

$$\partial f/\partial Z = (\partial/\partial Z)\,\mathbb{E}\mathrm{x}\,(f(R, Z));$$

and $\mathbb{N}\mathbb{E}\mathrm{x}(f(R, Z)) \equiv$ part of $f(R, Z)$ that is independent of Z, so that

$$(\partial/\partial Z)\,[\mathbb{E}\mathrm{x}(f(R, Z))] = 0.$$

In this problem, Z-dependent parts $\mathbb{E}\mathrm{x}\,(\cdot)$ decay exponentially with Z. Examining the expressions for r_1, r_3, r_4 and r_5 in (4.7), we observe the following:

$$\mu \nabla^2 \bar{\bar{u}} + 2\Sigma_1 r_4 = \mathbb{E}\mathrm{x}\,(\mu \nabla^2 \bar{\bar{u}}_2 + 2\Sigma_1 r_4), \tag{5.57a}$$

$$\mu\left(\nabla^2 \bar{\bar{w}} - \frac{\bar{\bar{w}}}{R^2}\right) + 2(-\eta_1 r_1 + \not{\eta} r_3 + \rho r_5)$$
$$= 2\mathbb{N}\mathbb{E}\mathrm{x}\,(-\eta_1 r_1 + \not{\eta} r_3 + \rho r_5) + \mathbb{E}\mathrm{x}\left(\mu\left(\nabla^2 \bar{\bar{w}} - \frac{\bar{\bar{w}}}{R^2}\right) + 2(-\eta_1 r_1 + \not{\eta} r_3 + \rho r_5)\right). \tag{5.57b}$$

Let

$$\bar{\bar{\Phi}}^{(1)}_{(j)}(R) = \mathbb{N}\mathbb{E}\mathrm{x}\,(\bar{\bar{\Phi}}_{(j)}), \tag{5.58a}$$

and

$$\bar{\bar{\Phi}}^{(2)}_{(j)}(R, Z) = \mathbb{E}\mathrm{x}(\bar{\bar{\Phi}}_{(j)}), \tag{5.58b}$$

then

$$\bar{\bar{\Phi}}_{(j)}(R, Z) = \bar{\bar{\Phi}}^{(1)}_{(j)}(R) + \bar{\bar{\Phi}}^{(2)}_{(j)}(R, Z). \tag{5.58c}$$

Using (5.58) and (5.57) in (5.56), we get

$$\bar{\bar{\Phi}}^{(2)}(R, Z) = \mathbb{E}\mathrm{x}\left[\int^Z (\mu \nabla^2 \bar{\bar{u}} + 2\Sigma_1 r_4)\,\mathrm{d}Z\right] \tag{5.59a}$$

and

$$\bar{\bar{\Phi}}^{(1)}(R, Z) = 2\mathbb{N}\mathbb{E}\mathrm{x}\left[\int_0^R (-\eta_1 r_1 + \not{\eta} r_3 + \rho r_5)\,\mathrm{d}R\right] + \text{constant } p. \tag{5.59b}$$

Integrating r_4 with respect to Z, we find that

$$\int^Z r_4 \mathrm{d}Z = 2R^2 |\omega^*_{,Z}|^2 + \int^Z \frac{1}{R}[R^3(\omega^*_{,R}\,\bar{\omega}^*_{,Z} + \bar{\omega}^*_{,R}\omega^*_{,Z})]_{,R}\,\mathrm{d}Z$$
$$= R^2\left(|\omega^*_{,Z}|^2 + |\omega^*_{,R}|^2 + \int^Z (A^2\omega^*\bar{\omega}^*_{,Z} + \bar{A}^2\bar{\omega}^*\omega^*_{,Z})\,\mathrm{d}Z\right),$$

where the second equality has been derived using (5.5*b*). It then follows that

$$\mathbb{E}\mathrm{x}\left[\int^{Z} r_4\,\mathrm{d}Z\right] = R^2\left\{\mathbb{E}\mathrm{x}\left[|\omega^*_{,R}|^2 + \int^{Z} (\mathbb{A}^2\omega^*\bar{\omega}^*_{,Z} + \bar{\mathbb{A}}^2\bar{\omega}^*\omega^*_{,Z})\,dZ\right] + |\omega^*_{,Z}|^2\right\}.$$

Substitution of first-order results into the preceding equation yields:

$$\begin{aligned}\mathbb{E}\mathrm{x}\left[\int^{Z} r_{(1)4}\,\mathrm{d}Z\right] = \sum_{n=1}^{\infty}\Bigg(&\frac{a\mathbb{A}_{(1)}}{2J_1(\mathrm{i}\mathbb{A}_{(1)}a)}\bar{C}_n\,e^{\bar{\beta}_{(1)n}Z}\left[\frac{\sigma_n}{a}J_2(\mathrm{i}\mathbb{A}_{(1)}R)\,J_2\left(\sigma_n\frac{R}{a}\right)\right.\\ &\left.-\mathrm{i}\mathbb{A}_{(1)}J_1(\mathrm{i}\mathbb{A}_{(1)}R)\,J_1\left(\sigma_n\frac{R}{a}\right)\right]+\text{conjugate}\Bigg)\\ &+\sum_{n=1}^{\infty}\sum_{m=1}^{\infty}\bar{C}_n C_m\,\mathrm{e}^{(\bar{\beta}_{(1)n}+\beta_{(1)m})Z}\left[\frac{\sigma_n\sigma_m}{a^2}J_2\left(\sigma_n\frac{R}{a}\right)J_2\left(\sigma_m\frac{R}{a}\right)\right.\\ &\left.+\left(\bar{\beta}_{(1)n}\beta_{(1)m}+\frac{\mathbb{A}^2_{(1)}\bar{\beta}_{(1)n}+\bar{\mathbb{A}}^2_{(1)}\beta_{(1)m}}{\bar{\beta}_{(1)n}+\beta_{(1)m}}\right)J_1\left(\sigma_n\frac{R}{a}\right)J_1\left(\sigma_m\frac{R}{a}\right)\right].\end{aligned}\tag{5.60}$$

The right-hand side of (5.60) can be simplified by approximations of the type (5.9) and (5.10). We denote

$$\begin{aligned}\gamma_{(1)n}(R) \equiv \Bigg(&\frac{a\mathbb{A}_{(1)}\bar{C}_n}{2J_1(\mathrm{i}\mathbb{A}_{(1)}a)}\left[\frac{\sigma_n}{a}J_2(\mathrm{i}\mathbb{A}_{(1)}R)\,J_2\left(\sigma_n\frac{R}{a}\right)\right.\\ &\left.-\mathrm{i}\mathbb{A}_{(1)}J_1(\mathrm{i}\mathbb{A}_{(1)}R)\,J_1\left(\sigma_n\frac{R}{a}\right)\right]+\text{conjugate}\Bigg),\end{aligned}\tag{5.61a}$$

$$\begin{aligned}\gamma_{(1)nm}(R) \equiv \bar{C}_n C_m\Bigg[&\frac{\sigma_n\sigma_m}{a^2}J_2\left(\sigma_n\frac{R}{a}\right)J_2\left(\sigma_m\frac{R}{a}\right)\\ &+\left(\frac{\sigma_n\sigma_m}{a^2}+\frac{\mathbb{A}^2_{(1)}\sigma_n+\bar{\mathbb{A}}^2_{(1)}\sigma_m}{\sigma_n+\sigma_m}\right)J_1\left(\sigma_n\frac{R}{a}\right)J_1\left(\sigma_m\frac{R}{a}\right)\Bigg]\end{aligned}\tag{5.61b}$$

and

$$\check{\gamma}_{(1)n}(R) \equiv \sum_{k=1}^{n-1}\gamma_{(1)k(n-k)} \quad (n \geqslant 2).\tag{5.61c}$$

$\gamma_{(2)n}$, $\gamma_{(2)nm}$, $\check{\gamma}_{(2)n}$ are defined exactly as in (5.16) with subscript (1) and coefficients C replaced by subscript (2) and coefficients D. The approximated version of (5.60) is of the form

$$\mathbb{E}\mathrm{x}\left[\int^{Z} r_{(j)4}\,\mathrm{d}z\right] = \sum_{n=1}^{\infty}\gamma_{(j)n}(R)\exp\left[(-1)^j\sigma_n\frac{Z}{a}\right] + \sum_{n=2}^{\infty}\check{\gamma}_{(j)n}(R)\exp\left[(-1)^j\check{\sigma}_n\frac{Z}{a}\right].\tag{5.62}$$

Since

$$\bar{\bar{u}}_{(j)} = \frac{1}{R}\frac{\partial}{\partial R}\psi_{(j)}$$

we have

$$\mathbb{E}\mathrm{x}\left[\int^{Z}\nabla^2\bar{\bar{u}}_{(j)}\,\mathrm{d}Z\right] = \int^{Z}\frac{1}{R}\frac{\partial}{\partial R}(\nabla^2\psi_{(j)})\,\mathrm{d}z.\tag{5.63}$$

Substituting (5.55) into the right-hand side of (5.63), and carrying out necessary differentiations and integrations, we get

$$\begin{aligned}\mathbb{E}\mathrm{x}\left[\int^{Z}\nabla^2\bar{\bar{u}}_{(j)}\,\mathrm{d}Z\right] = (-1)^j\Bigg\{&2\sum_{-\infty}^{\infty}\frac{a}{p_n}E_n\phi_3^{(n)}\exp\left[(-1)^j p_n\frac{Z}{a}\right]\\&+\sum_{n=1}^{\infty}\left\{\exp\left[(-1)^j\sigma_n\frac{Z}{a}\right]\right\}\frac{\pi}{2\sigma_n}\frac{a}{R}\Bigg[-\left(\frac{\sigma_n}{a}\right)^2\pi\int_0^a G_n(R,\xi)\,\mathscr{H}_{(j)n}(\xi)\,\mathrm{d}\xi\\&+\int_0^a\mathscr{P}_n(R,\xi)f_{(j)n}(\xi)\,\mathrm{d}\xi-Q_{(j)n}\,\mathscr{S}_n(R)\Bigg]\\&+\sum_{m=2}^{\infty}\left\{\exp\left[(-1)^j\check{\sigma}_m\frac{Z}{a}\right]\right\}\frac{\pi}{2\check{\sigma}_m}\frac{a}{R}\Bigg[-\left(\frac{\check{\sigma}_m}{a}\right)^2\pi\int_0^a\check{G}_m(R,\xi)\,\mathscr{H}_{(j)m}(\xi)\,\mathrm{d}\xi\\&+\int_0^a\check{\mathscr{P}}_m(R,\xi)\check{f}_{(j)m}(\xi)\,\mathrm{d}\xi-\check{Q}_{(j)m}\,\check{\mathscr{S}}_m(R)\Bigg]\Bigg\},\end{aligned}\tag{5.64}$$

where

$$\phi_3^{(n)}(R)\equiv 2\frac{J_1(p_n)}{aJ_0(p_n)}J_0\left(p_n\frac{R}{a}\right)-\left(1-2\frac{J_1(p_n)}{p_nJ_0(p_n)}\right)\frac{1}{R}J_1\left(p_n\frac{R}{a}\right),\tag{5.65a}$$

$$\mathscr{S}_n(R)\equiv\sigma_n\frac{R}{a}J_0\left(\sigma_n\frac{R}{a}\right)+2J_1\left(\sigma_n\frac{R}{a}\right),\tag{5.65b}$$

$$\mathscr{P}_n(R,\xi)\equiv\begin{cases}\left[\sigma_n\dfrac{R}{a}Y_0\left(\sigma_n\dfrac{R}{a}\right)+2Y_1\left(\sigma_n\dfrac{R}{a}\right)\right]J_1\left(\sigma_n\dfrac{\xi}{a}\right) & (\xi\leqslant R),\\[2ex]\left[\sigma_n\dfrac{R}{a}J_0\left(\sigma_n\dfrac{R}{a}\right)+2J_1\left(\sigma_n\dfrac{R}{a}\right)\right]Y_1\left(\sigma_n\dfrac{\xi}{a}\right) & (\xi\geqslant R),\end{cases}\tag{5.65c}$$

and $\check{\mathscr{S}}_n(R)$, $\check{\mathscr{P}}_m(R,\xi)$, with $m\geqslant 2$, are defined similarly as in (5.65b,c) with $\check{\sigma}_m$ replacing σ_n. We also recall that $G_n(R,\xi)$, $\mathscr{H}_{(j)n}(\xi)$, $Q_{(j)n}$ and their counterparts with symbol ($\check{\ }$) are defined in (5.19a–d).

We then substitute (5.62) and (5.64) into (5.59a) to obtain an explicit expression for $\bar{\bar{\Phi}}_{(j)}^{(2)}(R,Z)$:

$$\begin{aligned}\bar{\bar{\Phi}}_{(j)}^{(2)}(R,Z) = (-1)^j\Bigg\{&2\mu_{(j)}\sum_{-\infty}^{\infty}\frac{a}{p_n}E_n\phi_3^{(n)}\exp\left[(-1)^j p_n\frac{Z}{a}\right]\\&+\sum_{n=1}^{\infty}\left\{\exp\left[(-1)^j\sigma_n\frac{Z}{a}\right]\right\}\Bigg\langle\frac{\pi}{2\sigma_n}\frac{a}{R}\mu_{(j)}\Bigg[-\left(\frac{\sigma_n}{a}\right)^2\pi\int_0^a G_n(R,\xi)\,\mathscr{H}_{(j)n}(\xi)\,\mathrm{d}\xi\\&+\int_0^a\mathscr{P}_n(R,\xi)f_{(j)n}(\xi)\,\mathrm{d}\xi-Q_{(j)n}\,\mathscr{S}_n(R)\Bigg]+(-1)^j 2\Sigma_{(j)1}\gamma_{(j)n}(R)\Bigg\rangle\\&+\sum_{n=2}^{\infty}\left\{\exp\left[(-1)^j\check{\sigma}_n\frac{Z}{a}\right]\right\}\Bigg\langle\frac{\pi}{2\check{\sigma}_n}\frac{a}{R}\mu_{(j)}\Bigg[-\left(\frac{\check{\sigma}_n}{a}\right)^2\pi\int_0^a\check{G}_n(R,\xi)\,\mathscr{H}_{(j)n}(\xi)\,\mathrm{d}\xi\\&+\int_0^a\check{\mathscr{P}}_n(R,\xi)\check{f}_{(j)n}(\xi)\,\mathrm{d}\xi-\check{Q}_{(j)n}\,\check{\mathscr{S}}_n(R)\Bigg]+(-1)^j 2\Sigma_{(j)1}\check{\gamma}_{(j)n}(R)\Bigg\rangle\Bigg\}.\end{aligned}\tag{5.66}$$

We next derive the Z-independent part $\bar{\bar{\Phi}}_{(j)}^{(1)}(R)$ using (4.7) in (5.59b), and find that

$$\begin{aligned}\bar{\bar{\Phi}}_{(j)}^{(1)}(R) = \frac{a^2}{|J_1(\mathrm{i}\mathbb{A}_{(j)}a)|^2}\Bigg[&\Sigma_{(j)1}|\mathbb{A}_{(j)}|^2|J_2(\mathrm{i}\mathbb{A}_{(j)}R)|\\&+\int_0^R\left(\rho_{(j)}\frac{|J_1(\mathrm{i}\mathbb{A}_{(j)}\xi)|^2}{\xi}-2|\mathbb{A}_{(j)}|^2\eta_{(j)1}\frac{|J_2(\mathrm{i}\mathbb{A}_{(j)}\xi)|^2}{\xi}\right)\mathrm{d}\xi\Bigg]+\text{constant}\,\not{p}_{(j)},\end{aligned}\tag{5.67}$$

The mean pressure $\bar{\bar{\Phi}}_{(j)}(R, Z)$ is therefore determined, modulo an arbitrary constant $\not{p}_{(j)}$, by (5.58*c*), (5.66) and (5.67).

5.3. *The mean interfacial shape*

In this subsection we address the lowest-order deviation of the interface from the horizontally flat position for three special cases. In the first two cases, the interfacial surface tension is comparable to other forces, and the edge of the interface complies with the boundary conditions of the type (i) or (ii) in (4.17). In the third case, the interfacial tension parameter is practically zero, so that the normal stress difference between the two fluids vanishes.

We resume the analysis with the second-order differential equation (4.16):

$$-[\![\bar{\bar{\Phi}}]\!]+\left[\!\!\left[2\mu\frac{\partial\bar{\bar{u}}}{\partial Z}+2\mathring{\boldsymbol{S}}_{2ZZ}[\boldsymbol{U}_1]\right]\!\!\right]+[\![\rho]\!]g\bar{\bar{h}}=\sigma\left[\bar{\bar{h}}''+\frac{1}{R}\bar{\bar{h}}'\right].$$

The above equation is not completely determined, because of the unknown constant pressure difference $[\![\not{p}]\!] = \not{p}_{(2)}-\not{p}_{(1)}$. However, the equation for the slope,

$$X\equiv\frac{\mathrm{d}}{\mathrm{d}R}\bar{\bar{h}}(R), \tag{5.68}$$

is completely defined:

$$-[\![\bar{\bar{\Phi}}]\!]'+2\left[\!\!\left[\mu\frac{\partial\bar{\bar{u}}}{\partial Z}+\mathring{\boldsymbol{S}}_{2ZZ}[\boldsymbol{U}_1]\right]\!\!\right]'+[\![\rho]\!]gX=\sigma\left[X''+\frac{X'}{R}-\frac{X}{R^2}\right]. \tag{5.69}$$

We recall (4.19*b*) and (4.13*c*) and find that

$$2\left(\mu\frac{\partial\bar{\bar{u}}}{\partial Z}+\mathring{\boldsymbol{S}}_{2ZZ}[\boldsymbol{U}_1]\right)'=2\left(\mu\frac{\partial^2}{\partial R\,\partial Z}\left(\frac{1}{R}\frac{\partial}{\partial R}\psi\right)+2\frac{\partial}{\partial R}(R^2|\omega^*_{,Z}|^2)\,\Sigma_1\right). \tag{5.70}$$

Moreover, (5.56*b*) yields

$$\frac{\partial}{\partial R}\bar{\bar{\Phi}}=-\mu\left(\nabla^2-\frac{1}{R^2}\right)\frac{1}{R}\frac{\partial}{\partial Z}\psi+2(-\eta_1 r_1+\not{\eta} r_3+\rho r_5). \tag{5.71}$$

We now evaluate $(\bar{\bar{\Phi}}-2\mu\,\partial\bar{\bar{u}}/\partial Z-2\mathring{\boldsymbol{S}}_{2ZZ}[\boldsymbol{U}_1])'_{(1)}$ using (5.70) and (5.71), and then reduce the resulting expression, using (5.5*b*), to find that

$$\begin{aligned}\left(\bar{\bar{\Phi}}-2\mu\frac{\partial\bar{\bar{u}}}{\partial Z}-2\mathring{\boldsymbol{S}}_{2ZZ}[\boldsymbol{U}_1]\right)'_{(1)}&\\ =\Bigg[&-3\mu\left(\frac{\partial^2}{\partial R^2}+\frac{1}{R}\frac{\partial}{\partial R}-\frac{1}{R^2}\right)\frac{1}{R}\frac{\partial}{\partial Z}\psi-\mu\frac{1}{R}\frac{\partial^3}{\partial Z^3}\psi\\ &+2\Big\{\Sigma_1 R^2\left[\left(A^2\omega^*-\frac{\omega^*_{,R}}{R}+\omega^*_{,RR}\right)\bar{\omega}^*_{,R}+\text{conjugate}\right]\\ &-\Sigma_1(R^2|\omega^*_{,Z}|^2)_{,R}-2R\,[2\Sigma_2|\omega^*_{,Z}|^2+2\eta_1|\omega^*_{,R}|^2-\rho|w^*|^2]\Big\}\Bigg]_{(1)}.\end{aligned} \tag{5.72}$$

We can write similar expressions for fluid 2. Moreover, since the following conditions hold at $Z = 0$:

$$[\![\psi_{,Z}]\!]=[\![\omega^*]\!]=[\![\omega^*_{,Z}\eta]\!]=0, \tag{5.73}$$

the expression for $(\bar{\bar{\Phi}}-2\mu\,\partial\bar{\bar{u}}/\partial Z-2\mathring{\boldsymbol{S}}_{2ZZ}[\boldsymbol{U}_1])'_{(2)}$ at $Z = 0$ is conveniently expressed

partly in terms of functions defined for fluid 1. It then follows that

$$\left[\!\left[-\bar{\bar{\Phi}}+2\mu\frac{\partial\bar{\bar{u}}}{\partial Z}+2\mathring{\mathbf{S}}_{zzZ}[U_1]\right]\!\right]'$$

$$= 3[\![\mu]\!]\left(\frac{\partial^2}{\partial R^2}+\frac{1}{R}\frac{\partial}{\partial R}-\frac{1}{R^2}\right)\frac{1}{R}\frac{\partial}{\partial Z}\psi_{(1)}+\left[\!\left[\mu\frac{1}{R}\frac{\partial^3}{\partial Z^3}\psi\right]\!\right]$$
$$+2\left\{\left[-[\![\Sigma_1]\!]R^2\left(\omega^*_{(1),\,RR}-\frac{\omega^*_{(1),\,R}}{R}\right)\bar{\omega}^*_{(1),\,R}-[\![\Sigma_1\mathbb{A}^2]\!]R^2\omega^*_{(1)}\,\bar{\omega}^*_{(1),\,R}\right.\right.$$
$$\left.+\text{conjugate}\right]-\left(\Sigma_{(1)1}-\Sigma_{(2)1}\frac{|\eta_{(1)}|^2}{|\eta_{(2)}|^2}\right)(R^2|\omega^*_{(1),Z}|^2)_{,R}$$
$$\left.-2R\left[2\left(\Sigma_{(1)2}-\Sigma_{(2)2}\frac{|\eta_{(1)}|^2}{|\eta_{(2)}|^2}\right)|\omega^*_{(1),\,Z}|^2-2[\![\eta_1]\!]\,|\omega^*_{(1),\,R}|^2+[\![\rho]\!]\,|\omega^*_{(1)}|^2\right]\right\}. \tag{5.74}$$

Expression (5.74) is of the form

$$[\![-\bar{\bar{\Phi}}]\!]'+2\left[\!\left[\mu\frac{\partial\bar{\bar{u}}}{\partial Z}+\mathring{\mathbf{S}}_{zzZ}[U_1]\right]\!\right]' = \mathscr{R}(R) = \mathscr{R}_0(R)+\mathscr{R}_1(R), \tag{5.75a}$$

where $\mathscr{R}_0(R)$ is the only part of $\mathscr{R}(R)$ that arises when the Z-dependent contributions from the velocities at first and second orders are suppressed. The Z-dependent contributions are represented by $\mathscr{R}_1(R)$, which can be further decomposed into:

$$\mathscr{R}_1(R) = \mathscr{R}_{11}(R)+\mathscr{R}_{12}(R), \tag{5.75b}$$

where $\mathscr{R}_{11}(R)$ and $\mathscr{R}_{12}(R)$ are the contributions from first and second orders respectively. We now define

$$\left.\begin{aligned}
\Sigma_{(j)3} &\equiv (2\not{\eta}-3\eta_1)_{(j)},\\
\Sigma_{(j)4} &\equiv (3\not{\eta}-4\eta_1)_{(j)},\\
\mathscr{T}_1 &\equiv \Sigma_{(2)1}\left|\frac{\eta_{(1)}}{\eta_{(2)}}\right|^2-\Sigma_{(1)1},\\
\mathscr{T}_2 &\equiv [\![\Sigma_1\mathbb{A}^2]\!]+\mathbb{A}^2_{(1)}[\![\Sigma_1]\!],\\
\mathscr{T}_4 &\equiv \Sigma_{(2)4}\left|\frac{\eta_{(1)}}{\eta_{(2)}}\right|^2-\Sigma_{(1)4},\\
\mathscr{T}_{1m} &\equiv [\![\Sigma_1\mathbb{A}^2]\!]-\left(\frac{\sigma_m}{a}\right)^2[\![\Sigma_1]\!].
\end{aligned}\right\} \tag{5.76}$$

Using (3.20), (3.21), (5.55) and (5.76) in (5.74), and after lengthy manipulations and reductions of terms, we get

$$\mathscr{R}_0(R) = \frac{2a^2}{|J_1(\mathrm{i}\mathbb{A}_{(1)}a)|^2}\left[\frac{|\mathbb{A}_{(1)}|^2}{R}|J_2(\mathrm{i}\mathbb{A}_{(1)}R)|^2[\![\Sigma_3]\!]-\tfrac{1}{2}\frac{[\![\rho]\!]}{R}|J_1(\mathrm{i}\mathbb{A}_{(1)}R)|^2\right.$$
$$\left.-\frac{\mathrm{i}}{4}(\bar{\mathbb{A}}_{(1)}\mathscr{T}_2J_2(\mathrm{i}\bar{\mathbb{A}}_{(1)}R)\,J_1(\mathrm{i}\mathbb{A}_{(1)}R)-\text{conjugate})\right], \tag{5.77}$$

$$\mathscr{R}_{11}(R) = 2\left[\sum_{m=1}^{\infty}\left\{\frac{aC_m}{2J_1(\mathrm{i}\bar{\mathbb{A}}_{(1)}a)}J_1\left(\sigma_m\frac{R}{a}\right)\left[\bar{\mathbb{A}}_{(1)}\mathscr{T}_{1m}J_2(\mathrm{i}\bar{\mathbb{A}}_{(1)}R)-\frac{2\mathrm{i}[\![\rho]\!]}{R}J_1(\mathrm{i}\mathbb{A}_{(1)}R)\right]\right.\right.$$
$$\left.\left.+\frac{C_m\sigma_m}{2J_1(\mathrm{i}\bar{\mathbb{A}}_{(1)}a)}J_2\left(\sigma_m\frac{R}{a}\right)\left[\frac{4}{R}[\![\Sigma_3]\!]\,\bar{\mathbb{A}}_{(1)}J_2(\mathrm{i}\bar{\mathbb{A}}_{(1)}R)+i\bar{\mathscr{T}}_2J_1(\mathrm{i}\bar{\mathbb{A}}_{(1)}R)\right]+\text{conjugate}\right\}\right.$$

$$+\sum_{n=1}^{\infty}\sum_{m=1}^{\infty}\left\{(\bar{C}_n C_m[\mathscr{T}_{1m}-\mathscr{T}_1\beta_{(1)n}\bar{\beta}_{(1)m}]+\text{conjugate})\frac{\sigma_n}{a}J_2\left(\sigma_n\frac{R}{a}\right)J_1\left(\sigma_m\frac{R}{a}\right)\right.$$

$$+2\bar{C}_n C_m(\mathscr{T}_4\bar{\beta}_{(1)n}\beta_{(1)m}-[\![\rho]\!])\frac{1}{R}J_1\left(\sigma_n\frac{R}{a}\right)J_1\left(\sigma_m\frac{R}{a}\right)$$

$$\left.+4\frac{\sigma_n}{a}\frac{\sigma_m}{a}\bar{C}_n C_m[\![\Sigma_3]\!]\frac{1}{R}J_2\left(\sigma_n\frac{R}{a}\right)J_2\left(\sigma_m\frac{R}{a}\right)\right\}\Bigg] \tag{5.78}$$

and

$$\mathscr{R}_{12}(R)=\sum_{n=-\infty}^{\infty}-2(\mu_{(1)}A_n+\mu_{(2)}B_n)\left[\frac{p_n}{a}\frac{1}{R}\phi_1^{(n)}-\frac{3J_1(p_n)}{aJ_0(p_n)}J_1\left(p_n\frac{R}{a}\right)\right]$$

$$-\left(\frac{\pi}{2}\right)^2\sum_{n=1}^{\infty}\left\{2\left(\frac{\sigma_n}{a}\right)^3\int_0^a G_n(R,\xi)\,[\mu_{(1)}\mathscr{H}_{(1)n}(\xi)+\mu_{(2)}\mathscr{H}_{(2)n}(\xi)]\,\mathrm{d}\xi\right.$$

$$\left.-\frac{b}{\pi}\frac{\sigma_n}{a}\frac{1}{R}[\mu_{(1)}\mathscr{H}_{(1)n}(R)+\mu_{(2)}\mathscr{H}_{(2)n}(R)]\right\}$$

$$-\left(\frac{\pi}{2}\right)^2\sum_{n=2}^{\infty}\left\{2\left(\frac{\check{\sigma}_n}{a}\right)^3\int_0^a \check{G}_n(R,\xi)\,[\check{\mathscr{H}}_{(1)n}(\xi)\mu_{(1)}+\mu_{(2)}\check{\mathscr{H}}_{(2)n}(\xi)]\,\mathrm{d}\xi\right.$$

$$\left.-\frac{b}{\pi}\frac{\check{\sigma}_n}{a}\frac{1}{R}[\mu_{(1)}\check{\mathscr{H}}_{(1)n}(R)+\mu_{(2)}\check{\mathscr{H}}_{(2)n}(R)]\right\}. \tag{5.79}$$

So the forcing function $\mathscr{R}(R)=[\![-\bar{\bar{\Phi}}+2\mu\,\partial\bar{\bar{u}}/\partial Z+2\mathring{\boldsymbol{S}}_{2ZZ}[\boldsymbol{U}_1]]\!]'$ in (5.69) is considered known, computable from (5.75) and (5.77)–(5.79).

We next examine the case where the surface tension is not small and the interface satisfies the boundary conditions of the type (i) or (ii) in (4.17).

5.3.1. *Large interfacial tension*

Equation (5.69) can be rewritten as

$$X''+\frac{X'}{R}-\frac{X}{R^2}-\frac{[\![\rho]\!]g}{\sigma}X=\frac{1}{\sigma}\mathscr{R}(R) \tag{5.80}$$

We may non-dimensionalize (5.80) by multiplying the variable and functions $[R, X(R), \bar{\bar{h}}(R), \mathscr{R}(R)]$ with the scales $[1/a, \omega^2, \omega^2/a, \omega^2a^2/\sigma]$, and define the dimensionless parameter

$$\lambda^2\equiv\frac{[\![\rho]\!]ga^2}{\sigma}. \tag{5.81}$$

The dimensionless form of (5.80) is given by

$$\frac{\mathrm{d}^2}{\mathrm{d}R^2}X+\frac{1}{R}\frac{\mathrm{d}}{\mathrm{d}R}X-\left(\frac{1}{R^2}+\lambda^2\right)X=\mathscr{R}(R)\quad\text{with}\quad R\in[0,1], \tag{5.82}$$

and the boundary conditions corresponding to (i) and (ii) in (4.17) are given by (5.83a) and (5.83b) respectively:

$$X(0)=0,\quad X(1)=\omega^2\bar{\bar{\alpha}}, \tag{5.83a}$$

$$X(0)=0,\quad \bar{\bar{h}}(1)=0. \tag{5.83b}$$

The constraint of constant volumes (4.18) becomes

$$\int_0^1 R\bar{\bar{h}}(R)\,\mathrm{d}R=0, \tag{5.84a}$$

or in terms of the slope $X(R)$:

$$\tfrac{1}{2}\bar{\bar{h}}(0)+\int_0^1\left[\int_0^R X(\xi)\,\mathrm{d}\xi\right]R\,\mathrm{d}R=0. \tag{5.84b}$$

The differential equation (5.82) subject to boundary conditions (5.83a or b) and constraint (5.84) can be solved by the method of variation of parameters. In fact, the general form of a solution of (5.82), which satisfies $X(0)=0$, is given by (see Tieu 1983)

$$X(R)=-\int_0^1 H_\lambda(R,\xi)\,\mathscr{R}(\xi)\,\xi\,\mathrm{d}\xi+bI_1(\lambda R), \tag{5.85}$$

where the constant b is chosen to satisfy the edge condition at $R=1$, and the kernel $H_\lambda(R,\xi)$ is defined as follows:

$$H_\lambda(R,\xi)=\begin{cases}K_1(\lambda R)\,I_1(\lambda\xi) & (R\geqslant\xi),\\ I_1(\lambda R)\,K_1(\lambda\xi) & (R\leqslant\xi).\end{cases} \tag{5.86}$$

$I_1(R)$ and $K_1(R)$ are modified Bessel functions of the first and second kind respectively. The corresponding interfacial shape correction $\bar{\bar{h}}(R)$ is therefore

$$\bar{\bar{h}}(R)=\bar{\bar{h}}(0)+\int_0^R\left[-\int_0^1 H_\lambda(\zeta,\xi)\,\mathscr{R}(\xi)\,\mathrm{d}\xi+bI_1(\lambda\zeta)\right]\mathrm{d}\zeta, \tag{5.87}$$

where the unknown constants $\bar{\bar{h}}(0)$ and b are to be determined from boundary condition at $R=1$, and constraint (5.84).

If the contact angle is prescribed, i.e. when conditions (5.83a) hold, b is found to be

$$b=\frac{1}{I_1(\lambda)}\left[\omega^2\bar{\bar{\alpha}}+K_1(\lambda)\int_0^1\xi I_1(\lambda\xi)\,\mathscr{R}(\xi)\,\mathrm{d}\xi\right]. \tag{5.88}$$

Substitution of (5.87) in (5.84b) yields

$$\bar{\bar{h}}(0)=-2\int_0^1 R\left[\int_0^R\left\langle-\int_0^1 H_\lambda(\zeta,\xi)\,\mathscr{R}(\xi)\,\xi\,\mathrm{d}\xi+bI_1(\lambda\zeta)\right\rangle\mathrm{d}\zeta\right]\mathrm{d}R. \tag{5.89}$$

If the contact line is fixed at $R=1$, i.e. when boundary conditions (5.83b) hold, integration by parts of (5.84a) leads to

$$\int_0^1 R^2X(R)\,\mathrm{d}R=0. \tag{5.90}$$

Substitution of (5.85) in (5.90) yields

$$b=\frac{\displaystyle\int_0^1 R^2\int_0^1 H_\lambda(R,\xi)\,\mathscr{R}(\xi)\,\xi\,\mathrm{d}\xi\,\mathrm{d}R}{\displaystyle\int_0^1 R^2I_1(\lambda R)\,\mathrm{d}R}. \tag{5.91}$$

We may determine $\bar{\bar{h}}(0)$ by using the condition $\bar{\bar{h}}(1)=0$, and find that

$$\bar{\bar{h}}(0)=\int_0^1\left[\int_0^1 H_\lambda(R,\xi)\,\mathscr{R}(\xi)\,\xi\,\mathrm{d}\xi-bI_1(\lambda R)\right]\mathrm{d}R. \tag{5.92}$$

5.3.2. *Zero interfacial tension*

The expressions for interfacial shapes derived in the preceding cases are applicable when λ^2 is about $O(1)$ or $o(1)$. In the case $\lambda^2\gg 1$, the problem defined by (5.82) and

boundary conditions of the type (5.83) should be solved by singular perturbations. In the limit $\sigma = 0$ (5.80) is no longer well defined and should be replaced by

$$[\![\rho]\!] gX = -\mathscr{R}(R). \tag{5.93}$$

Again we may non-dimensionalize the variable and functions $[R, X(R), \bar{\bar{h}}(R), \mathscr{R}(R)]$ by multiplications with the scales $[1/a, \omega^2, \omega^2/a, \omega^2/[\![\rho]\!] g]$. The dimensionless form of (5.93) is thus

$$X(R) = -\mathscr{R}(R). \tag{5.94}$$

It then follows that

$$\bar{\bar{h}}(R) = -\int_0^R \mathscr{R}(\xi)\,\mathrm{d}\xi + \bar{\bar{h}}(0), \tag{5.95a}$$

where $\bar{\bar{h}}(0)$ is chosen such that the condition of constant volume is satisfied:

$$\bar{\bar{h}}(0) = \frac{1}{2}\int_0^1 R \int_0^R \mathscr{R}(\xi)\,\mathrm{d}\xi\,\mathrm{d}R. \tag{5.95b}$$

The solution we constructed is such that $\mathscr{R}(0) = 0$; therefore the condition $X(0) = 0$ is automatically satisfied. However, the edge condition at $R = 1$ cannot be fulfilled. This is expected, because in the absence of interfacial tension the boundary between two media is determined entirely by the balance of normal stress. When interfacial tension is zero, the interface cannot sustain tension forces, and it is impossible to apply boundary conditions that are independent of motions of the two media.

We now determine the order of magnitude of the dimensionless $\bar{\bar{h}}(R;\omega)$ when ω approaches zero. The dependence of (5.11) and (5.49) on ω is found, using (3.26) and (3.27), to be

$$f_{(j)}(R, Z;\omega) = O(\omega^2), \tag{5.96a}$$

and

$$\begin{bmatrix} y_1(R;\omega) \\ y_2(R;\omega) \end{bmatrix} = O(\omega^2), \quad \begin{bmatrix} \tilde{Y}_1(R;\omega) \\ \tilde{Y}_2(R;\omega) \end{bmatrix} = O(\omega^2). \tag{5.96b,c}$$

These results imply that

$$\psi_{(j)}(R, Z;\omega) = O(\omega^2). \tag{5.97}$$

The order estimates in (3.26), (3.27) and (5.97) then lead to the orders of magnitude of the dimensional forcing function $\mathscr{R}(R)$ and its components, as defined in (5.75)–(5.79), as follows:

$$\mathscr{R}_0(R;\omega) = -[\![\rho]\!] R + O(\omega^2), \quad \mathscr{R}_{11}(R;\omega) = O(\omega^2), \quad \mathscr{R}_{12}(R;\omega) = O(\omega^2);$$

and therefore

$$\mathscr{R}(R;\omega) = -[\![\rho]\!] R + O(\omega^2). \tag{5.98}$$

Of particular interest is the case of zero interfacial tension. Application of (5.98) in (5.95) yields a simple decomposition of the dimensionless mean interfacial-shape correction:

$$\bar{\bar{h}}(R;\omega) = \omega^2\left[\frac{a}{2g}(R^2 - \tfrac{1}{2}) + h^*(R;\omega)\right] \tag{5.99a}$$

for $R \in [0, 1]$, where

$$h^*(R, \omega) = O(\omega^2). \tag{5.99b}$$

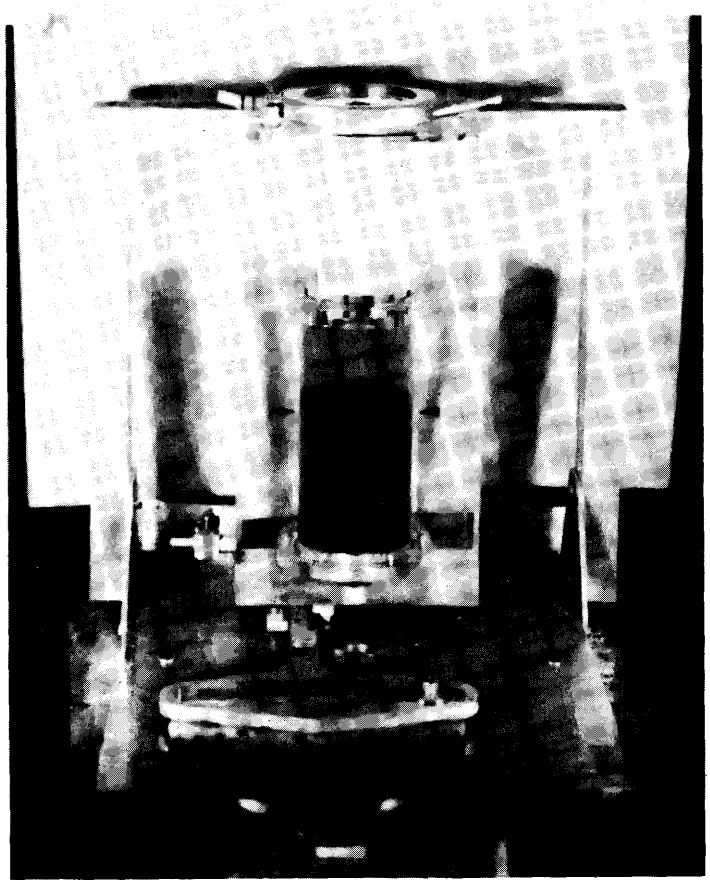

FIGURE 2. Overall view of the experimental equipment.

The first term in the square bracket of (5.99a) represents a parabolic shape which is the exact interfacial shape when the two fluids execute the same solid-body motion as the cylinder. The term $h^*(R;\omega)$ represents the deviation of the interface shape from a parabolic profile, when the fluids do not undergo a solid-body rotation.

6. Experiments

6.1. *Apparatus*

The central part of the apparatus consists of a vertical Plexiglas cylinder with an inner radius of 5.68 cm and a height of 42.00 cm. The cylinder is located inside a fixed Plexiglas housing of 18.0 cm × 23.0 cm rectangular section and of approximately the same height as the cylinder, as shown in figure 2. The oscillatory motion is transmitted to the cylinder by means of a driving mechanism consisting of a motor, a reduction gear, a Scotch yoke and a rack-and-pinion system.

The cylinder is supported at its upper end by a ring bearing which is attached to a rigid aluminium support frame. The frame in turn is attached to a rigid aluminium table upon which the apparatus is situated. The bottom end of the cylinder is sealed by means of an aluminium endplate. This component has a central stud which passes through a ball bearing located in the support table. The stud carries a pinion gear

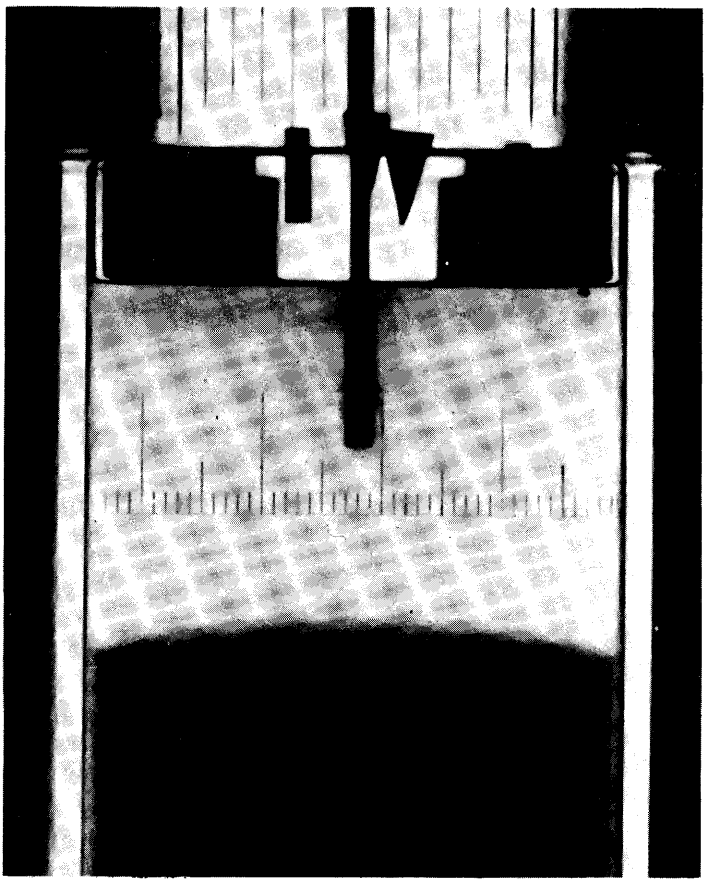

FIGURE 3. Calibration of the system for optical distortion. A scale with equally spaced marks is immersed in STP within the circular cylinder. The picture is taken through glycerol occupying the space between the circular cylinder and a surrounding rectangular box. The divisions on the scale remain uniform in this view across the whole diameter of the cylinder.

which meshes with and is driven by a rack attached to the Scotch-yoke mechanism described later.

The outer Plexiglas housing is fixed to the support frame, and has a liquid-proof seal in the bottom, through which the cylinder driving stud passes. The space between the housing and the cylinder is filled with glycerol, whose refractive index is extremely close to the refractive indices of STP and TLA227 so that there is no measurable distortion of light paths going through the cylinder to an outside observer. This is illustrated in figure 3 which shows a photograph of a calibration scale, with equally spaced marks, immersed in the STP. The distances between graduations on the photograph were checked by means of a travelling microscope, and found to be uniform.

The driving mechanism is powered by an Electro-Craft servo motor, type 0703-05-052. The motor is connected to a gear box of reduction ratio 9.5. The output shaft of the gear box is connected to a steel disk of a Scotch-yoke mechanism which transforms steady input rotations to a harmonic rectilinear motion of the yoke. There are 13 threaded holes on the disk, and corresponding unthreaded holes are located diametrically symmetric to the threaded holes to balance the disk dynamically. The

yoke is constrained to move horizontally by pairs of roller bearings and has a rack attached along part of its length. The rack meshes with the pinion on the cylinder bottom plate, thus providing the sinusoidal oscillations of the cylinder. The speed of the motor is regulated by an Electro-Craft feedback controller, type E.710. This maintains a constant speed from the motor under varying torque conditions, which in turn assures true sinusoidal motion of the cylinder.

The angular frequency of the cylinder is directly related to the gear ratio and the motor shaft angular velocity, which is monitored by means of a Kaman proximity gauge, is displayed on an electronic counter. To monitor the instantaneous motion of the cylinder, evenly spaced marks are scribed on the outside surface of the cylinder. The amplitude of the cylinder motion can be adjusted by changing the position of the crank pin on the steel disk.

6.2. *The test fluids*

The test fluids used in the current experiments are lubricating-oil additives TLA227 and STP. The former is a solution of methacrylate copolymer in petroleum oil, and the latter is a solution of polyisobutylene in oil. Both fluids have been used extensively in the studies of steady and unsteady rod climbing problems (Joseph *et al.* 1973; Joseph & Beavers 1976). The present samples come from different production batches from the fluid samples used in earlier experiments. Thus it was necessary to measure the material constants of these fluids as a prelude to the oscillating-cylinder experiments.

The densities of the fluids were measured using standard specific-gravity bottles. These measurements were repeated several times, using bottles of different volumes. An average density for each fluid was then computed from these measurements.

The variations of shear stress and first normal stress difference with shear rate were measured in cone-and-plate and parallel-plate geometries using a Rheometrics mechanical spectrometer. For a small range of shear rates near zero, the shear stress varies linearly with shear rate and therefore the zero-shear viscosity of each fluid can be determined with good accuracy. However, a limitation of mechanical viscometers is that readings of the first normal-stress difference at very small shear rates are not very reliable. These readings are thus subject to possible error from the extrapolation procedure described below.

It is always the case that some backward extrapolation is necessary to determine the first normal stress difference at infinitesimal shear rate $\dot{\gamma}$. Theoretically, this normal stress difference is proportional to the square of the shear rate $\dot{\gamma}^2$, for very small $\dot{\gamma}$, where the proportionality constant is $-2\alpha_1$. The material constant α_1 can thus be deduced from a graph of the first normal stress difference versus shear rate. From the rod-climbing experiments, the climbing constant $\hat{\beta} = 3\alpha_1 + 2\alpha_2$ is evaluated (see Beavers & Joseph 1975), and therefore the constant α_2 can be determined next.

Another physical property required in this work is the interfacial tension between STP and TLA227, which at room temperature is very small. The interfacial tension is very difficult to measure accurately for this pair of polymer solutions. Using a standard electrobalance ring tensiometer, it was consistently found that the interfacial tension σ was less than 0.4 dyn/cm and was probably about 0.1 dyn/cm. Thus for present work it is a reasonable approximation to take the interfacial tension σ to be zero. This approximation is equivalent to assuming that the Bond number is infinitely large.

The next material functions to be determined are the linear and quadratic shear relaxation functions $G(s)$ and $\gamma(s_1, s_2)$ that appear in (2.19). The most widely used

forms of these functions are the generalized Maxwell models (Joseph & Beavers 1976; Bird, Armstrong and Hassager 1977):

$$G_N(s) = -\frac{\mu^2}{\alpha_1} \sum_1^N \frac{a_n^2}{b_n} \exp\left(\frac{\mu}{\alpha_1}\frac{a_n}{b_n} s\right) \tag{6.1}$$

and

$$\gamma_M(s_1, s_2) = \alpha_2 \sum_1^M c_n k_n^2 \exp\left(-k_n(s_1+s_2)\right), \tag{6.2}$$

where

$$\sum_1^N a_n = \sum_1^N b_n = \sum_1^M c_n = 1. \tag{6.3}$$

In the works of Joseph & Beavers (1976), and Kolpin *et al.* (1980), the second order theoretical predictions for unsteady rod climbing have been found best fitted to experimental observations on TLA227 for the following choice of parameter values:

$$k_1^2 = 15.43 \quad \text{when} \quad N = M = 1 \quad \text{and} \quad 0 \leqslant \omega^2 < 30.$$

And

$$k_1^2 = 14.50, \quad k_2^2 = 307.00, \quad c_1 = 0.9735$$

when

$$N = 1, \quad M = 2 \quad \text{and} \quad 0 \leqslant \omega^2 < 450.$$

If the Maxwell models (6.1)–(6.3) are good, then the findings in the oscillatory rod-climbing investigation should be applicable in some sense to other flow situations. It might be expected that in general, for TLA227, the above constants a_n, b_n, c_n and k_n remain the same, but that the range of best fit on ω^2 varies from one type of flow to another. We do not claim, however, that these fitting constants should have the same values for STP. Still, if these constants for STP are temporarily unknown, a good first approximation is to use the same values as for TLA227, particularly in view of the experimental observation that the parameter values for Paratone (another oil-based polymer similar to STP and TLA227) are almost the same as for TLA227 (Kolpin *et al.* (1980). We note that the asymptotic values of the only material-related functions (i.e. $\not{\eta}(\omega)$ and $\eta_1(\omega)$) occurring in the mean problem at second order are independent of these fitting constants as ω approaches zero. So, if we choose an arbitrary set of values for a_n, b_n, c_n and k_n consistent with (6.3), but not close to the true values of these coefficients, then we will find that, for sufficiently small angular frequency ω, the theoretical interfacial shape would look similar to the true surface shape. The predicted interfacial deformations may however differ from the experimental measurements at higher ω^2.

Estimates for the material constants of STP and TLA227 at room temperatures based on the earlier oscillating rod experiments of Joseph and co-workers are listed in table 2.

6.3. *Experimental procedures*

The cylinder is filled with TLA 227 to 14.5 cm in depth and then STP is added on top to 7.0 cm in depth. The glycerol level is kept a few centimetres above the air–STP interface. The STP is not filled to a greater depth, because our analysis shows that flow conditions at positions away from the STP–TLA227 interface greater than one cylinder radius (≈ 5.68 cm) are almost identical with flow conditions at an infinite distance from the interface. Moreover, unnecessarily larger depths of STP and TLA227 require a greater depth of glycerol; and greater depths of the test fluids and the glycerol cause larger fluctuations in applied torques as the cylinder undergoes

	STP	TLA227
Density (g/cm^3)	0.86	0.90
Viscosity (P)	120.00	200.00
α_1 (g/cm)	−0.90	−50.00
α_2 (g/cm)	1.80	85.00
k_1^2	14.50	14.50
k_2^2	307.00	307.00
c_1	0.9735	0.9735

TABLE 2

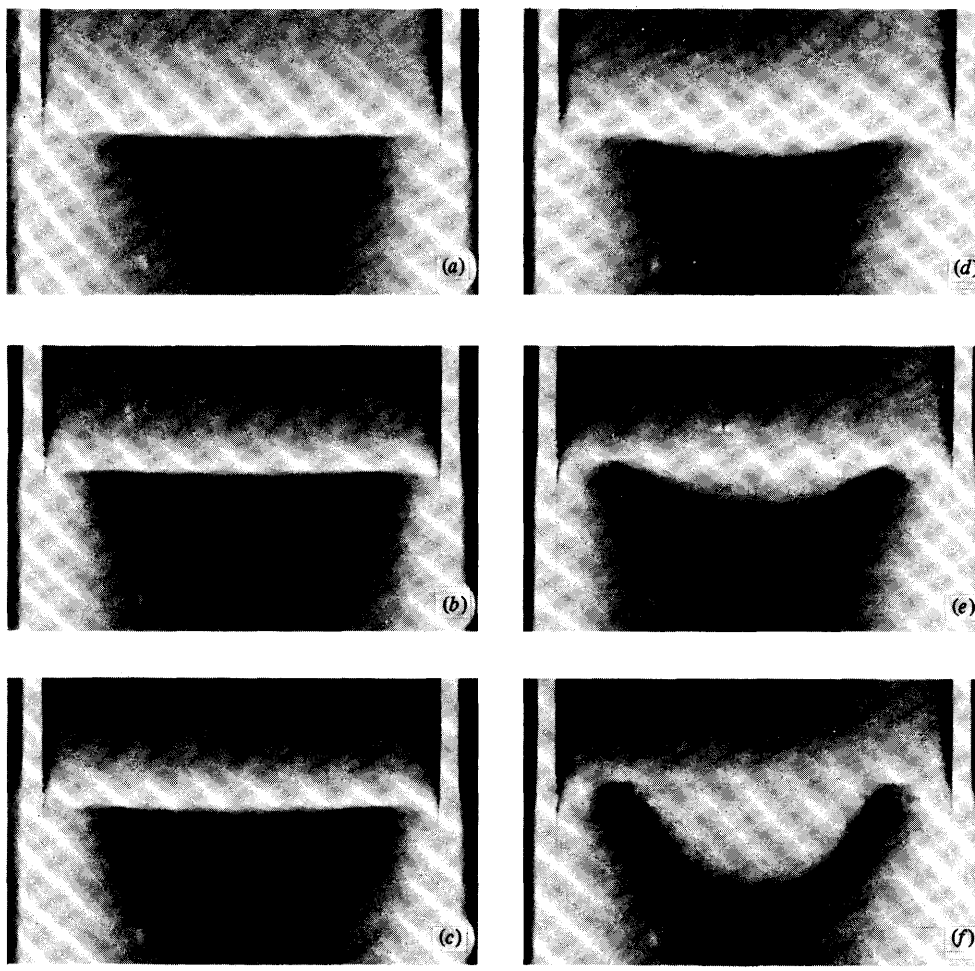

FIGURE 4. Interfacial shapes between STP and TLA227 in fixed-amplitude oscillations; $\Theta = 2.50$ rad. Frequency ω (rad/s): (*a*) 5.10; (*b*) 6.08; (*c*) 6.62; (*d*) 8.40; (*e*) 10.71; (*f*) 14.29.

oscillatory motions. After adding the fluids to the cylinder, they are allowed to sit for about a day to let all air bubbles escape.

In each experimental run, a fixed angle of twist Θ of the cylinder was selected, and the interfacial shape was observed for increasing values of the angular frequency ω from zero to a large value which was clearly beyond the limit of validity of the second-

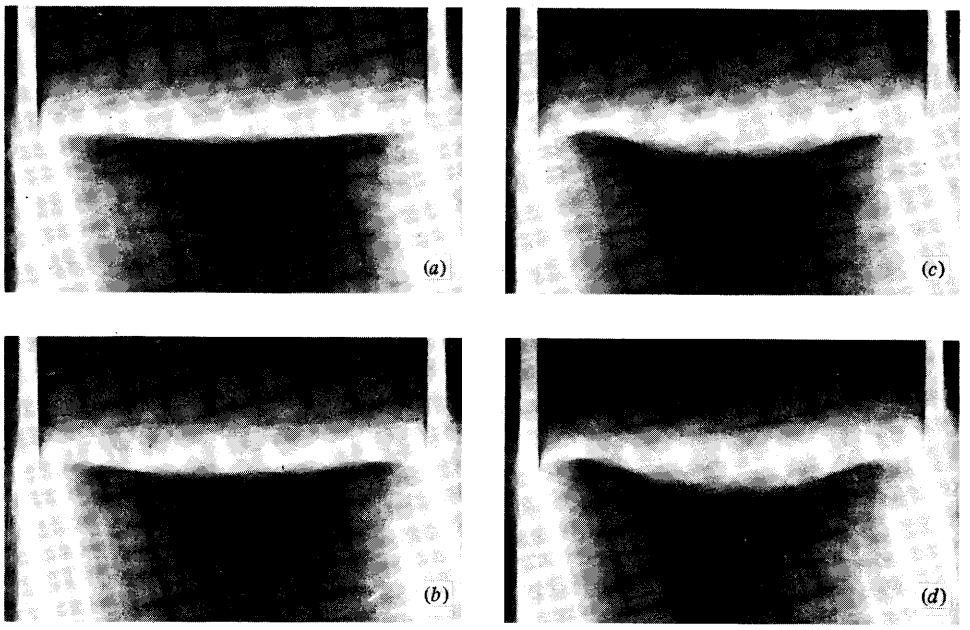

FIGURE 5. Interfacial shapes between STP and TLA227 in fixed-amplitude oscillations; $\Theta = 3.98$ rad. Frequency ω (rad/s): (*a*) 4.03; (*b*) 4.83; (*c*) 6.08; (*d*) 6.62.

order theory. Photographs of the interfacial shape were obtained using a camera installed exactly at the level of the undisturbed STP–TLA 227 interface and aligned with the centreline of the cylinder. At every angular frequency ω, a sequence of six to ten pictures was taken at different angular positions of the cylinder. The position of the cylinder in a cycle can be determined by examining the position of the marked labels on the cylinder wall.

Proper lighting and fast camera shutter speed play important roles in obtaining clear pictures of the fluid interface. The shutter is set at the fastest speed that film sensitivity allows. The difference in colours of the test fluids is not great, so that photographing the interfacial shape through the slightly opaque TLA227 presents a difficulty with regard to obtaining a sharply defined image of the interface. Various lighting arrangements were tried, and it was found that the best images of the interface were obtained for a lighting system consisting of a slit of intense light (about 0.5 cm wide) across the cylinder at the location of the undisturbed interface.

Each experimental run was performed as quickly as possible to avoid undesirable heating by fluid shearing and from the light source. After completion of each experimental run the fluids were allowed to sit for several hours before preparing for another run with a different angle of twist Θ.

Theoretical mean interfacial shapes are computed for different angles of twist Θ and angular frequencies ω in §7.3 and compared with experimentally observed shapes. The relation between ϵ, Θ and ω for sinusoidal oscillations of the cylinder is

$$\epsilon = \tfrac{1}{2}\omega\Theta.$$

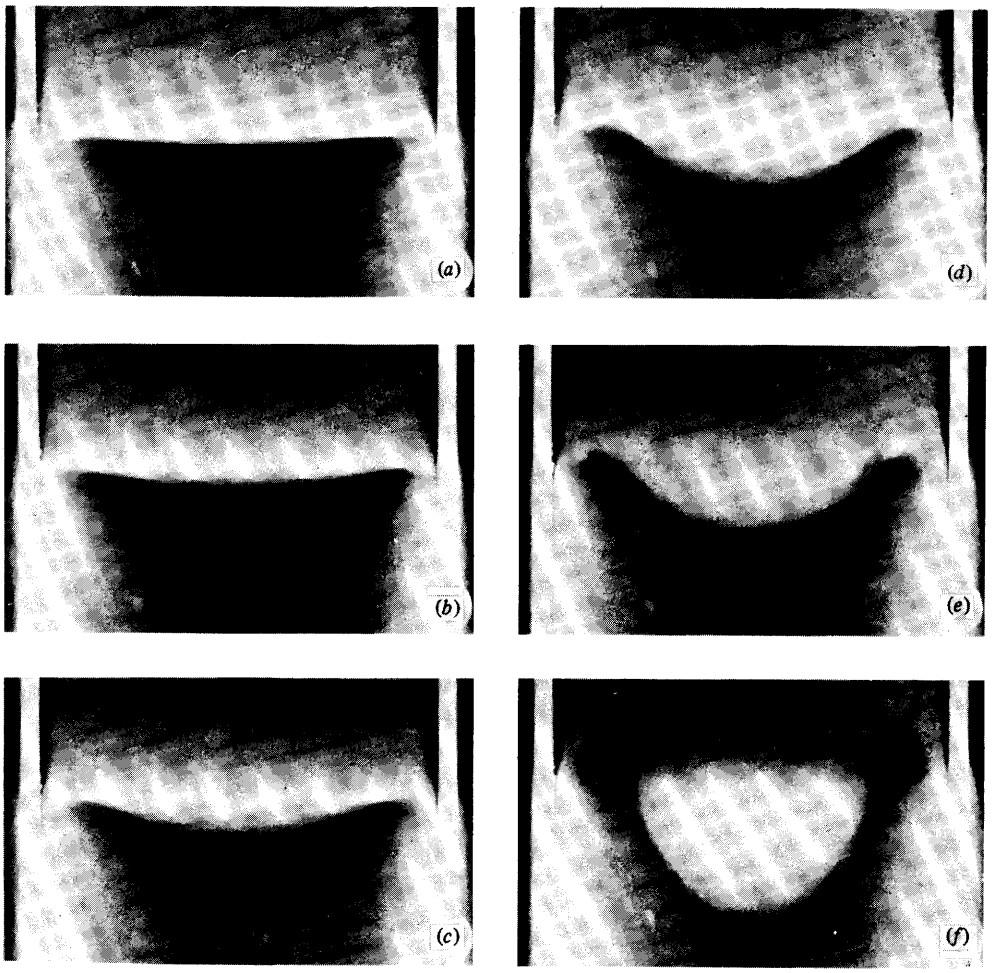

FIGURE 6. Interfacial shapes between STP and TLA227 in fixed-amplitude oscillations; $\Theta = 5.48$ rad. Frequency ω (rad/s): (*a*) 3.17; (*b*) 4.03; (*c*) 4.96; (*d*) 6.02; (*e*) 6.62; (*f*) 10.52.

6.4. *Qualitative observations*

Before comparing the experimentally measured profiles with those predicted from the analysis of §§4 and 5, we present here some general qualitative observations on the variation of the interfacial shape with changes in ω and Θ.

Figures 4–6 show pictures of the STP–TLA227 interfacial shape in three experimental runs with angles of twist $\Theta = 2.50$, 3.98 and 5.48 rad respectively. Each figure illustrates the change in the interfacial shape as the angular frequency is increased at a fixed value of the angle of twist. All the photographs in these three figures were taken with the cylinder at or very close to the minimum-velocity position. As the angular frequency ω increases, the centre of the interface falls below the undeformed location, the fluid interface near the outer perimeter climbs above the undeformed location, while the fluid interface at the cylinder wall remains fixed at the undisturbed location. The trend continues to become increasingly pronounced, until at a high-enough angular frequency the interface begins to lose its smooth appearance. Wavelike irregularities start to form on the deformed STP–TLA227 interface; and

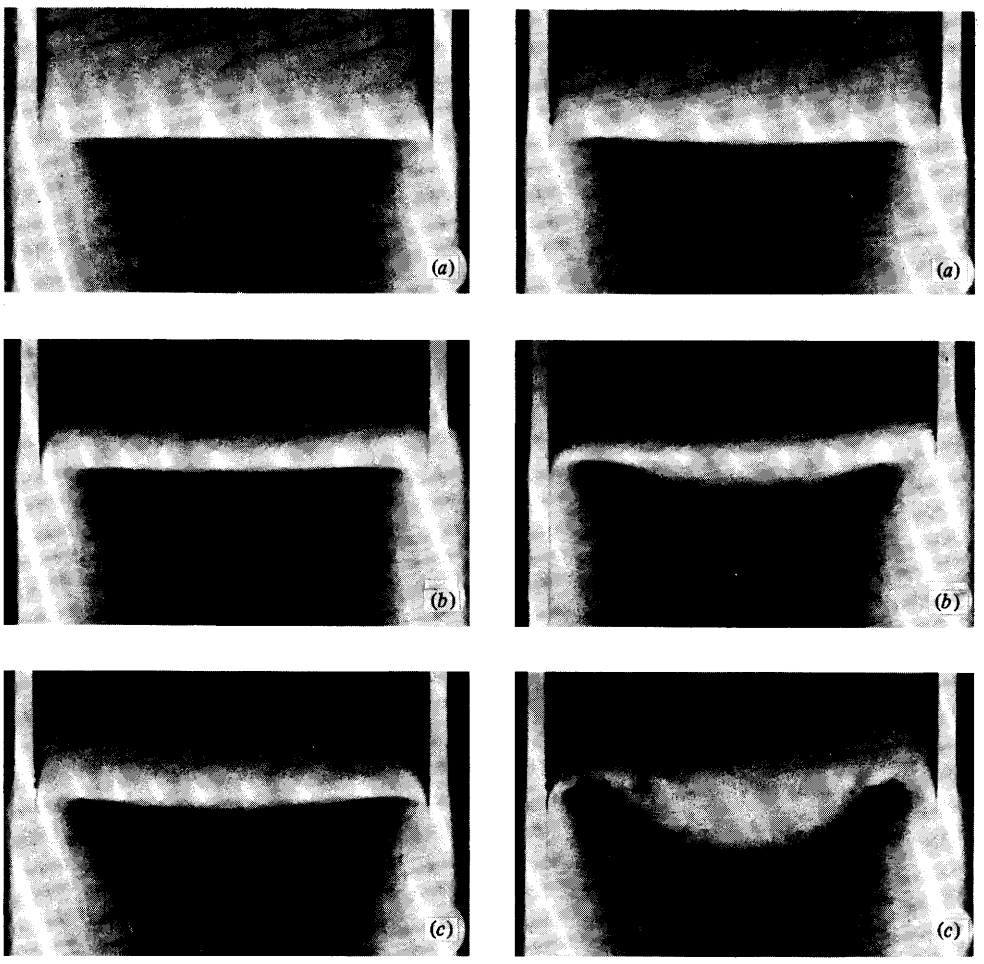

FIGURE 7. Dependence of the STP–TLA227 interfacial shape on the amplitude Θ of sinusoidal oscillations at fixed angular frequencies. Θ (rad): (*a*) 2.50; (*b*) 3.98; (*c*) 5.48.

finally as the frequency is increased further the interface breaks up and the two fluids tend to form an emulsion in the vicinity of the original interface. During the process of destruction of the STP–TLA227 interface, the air–STP interface remains smooth and assumes a paraboloid-like shape.

The photographs in figure 7 show the changes in the STP–TLA227 interfacial shape with increasing angle of twist, keeping angular frequency ω fixed. At a constant frequency the interface becomes increasingly more deformed as the angle of twist is increased. If the angular frequency is high enough, break-up of the interface takes place as the amplitude of the motion is increased.

In all experimental runs, the time-dependent part of the deformation of the STP–TLA227 interface is observed to be small (almost negligible) compared with the mean part. The time-dependent part varies at a frequency twice as large as the frequency of the cylinder, and is better observed at the air–STP interface, where the ratio of the time-dependent part to the mean is slightly higher than the ratio for

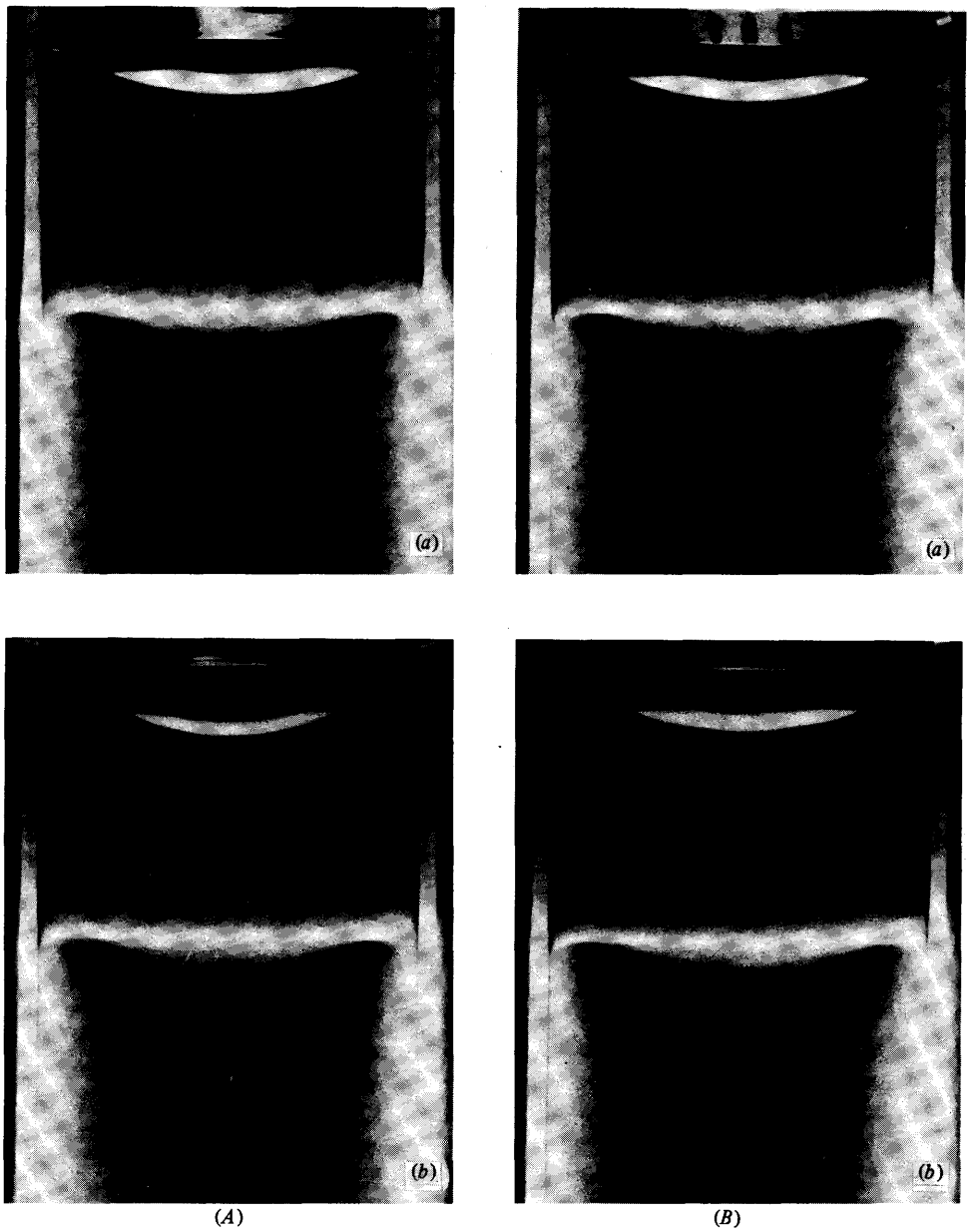

FIGURE 8. The time-dependent versus the mean contributions in the STP–TLA227 interfacial shapes: (*A*) near maximum velocity; (*B*) near minimum velocity. $\Theta = 3.98$ rad. ω (rad/s): (*a*) 6.08; (*b*) 6.62.

the STP–TLA227 interface. Figures 8 and 9 show the shapes of both interfaces at times when the speed of the cylinder is nearly at its maximum value (part *A*) and is nearly zero (part *B*) for various angles of twist and angular frequencies. At the lower angle of twist (e.g. figure 8) it is difficult to identify any difference between the shapes at two extremes in the cycle, but at the higher angle of twist (e.g. figure 9) the difference is quite evident, particularly at the air–STP interface.

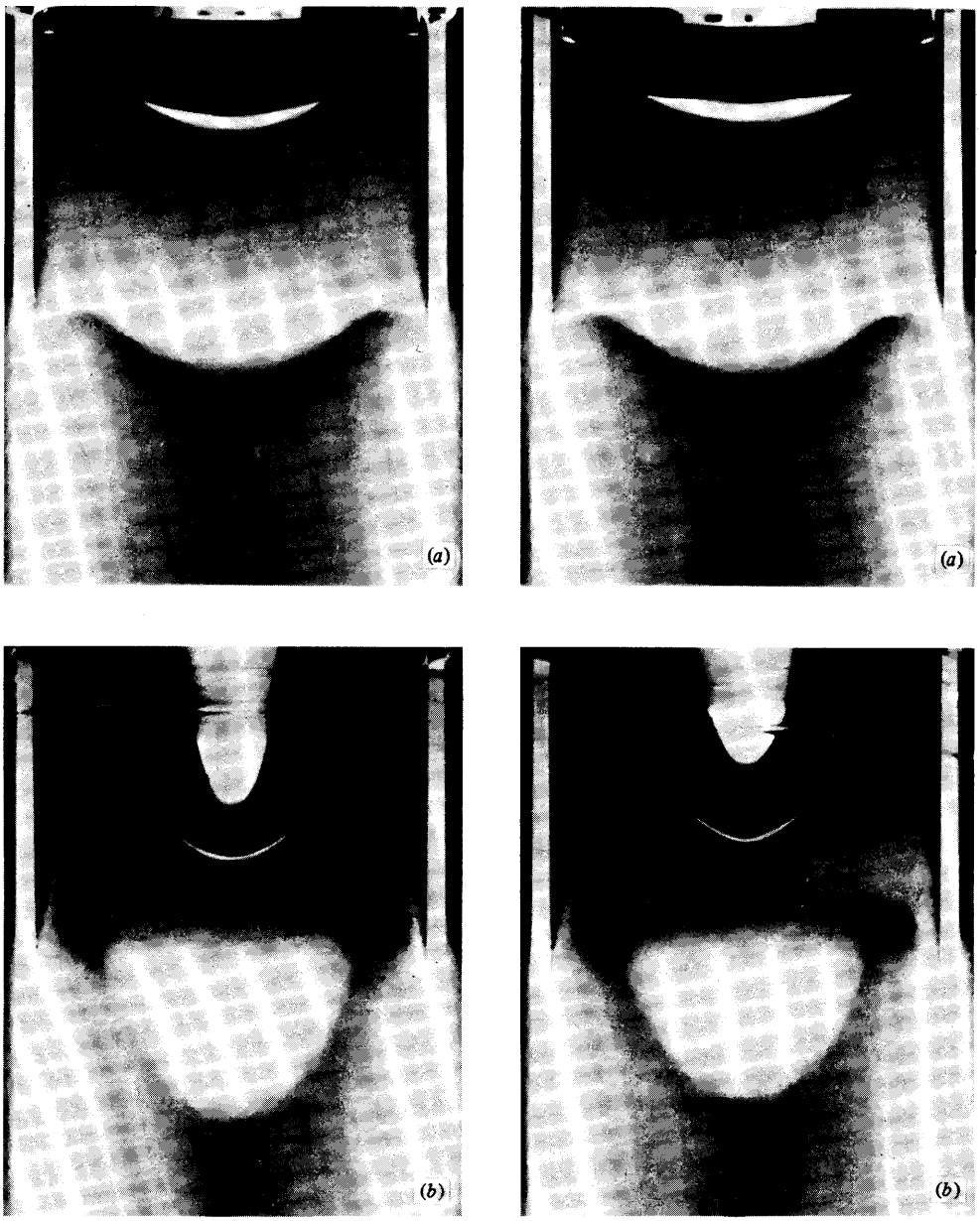

FIGURE 9. The time-dependent versus the mean contributions in the STP-TLA227 interfacial shapes: (*A*) near maximum velocity; (*B*) near minimum velocity. $\Theta = 5.48$ rad. ω (rad/s): (*a*) 6.02; (*b*) 10.52.

7. Results

7.1. *First-order velocity distributions*

In §3.2 we showed that, when ω approaches zero, the first-order azimuthal velocity distribution is a solid-body oscillation. When $\omega \neq 0$, the velocity distribution will deviate from this asymptotic form. It is best to illustrate the deviation by plotting the distributions of $2|\omega^*_{(j)}(R, Z; \omega)|$ and phase lag $\delta_{(j)}(R, Z; \omega)$. The more these

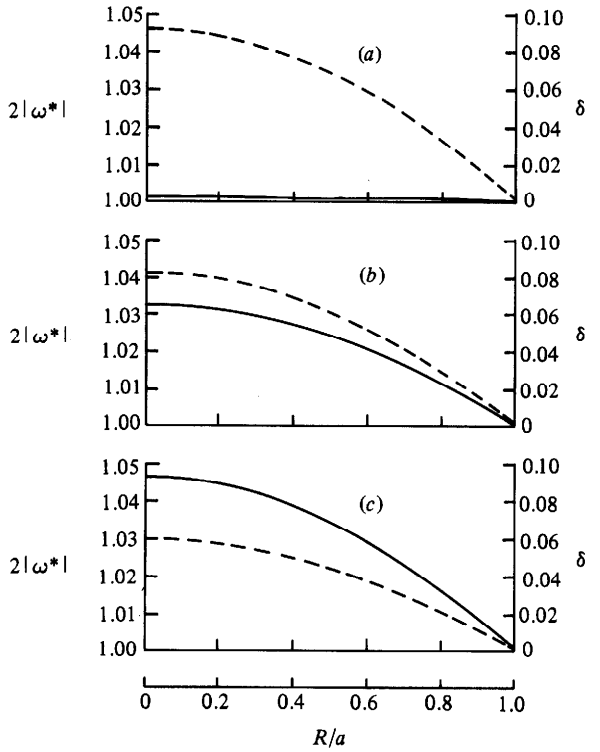

FIGURE 10. Radial distributions of the modulus and the phase lag of the first-order azimuthal angular velocity $\omega^*(R, Z; \omega)$ at $\omega = 3.173$ rad/s. ——, $2|\omega^*|$; – – –, δ. (*a*) $z/a \to +\infty$; (*b*) $z/a = 0$; (*c*) $z/a \to -\infty$.

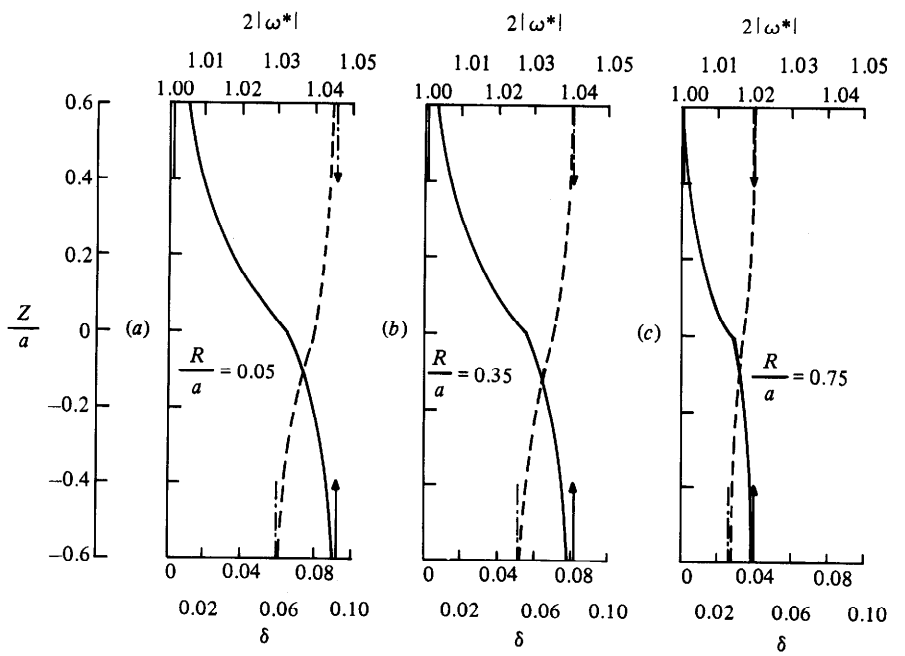

FIGURE 11. Axial distributions of the modulus $2|\omega^*|$ (——) and the phase lag δ(– – –) of the first-order azimuthal angular velocity at $\omega = 3.173$ rad/s. Asymptotic values at infinity: ——, $2|\omega^*|$; —·—, δ.

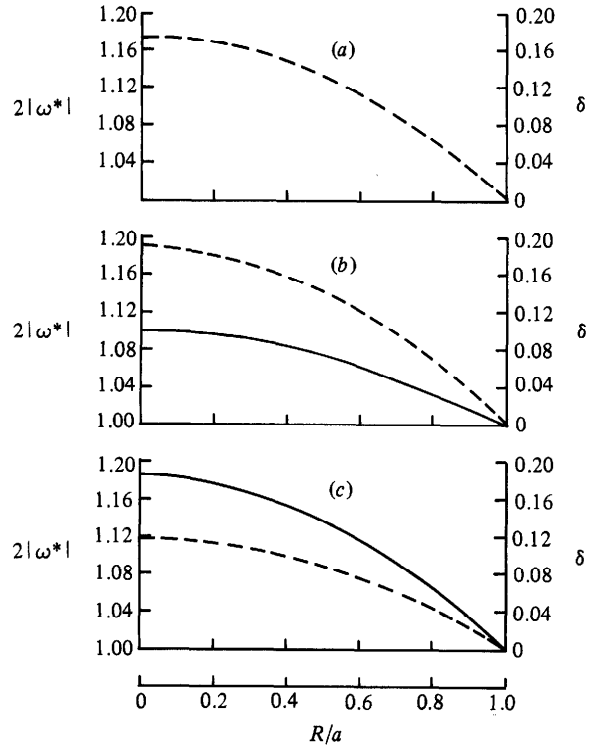

FIGURE 12. Radial distributions of the modulus and the phase lag of the first-order azimuthal angular velocity $\omega^*(R, Z; \omega)$ at $\omega = 6.082$ rad/s. For legend see figure 10.

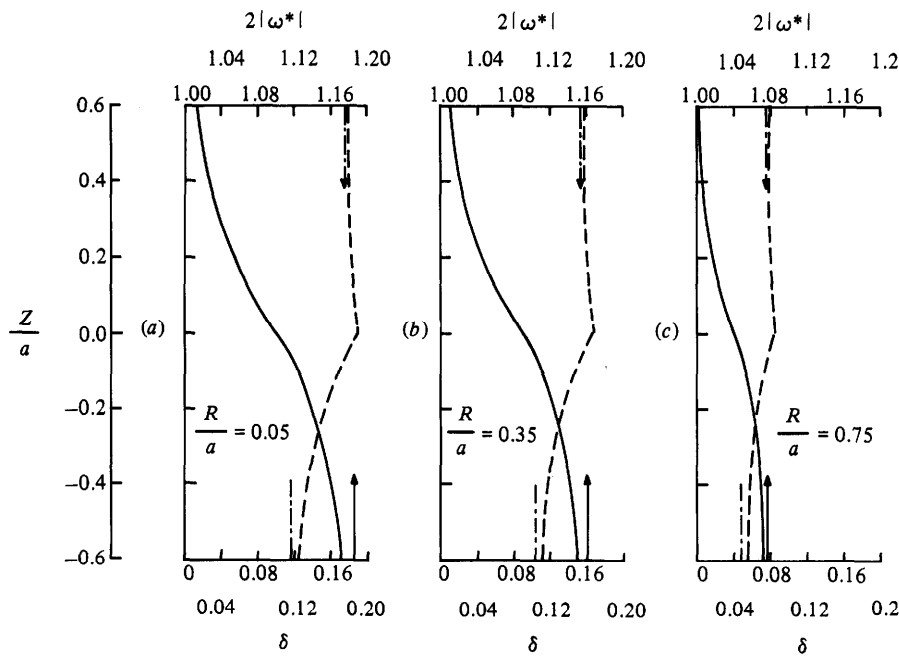

FIGURE 13. Axial distributions of the modulus $2|\omega^*|$ and the phase lag δ of the first-order azimuthal angular velocity at $\omega = 6.082$ rad/s. For legend see figure 11.

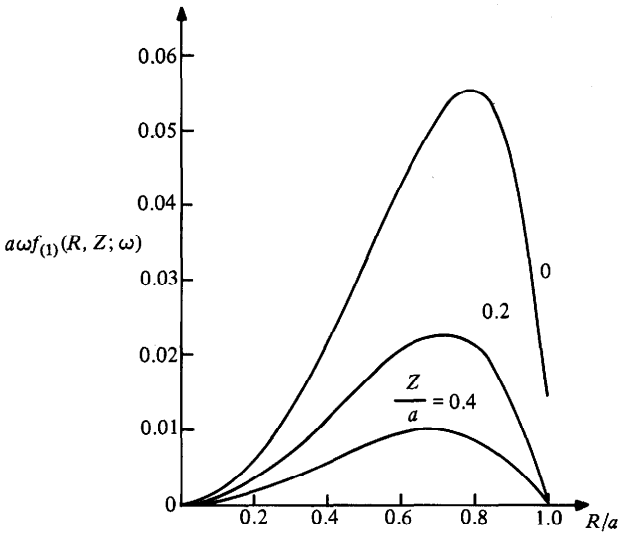

FIGURE 14. Radial distributions of $a\omega f_{(1)}(R, Z; \omega)$, where $f_{(1)}(R, Z; \omega)$ is the forcing function in (5.2a) with $j = 1$ and $\omega = 3.173$ rad/s. ——, $f_{(j)}(R, Z; \omega)$ is computed using (5.11), with $L = 10$ and $M = N = 9$; – – –, $f_{(j)}(R, Z; \omega)$ is approximated by (5.17), with $N = M = 10$. (At small ω, e.g. $\omega = 3.173$ rad/s, the curves of the two families ((5.11) and (5.17)) coincide.)

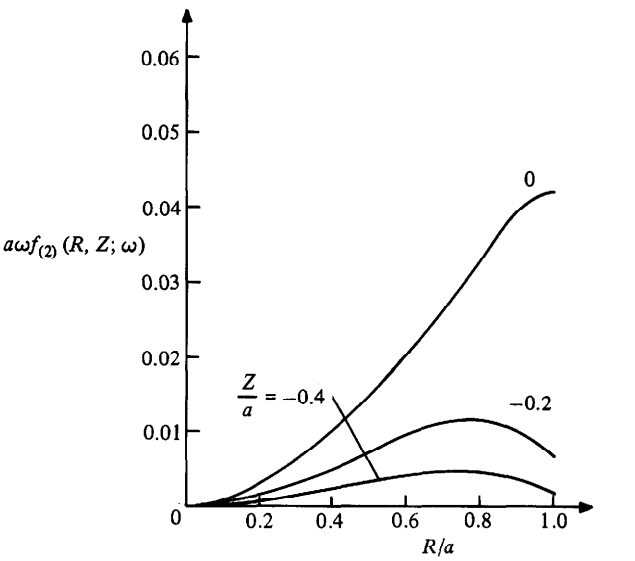

FIGURE 15. Radial distributions of $a\omega f_{(2)}(R, Z; \omega)$, where $f_{(2)}(R, Z; \omega)$ is the forcing function in (5.2a) with $j = 2$ and $\omega = 3.173$ rad/s. For legend see figure 14.

functions differ from unity and zero respectively, the larger the discrepancy between the distribution of $V_{(j)}(R, Z, t; \omega)$ and the solid-body oscillation (3.29).

With the fluid properties given in table 2, we will compute, using the results given in § 3.1, the function $\omega^*(R, Z; \omega) = \omega^*_{(j)}(R, Z; \omega)$ in which $j = 1$ when $Z \geqslant 0$ and $j = 2$ when $Z \leqslant 0$. The truncation number N, appearing in (3.20a, b), is taken to be 10. The modulus $2|\omega^*(R, Z; \omega)|$ and phase lag $\delta(R, Z; \omega)$ are next computed and plotted in figures 10–13. Figure 10 shows radial distributions of $2|\omega^*(R, Z; \omega)|$ and $\delta(R, Z; \omega)$ at

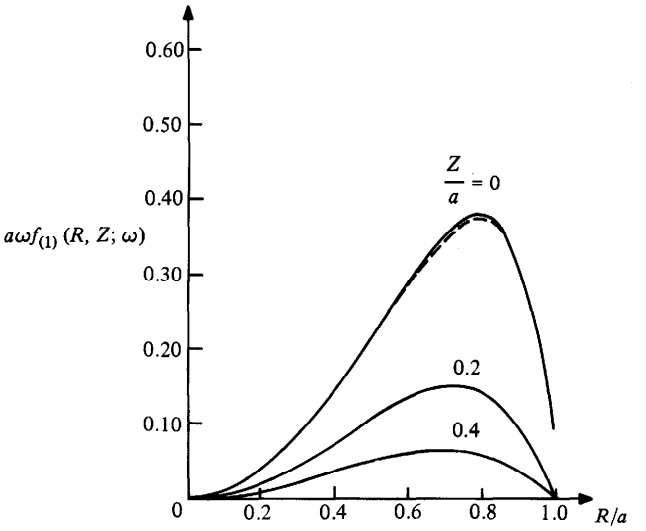

FIGURE 16. Radial distributions of $a\omega f_{(j)}(R, Z; \omega)$ with $j = 1$ and $\omega = 6.082$ rad/s. For legend see figure 14.

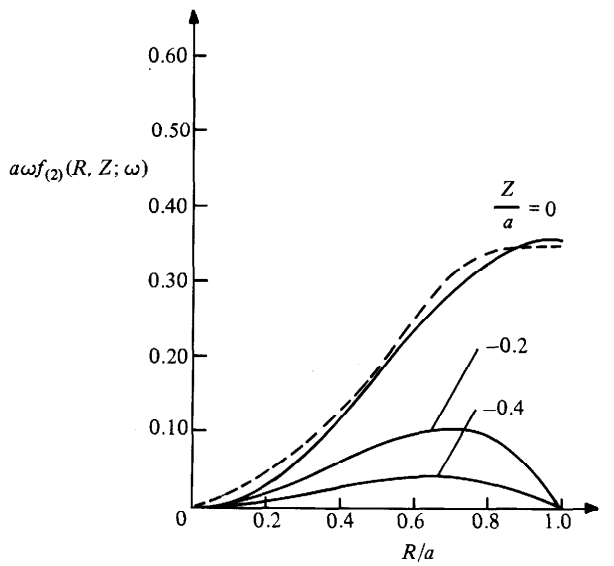

FIGURE 17. Radial distributions of $a\omega f_{(j)}(R, Z; \omega)$ with $j = 2$ and $\omega = 6.082$ rad/s. For legend see figure 14.

$Z = \pm\infty$ and at the undisturbed interface, for $\omega = 3.173$ rad/s. Figure 11 shows axial distributions of these functions at $R/a = 0.05$, 0.35 and 0.75 for the same angular frequency ω. The expressions for velocities in (3.20) and (3.21) should agree at $Z = 0$ for all $R/a \in [0, 1]$. In fact we achieve agreement with the approximation associated with $N = 10$. Figures 10 and 11 demonstrate that $V_{(j)}(R, Z, t; \omega)$, with $\omega = 3.173$ rad/s, deviates only mildly from solid-body oscillation $V = R \sin \omega t$. As the angular frequency ω is increased, this deviation becomes more pronounced. Figures 12 and 13 show the corresponding distributions at $\omega = 6.082$ rad/s.

At any particular angular frequency ω, the difference between $\omega^*(R, Z; \omega)$ and

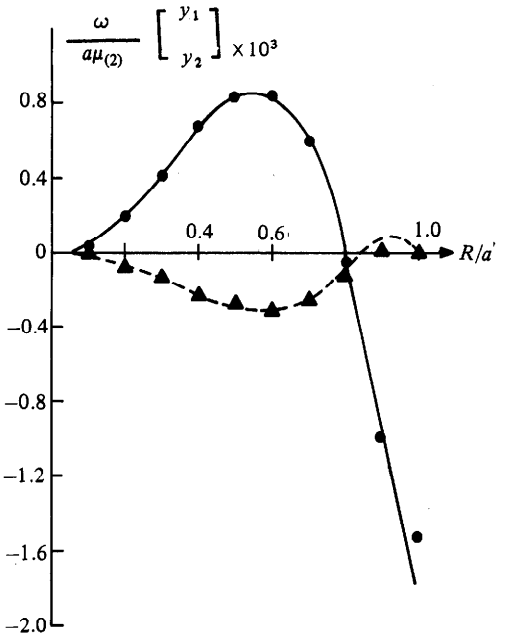

FIGURE 18. Representation of the components of the vector $\begin{bmatrix} y_1 \\ y_2 \end{bmatrix}$, defined in (5.49$a$), by the truncated series

$$\sum_{-10}^{10} a_n \begin{bmatrix} \phi_1^{(n)} \\ \phi_2^{(n)} \end{bmatrix},$$

at $\omega = 3.173$ rad/s.

$$\left\{\begin{matrix}---\\ \text{——}\end{matrix}\right\}, \frac{\omega}{a\mu_{(2)}} \times 10^3 \begin{Bmatrix} y_1 \\ y_2 \end{Bmatrix}; \quad \left\{\begin{matrix}\blacktriangle \\ \bullet\end{matrix}\right\}, \frac{\omega}{a\mu_{(2)}} \times 10^3 \sum_{-10}^{10} a_n \begin{Bmatrix} \phi_1^{(n)} \\ \phi_2^{(n)} \end{Bmatrix}.$$

solid-body oscillation is largest along the centreline of the cylinder, and zero along the cylinder wall. The Z-dependence of $\omega_{(j)}^*(R, Z; \omega)$ is significant only in the vicinity of the STP–TLA227 interface. As seen in figures 11 and 13, the functions $\omega_{(j)}(R, Z; \omega)$ have nearly attained, at distance about $0.6a$ away from the undisturbed interface, their values at $Z = \pm\infty$.

7.2. *Second-order mean motion*

We now compute the forcing function $f_{(j)}(R, Z; \omega)$ in (5.2a) for the stream function $\psi_{(j)}(R, Z; \omega)$ of the mean motion. To illustrate the validity of the approximations in (5.9) and (5.10) we compute the dimensionless function $a\omega f_{(j)}(R, Z; \omega)$, using the truncated version of (5.11), in which the limits of summations on l, m and n subscripts are $L = 10$ and $M = N = 9$ respectively. The above function is denoted by $a\omega f_{(j)}^{\langle 10, 9, 9\rangle}(R, Z; \omega)$.

Radial distributions of $a\omega f_{(j)}^{\langle 10, 9, 9\rangle}(R, Z; \omega)$ at the undisturbed interface and at distances $0.2a$ and $0.4a$ away from the undisturbed interface are plotted with solid lines in figures 14 and 15, in which $\omega = 3.173$ rad/s, and in figures 16 and 17, in which $\omega = 6.032$ rad/s. The approximate version for $f_{(j)}^{\langle 10, 9, 9\rangle}(R, Z; \omega)$ is the expression (5.17), where the limits of summations are $N = M = 10$. This approximate function is also used to compute $a\omega f_{(j)}(R, Z; \omega)$ which is plotted with dashed lines in figures 14–17. At low angular frequency ω, e.g. $\omega = 3.173$ rad/s, the approximate function

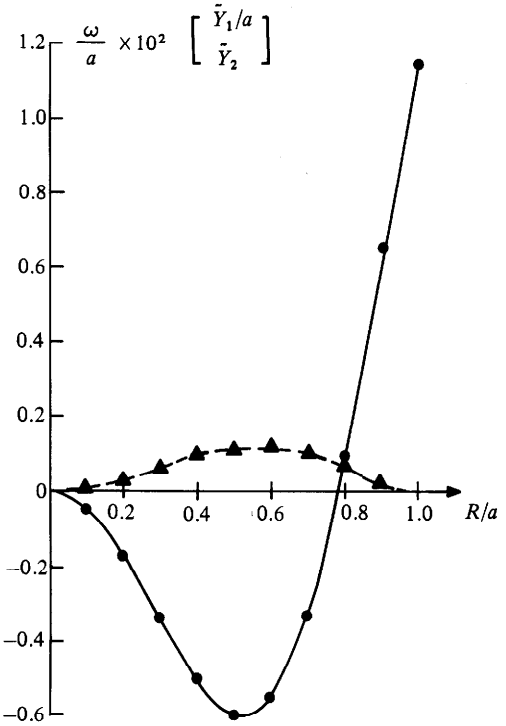

FIGURE 19. Representation of the components of the vector $\begin{bmatrix} \tilde{Y}_1 \\ \tilde{Y}_2 \end{bmatrix}$, defined in (5.49*b*), by the truncated series

$$\sum_{-10}^{10} b_n \begin{bmatrix} \phi_1^{(n)}/P_n \\ \phi_2^{(n)} \end{bmatrix}$$

at $\omega = 3.173$ rad/s.

$$\left\{\begin{matrix}---\\ \text{———}\end{matrix}\right\}, \frac{\omega}{a} \times 10^2 \begin{Bmatrix} \tilde{Y}_1/a \\ \tilde{Y}_2 \end{Bmatrix}; \quad \left\{\begin{matrix}\blacktriangle \\ \bullet\end{matrix}\right\}, \quad \frac{\omega}{a} \times 10^2 \sum_{-10}^{10} b_n \begin{Bmatrix} \phi_1^{(n)}/P_n \\ \phi_2^{(n)} \end{Bmatrix}.$$

(5.17) gives more or less the same values as the original function (5.11). The dashed lines coincide with the solid lines in figures 14 and 15. At larger ω some discrepancy between the approximate and original functions $f_{(j)}(R, Z; \omega)$ is noticeable. The discrepancy is most conspicuous along the interface, and is smaller at distances further away from the interface. Figures 16 and 17 show the distributions of the approximate and original functions $f_{(j)}(R, Z; \omega)$ at $\omega = 6.082$ rad/s. In these figures, a small discrepancy is observed between the distributions along the undisturbed interface, but the discrepancies at distances $0.2a$ and $0.4a$ away from the interface are too small to be graphically distinguishable.

The discrepancy for TLA227 on figure 17 is relatively larger than the one for STP on figure 16. This is expected because, as ω increases, $\mathcal{A}^2_{(2)}(\omega)$ grows in magnitude faster than $\mathcal{A}^2_{(1)}(\omega)$; therefore the approximation in (5.9) for TLA227 becomes less accurate before the one for STP does. In computing the mean motion $\psi_{(j)}(R, Z; \omega)$ at second order, we will use the approximate expression (5.17) with $N = M = 10$ for $f_{(j)}(R, Z; \omega)$, and (3.20*a*, *b*) with $N = 10$.

Once the forcing function $f_{(j)}(R, Z; \omega)$ is known, the integrals in (5.8) and (5.19) can be evaluated, using Simpson's rule, to determine the particular function $\psi_{P(j)}(R, Z; \omega)$, which is defined by (5.1) and (5.2). On the other hand, the stream

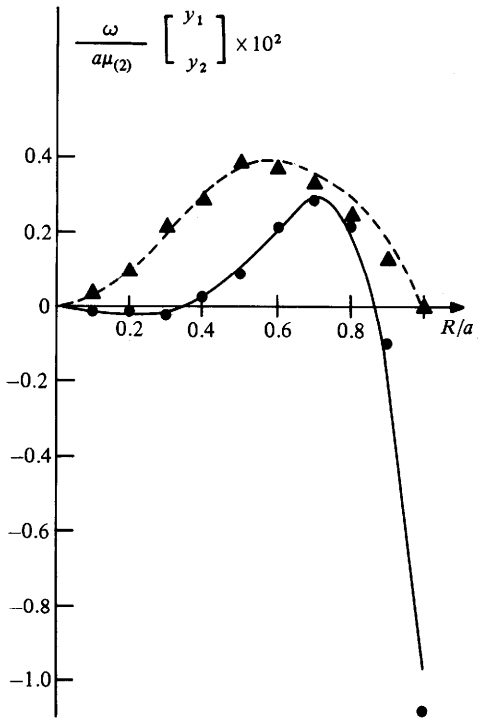

FIGURE 20. Representation of the components of the vector $\begin{bmatrix} y_1 \\ y_2 \end{bmatrix}$ at $\omega = 6.082$ rad/s.

$$\left\{\begin{matrix} --- \\ —— \end{matrix}\right\}, \frac{\omega}{a\mu_{(2)}} \times 10^2 \begin{Bmatrix} y_1 \\ y_2 \end{Bmatrix}; \quad \left\{\begin{matrix} \blacktriangle \\ \bullet \end{matrix}\right\}, \frac{\omega}{a\mu_{(2)}} \times 10^2 \sum_{-10}^{10} a_n \begin{Bmatrix} \phi_1^{(n)} \\ \phi_2^{(n)} \end{Bmatrix}.$$

function $\Psi_{\mathrm{H}(j)}(R, Z; \omega)$, which satisfies the homogeneous problem (5.2) where $f_{(j)}(R, Z; \omega) = 0$, is given by the biorthogonal series (5.20). Since the eigenvalues p_n are known (Yoo 1977), it remains for us to find the coefficients A_n and B_n in (5.20). To this end, we combine A_n and B_n, using (5.50), into new unknowns a_n and b_n. The new unknowns can be calculated from (5.54), and from solving a truncated system of linear equations in (5.53*b*).

The procedure for obtaining the unknowns a_n and b_n requires the vectors $\begin{bmatrix} y_1 \\ y_2 \end{bmatrix}$ and $\begin{bmatrix} \tilde{Y}_1 \\ \tilde{Y}_2 \end{bmatrix}$, defined in (5.49*a*, *b*). Since $\omega_{(j)}^*$ and $\psi_{\mathrm{P}(j)}$ have been completely determined, it is possible to derive explicit expressions for components of these vectors, as given in the Appendix. We note that since the components y_1, y_2, $\tilde{Y}_1$ and $\tilde{Y}_2$ are real, the coefficients a_n and $a_{(-n)}$, and b_n and $b_{(-n)}$ are complex-conjugate pairs. For practical purposes, we only need to compute the first ten coefficients a_n and b_n, $n = 1, 2, \ldots, 10$.

The series on the left-hand sides of (5.52*a*, *b*), with $N = 10$, are already good approximations for the vectors $\boldsymbol{y}$ and $\boldsymbol{Y}$. In figures 18 and 19 we plot dimensionless components of

$$\frac{\omega}{a\mu_{(2)}}\begin{bmatrix} y_1 \\ y_2 \end{bmatrix} \quad \text{and} \quad \frac{\omega}{a}\begin{bmatrix} \tilde{Y}_1/a \\ \tilde{Y}_2 \end{bmatrix}$$

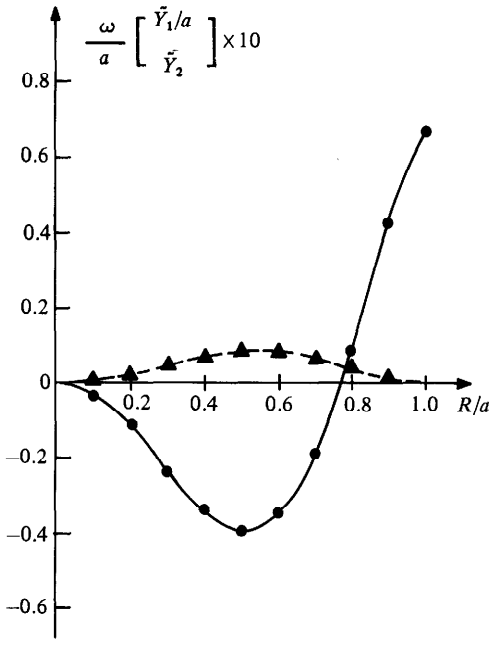

FIGURE 21. Representation of the components of the vector $\begin{bmatrix}\tilde{Y}_1\\ \tilde{Y}_2\end{bmatrix}$ at $\omega = 6.082$ rad/s.

$$\left\{\begin{matrix}---\\ \_\_\_\end{matrix}\right\};\quad 10\frac{\omega}{a}\begin{Bmatrix}\tilde{Y}_1/a\\ \tilde{Y}_2\end{Bmatrix};\quad \left\{\begin{matrix}\blacktriangle\\ \bullet\end{matrix}\right\},\ 10\frac{\omega}{a}\sum_{-10}^{10} b_n\begin{Bmatrix}\phi_1^{(n)}/P_n\\ \phi_2^{(n)}\end{Bmatrix}.$$

for $\omega = 3.173$ rad/s by continuous and broken lines, while values of the corresponding biorthogonal series

$$\frac{\omega}{a\mu_{(2)}}\left\{\sum_{-10}^{10} a_n \boldsymbol{\phi}^{(n)}\right\} \quad \text{and} \quad \frac{\omega}{a}\left\{\sum_{-10}^{10} b_n\begin{bmatrix}\phi_1^{(n)}/P_n\\ \phi_2^{(n)}\end{bmatrix}\right\}$$

are plotted with dots. Figures 20 and 21 show graphs of the above functions at $\omega = 6.082$ rad/s. We observe, from these four figures, that the series in (5.52*b*) approximates to $\tilde{\boldsymbol{Y}}$ more closely than the series in (5.52*a*) does to $\boldsymbol{y}$.

Given a_n and b_n, we can calculate A_n and B_n, using the inversion (5.51). In this way, the stream function $\psi_{\mathrm{H}(j)}$ is determined. For each $j = 1, 2$, level lines of $\psi_{\mathrm{H}(j)}$ form a series of alternate eddies of opposite direction. Each series starts at the interface with a half-eddy in clockwise rotation. The magnitude of $\psi_{\mathrm{H}(j)}$ decreases exponentially with $|Z|$. Typical level lines of $\psi_{\mathrm{H}(j)}$ are shown in figures 22 and 23, where the angular frequency ω is 3.173 rad/s.

The total stream function $\psi_{(j)}(R, Z; \omega)$ of the mean motion at second order is found by adding $\psi_{\mathrm{H}(j)}$ to $\psi_{\mathrm{P}(j)}$. For each $j = 1, 2$, the level lines of $\psi_{(j)}$ form a single eddy. Figures 24 and 25 show these level lines at $\omega = 3.173$ rad/s. The two eddies, one being above and one below the interface, rotate in the same (counterclockwise) direction.

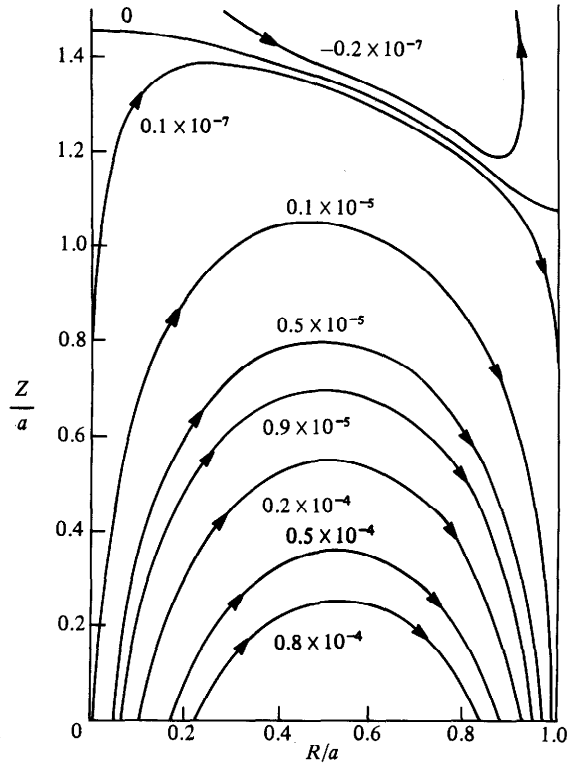

FIGURE 22. Level lines at $\omega = 3.173$ rad/s for the upper biharmonic series $(\omega/a^3)\psi_{H(1)}$.

7.3. *Mean interfacial shape*

Since the interfacial tension is zero, the mean interfacial shape is obtained from the relation

$$\frac{\mathring{h}\left(\frac{R}{a};\epsilon\right)}{a} = \frac{1}{a}\left(\frac{\epsilon^2}{2}\frac{a}{\omega^2}\bar{\bar{h}}\left(\frac{R}{a};\omega\right)\right) = \frac{1}{2}\left(\frac{\epsilon}{\omega}\right)^2\bar{\bar{h}}\left(\frac{R}{a};\omega\right) \tag{7.1}$$

where $\bar{\bar{h}}$ is given by (5.95a,b). The relation between ϵ and angular frequency ω and angle of twist Θ of the cylinder can be shown, from the sinusoidal oscillations of the cylinder, to be

$$\epsilon = \tfrac{1}{2}\omega\Theta. \tag{7.2}$$

Substituting (7.2) in (7.1), we get

$$\frac{\mathring{h}}{a}\left(\frac{R}{a};\epsilon\right) = \tfrac{1}{8}\Theta^2\bar{\bar{h}}\left(\frac{R}{a};\omega\right). \tag{7.3}$$

The theoretical mean interfacial shape $\mathring{h}(R/a;\epsilon)/a$ will be computed at different angles of twist and angular frequencies, and compared with the ones observed in the experiments. Figures 26–28 show series of mean interfacial shapes $\mathring{h}(R/a;\epsilon)/a$ for increasing sequences of ω, at angles of twist $\Theta = 2.50$, 3.98 and 5.48 rad respectively. Table 3 gives the angular frequency ω and the corresponding ϵ for each case, from (a) to (e), of these figures.

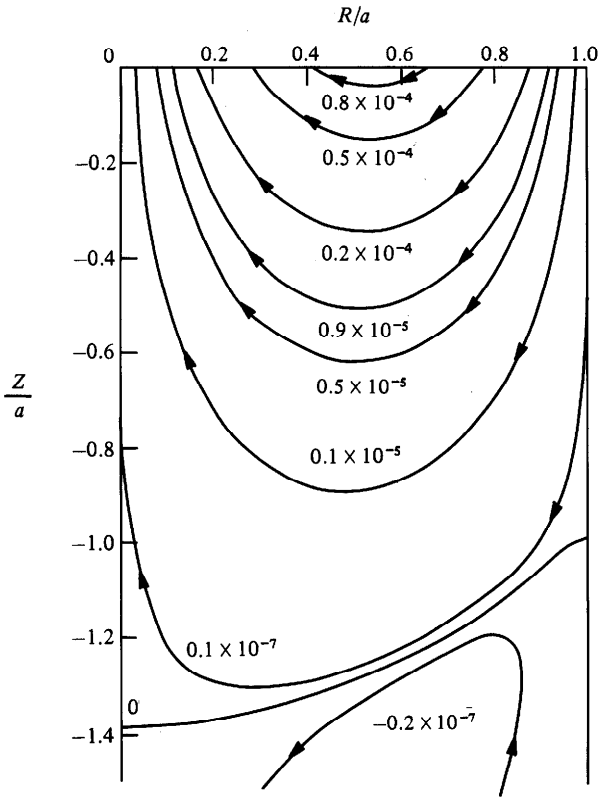

FIGURE 23. Level lines at $\omega = 3.173$ rad/s for the lower biharmonic series $(\omega/a^3)\psi_{H(2)}$.

In the above figures, the theoretical predictions are plotted with dotted lines, and the observed mean interfacial shapes are shown as solid lines. Careful study of these graphs reveals the following results.

Our theoretical prediction, with interfacial tension being neglected, is that the curvature of the STP–TLA227 interface is convex at the centre of the cylinder and concave at the edge. In all cases, except that in figure 26(*e*), predicted interfacial shapes fall slightly below the undisturbed level ($Z = 0$) at the cylinder wall ($R = a$). It is only a coincidence in figure 26(*e*) that the theoretical shape joins the wall at $Z = 0$. The experimental interfaces also have the characteristic of being convex at the centerline, and concave at the outer edge. However, the edge of a real STP–TLA 227 interface is observed to be fixed, so that when the real interface tends to drop below the undisturbed level, its curvature becomes convex. This secondary change in curvature in a small neighbourhood of the cylinder wall is caused by the action of interfacial tension coupled with the fixed-edged condition, and can be seen in case (*e*) of figures 26 and 27.

At each angle of twist, the first graph (*a*) shows a good agreement between our theory and experiments. As ω (hence ϵ) is increased, the discrepancy between second-order theoretical prediction and experimental measurements grows. The predicted interface, however, retain shapes qualitatively the same as the experimental ones when ω is less than 6.62 rad/s.

One way to check the validity of a second-order theory is to study the change of

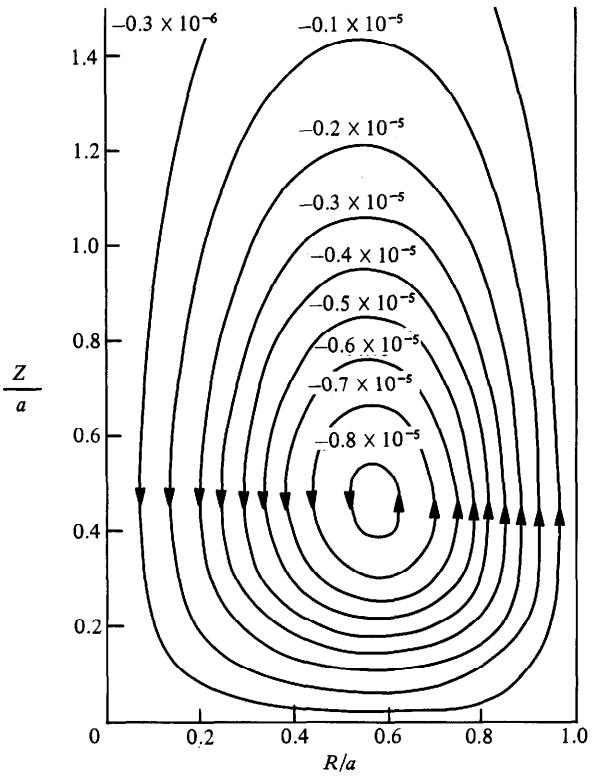

FIGURE 24. Level lines at $\omega = 3.173$ rad/s for the upper stream function $(\omega/a^3)\psi_{(1)}$.

a physical interfacial shape caused by a variation in angle of twist Θ. A physical interfacial shape is well monitored by a second-order theory only when the physical interfacial shape, itself, is indeed proportional to ϵ^2, and therefore to Θ^2. We thus compare physical interfacial shapes at a fixed angular frequency but with different angles of twist. Close examination of the solid lines in the following pairs of graphs 27(*a*) and 28(*b*), 26(*c*) and 27(*d*), and 26(*d*) and 27(*e*) reveals that these physical interface shapes at the same angular frequency, but with different angles of twist, are not exactly proportional to each other. A general trend, observed from these pairs of graphs, is that the intersection between a physical interfacial shape and the line $Z = 0$ is shifted nearer to the cylinder wall as Θ is increased. The average value of ϵ in these cases is roughly 10 rad^2/s. Experimental data have thus indicated that at these values of Θ and ϵ, there is noticeable contribution from terms $o(\epsilon^2)$.

7.4. *Region of validity of the analysis*

We shall follow the approach of Joseph *et al.* (1973) and use the criterion

$$\mathbb{F} \ll 1 \tag{7.4}$$

to estimate the region of validity for our second-order theory. The Froude number $\mathbb{F}$ is defined here as follows:

$$\mathbb{F} \equiv \frac{\boldsymbol{\Omega}^2 l}{[\![\rho]\!] g/\rho_{(2)}}, \tag{7.5}$$

where $\boldsymbol{\Omega}^2 = \frac{1}{2}\epsilon^2 = \frac{1}{8}\Theta^2\omega^2$ is the mean-square angular velocity and l is a characteristic

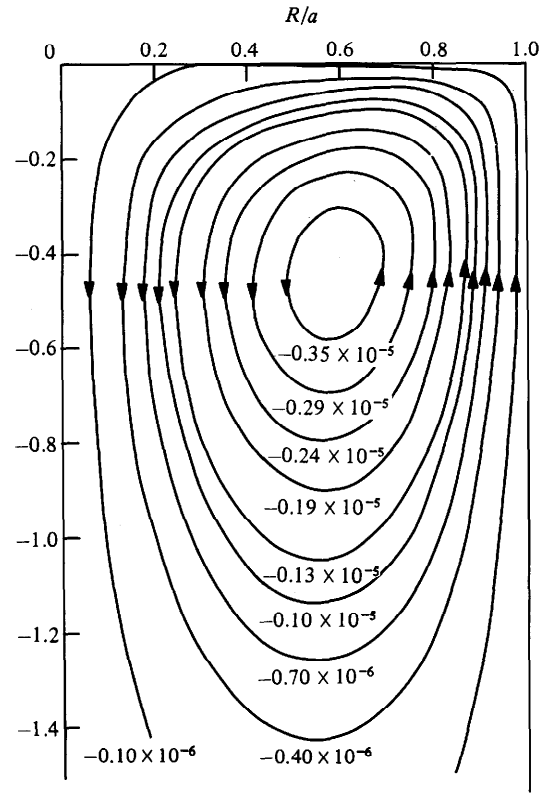

FIGURE 25. Level lines at $\omega = 3.173$ rad/s for the lower stream function $(\omega/a^3)\psi_{(2)}$.

lengthscale, dependent on fluid properties, angular frequency ω and the cylinder radius a. This lengthscale can be chosen as

$$l = \tfrac{1}{8}\Theta^2\omega^2|ah^*(1;\omega)|,$$

where $h^*(R;\omega)$ has been introduced in (5.99). Our analysis does not show a simple expression for $h^*(a;\omega)$. Nevertheless, $h^*(a;\omega)$ can be computed, using the formula

$$h^*(1;\omega) = \frac{\bar{\bar{h}}(1;\omega)}{\omega^2} - \frac{a}{4g}. \tag{7.7}$$

Substitution of (7.7) in (7.6) yields

$$l = \frac{a\Theta^2}{8}\left|\hat{h}(1;\omega) - \frac{a\omega^2}{4g}\right|. \tag{7.8}$$

In particular for the STP–TLA227 interface, our calculations have consistently shown that $\hat{h}(1;\omega) < 0$ for small ω, and therefore by (7.8), we have

$$l > \frac{a^2\Theta^2\omega^2}{32g}. \tag{7.9}$$

The criterion (7.4) and the definition (7.5) moreover imply that, for a given Θ, larger l requires smaller limiting ω_c. Hence, if we take

$$l = \frac{a^2\Theta^2\omega^2}{32g}, \tag{7.10}$$

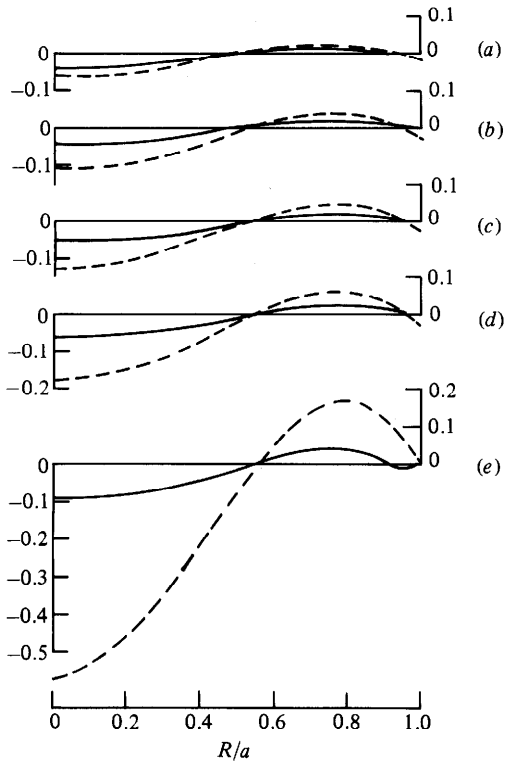

FIGURE 26. The mean interfacial shapes $\hat{h}/a$ between STP and TLA227, at angle of twist $\Theta = 2.50$ rad. See table 3 for details. – – –, theoretical predictions; ——, experimental observations.

we will obtain a larger limiting value for ω_c. Using (7.5) and (7.6) in (7.4), we find

$$\omega \ll \omega_c = \frac{4}{\Theta}\left[\frac{g\left(\frac{[\![\rho]\!]}{\rho_{(2)}}\right)^{\frac{1}{2}}}{a}\right]^{\frac{1}{2}}. \tag{7.11}$$

Limiting values ω_c for some specific angles of twist used in the experiments are given in table 4. These limits are consistent with our results in § 7.3.

This work was supported by the U.S. Army Research Office.

Appendix. Expressions for the components of y and $\tilde{Y}$ as defined by (5.49)

Using the first-order solution (3.19), (3.20) and the approximations (5.9), we find that at $z = 0$

$$\omega^*_{(1),z} = \sum_{n=1}^{\infty} -\frac{\sigma_n}{a} C_n \frac{1}{R} J_1\left(\sigma_n \frac{R}{a}\right), \tag{A 1a}$$

$$\omega^*_{(2),z} = \sum_{n=1}^{\infty} \frac{\sigma_n}{a} D_n \frac{1}{R} J_1\left(\sigma_n \frac{R}{a}\right), \tag{A 1b}$$

$$\omega^*_{(1),R} = -\left[\frac{a}{2}\frac{\mathbb{A}_{(1)}}{J_1(\mathrm{i}\mathbb{A}_{(1)}a)}\frac{J_2(\mathrm{i}\mathbb{A}_{(1)}R)}{R} + \sum_{n=1}^{\infty} C_n \frac{\sigma_n}{a}\frac{J_2\left(\sigma_n \frac{R}{a}\right)}{R}\right], \tag{A 1c}$$

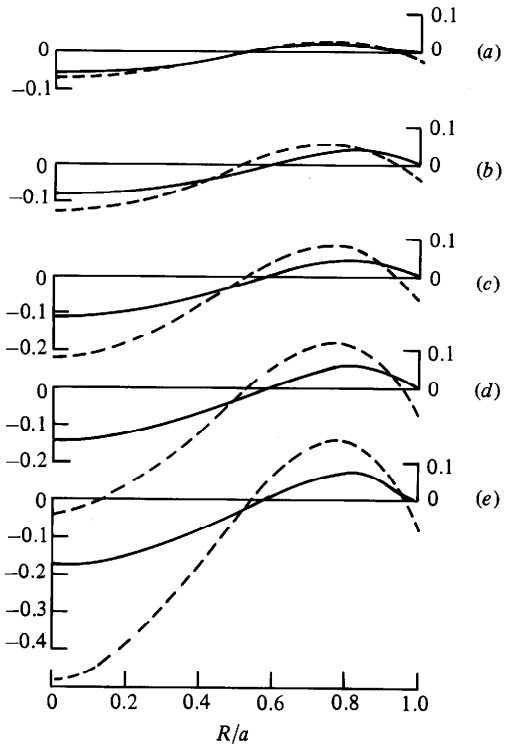

FIGURE 27. The mean interfacial shapes $\hat{h}/a$ between STP and TLA227, at angle of twist $\Theta = 3.98$ rad. See caption of figure 26 and table 3 for details.

and $\omega^*_{(2),R}$ can be expressed similarly as $\omega^*_{(1),R}$ with subscript (2) and coefficient D_n replacing subscript (1) and coefficient C_n respectively. Moreover, (4.13*b*) leads us to

$$2R[\![\hat{\boldsymbol{S}}_{2RZ}[\boldsymbol{U}_1]]\!] = [\![2R^3(\omega^*_{,Z}\bar{\omega}^*_{,R}+\bar{\omega}^*_{,Z}\omega^*_{,R})\Sigma_1]\!]. \tag{A 2}$$

Substituting (A 1) into (A 2), and rearranging terms on the right-hand side, (A 2) may be written in the form

$$2R[\![\hat{\boldsymbol{S}}_{2RZ}[\boldsymbol{U}_1]]\!] = \sum_{n=1}^{\infty} \mathscr{M}_n(R) + \sum_{m=2}^{\infty} \check{\mathscr{M}}_m(R), \tag{A 3}$$

where

$$\mathscr{M}_n(R) = -2R\sigma_n J_1\left(\sigma_n \frac{R}{a}\right) \mathrm{Re}\left\{\frac{\mathbb{A}_{(2)} J_2(\mathrm{i}\mathbb{A}_{(2)}R)}{J_1(\mathrm{i}\mathbb{A}_{(2)}a)} \bar{D}_n \Sigma_{(2)1} + \frac{\mathbb{A}_{(1)} J_2(\mathrm{i}\mathbb{A}_{(2)}R)}{J_1(\mathrm{i}\mathbb{A}_{(1)}a)} \bar{C}_n \Sigma_{(1)1}\right\}, \tag{A 4a}$$

$$\check{\mathscr{M}}_m(R) = \sum_{n=1}^{m-1} \mathscr{M}_{(m-n)n}(R) \quad (m \geqslant 2) \tag{A 4b}$$

and

$$\mathscr{M}_{ln}(R) = -4R\frac{\sigma_l\sigma_n}{a^2} J_2\left(\sigma_l \frac{R}{a}\right) J_1\left(\sigma_n \frac{R}{a}\right) \mathrm{Re}\{D_l \bar{D}_n \Sigma_{(2)1} + C_l \bar{C}_n \Sigma_{(1)1}\}. \tag{A 4c}$$

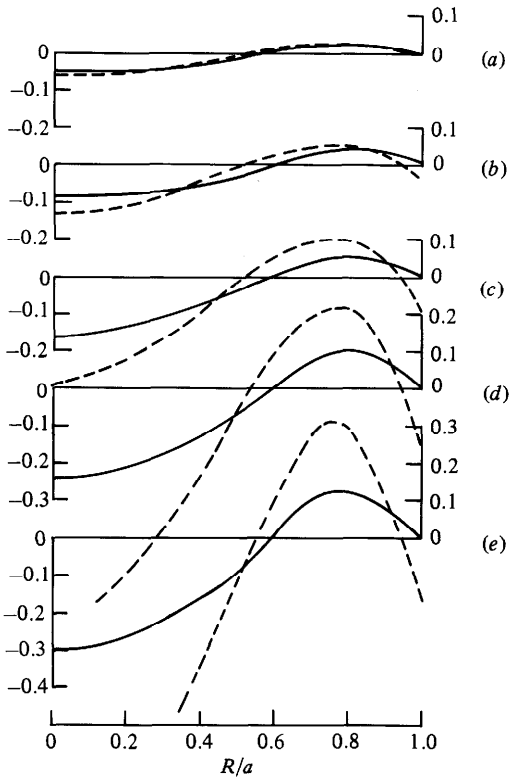

FIGURE 28. The mean interfacial shapes $\hat{h}/a$ between STP and TLA227, at angle of twist $\Theta = 5.48$ rad. See caption of figure 26 and table 3 for details.

		Angular frequency ω (rad/s) ϵ (rad^2/s)				
Figure	Θ (rad)	(*a*)	(*b*)	(*c*)	(*d*)	(*e*)
26	2.50	5.10	5.82	6.08	6.62	8.40
		6.37	7.27	7.60	8.27	10.50
27	3.98	4.03	4.83	5.55	6.08	6.62
		8.02	9.61	11.04	12.10	13.17
28	5.48	3.17	4.03	4.96	6.02	6.62
		8.69	11.04	13.59	16.49	18.14

TABLE 3

Θ (rad)	2.50	3.98	5.48
ω_c (rad/s)	9.65	6.06	4.40

TABLE 4

We next recall the expression (5.18) for $\psi_{(j)\mathrm{P}}$ and the differentiation operator Γ defined in §5 as

$$\Gamma(\cdot) = R\frac{\mathrm{d}}{\mathrm{d}R}\left(\frac{1}{R}\frac{\mathrm{d}}{\mathrm{d}R}\right)(\cdot) \equiv (\cdot)^{\bigstar}.$$

Substituting $Z = 0$ in (5.18) and applying $\Gamma(\cdot)$ to both sides of the resulting equation, we get

$$\psi_{(j)\mathrm{P}}(R,0)^{\bigstar} = \sum_{n=1}^{\infty} [\tfrac{1}{2}\pi \mathscr{H}_{(j)n}(R) - \mathscr{N}_{(j)n}(R)] + \sum_{m=2}^{\infty} [\tfrac{1}{2}\pi \check{\mathscr{H}}_{(j)m}(R) - \check{\mathscr{N}}_{(j)m}(R)], \quad \text{(A 5)}$$

where

$$\mathscr{N}_{(j)n}(R) \equiv \left(\frac{\pi}{2}\frac{\sigma_n}{a}\right)^2 R\int_0^a G_n(R,\xi)\,\mathscr{H}_{(j)n}(\xi)\,\mathrm{d}\xi \quad \text{(A 6}a\text{)}$$

and

$$\check{\mathscr{N}}_{(j)m}(R) \equiv \left(\frac{\pi}{2}\frac{\check{\sigma}_m}{a}\right)^2 R\int_0^a \check{G}_m(R,\xi)\,\check{\mathscr{H}}_{(j)m}(\xi)\,\mathrm{d}\xi. \quad \text{(A 6}b\text{)}$$

Using (5.18), (A 3), (A 5) and (A 6) in (5.49a,b), we finally obtain the following expressions:

$$y_1(R) = \sum_{n=1}^{\infty} (\mathscr{M}_n(R) - [\![\mu\mathscr{N}_n(R)]\!]) + \sum_{m=2}^{\infty} (\check{\mathscr{M}}_m(R) - [\![\mu\check{\mathscr{N}}_m(R)]\!]), \quad \text{(A 7}a\text{)}$$

$$y_2(R) = \sum_{n=1}^{\infty} (-\tfrac{1}{2}\pi [\![\mu\mathscr{H}_n(R)]\!] + [\![\mu\mathscr{N}_n(R)]\!]) + \sum_{m=2}^{\infty} (-\tfrac{1}{2}\pi[\![\mu\check{\mathscr{H}}_m(R)]\!] + [\![\mu\check{\mathscr{N}}_m(R)]\!]), \quad \text{(A 7}b\text{)}$$

$$\tilde{Y}_1(R) = -\sum_{n=1}^{\infty} \frac{a}{\sigma_n}(\mathscr{N}_{(1)n} + \mathscr{N}_{(2)n}) - \sum_{m=2}^{\infty} \frac{a}{\check{\sigma}_m}(\check{\mathscr{N}}_{(1)m} + \check{\mathscr{N}}_{(2)m}), \quad \text{(A 7}c\text{)}$$

$$\tilde{Y}_2(R) = \sum_{n=1}^{\infty} (-\tfrac{1}{2}\pi[\mathscr{H}_{(1)n} + \mathscr{H}_{(2)n}] + [\mathscr{N}_{(1)n} + \mathscr{N}_{(2)n}])$$

$$+ \sum_{m=2}^{\infty} (-\tfrac{1}{2}\pi[\check{\mathscr{H}}_{(1)m} + \check{\mathscr{H}}_{(2)m}] + [\check{\mathscr{N}}_{(1)m} + \check{\mathscr{N}}_{(2)m}]). \quad \text{(A 7}d\text{)}$$

REFERENCES

Abramowitz, M. & Stegun, I. A. 1970 *Handbook of Mathematical Functions*. Dover.

Beavers, G. S. & Joseph, D. D. 1975 The rotating rod viscometer. *J. Fluid Mech.* **69**, 475.

Beavers, G. S. & Joseph, D. D. 1977 Novel Weissenberg effects. *J. Fluid Mech.* **81**, 265.

Bird, R. B., Armstrong, R. C. & Hassager, O. 1977 *Dynamics of Polymeric Liquids*, vol. I. Wiley.

Joseph, D. D. 1976 *Stability of Fluid Motions*, vol. II. Springer.

Joseph, D. D. 1977 A new separation of variables theory for problems of Stokes flow and elasticity. In *Proc. Symp. on Trends in Applications of Pure Mathematics to Mechanics, Kozubnik, Poland.*

Joseph, D. D. & Beavers, G. S. 1977 Free surface problems in rheological fluid mechanics. *Rheol. Acta* **16**, 169.

Joseph, D. D., Beavers, G. S. & Fosdick, R. L. 1973 The free surface on a liquid between cylinders rotating at different speeds. Part II. *Arch. Rat. Mech. Anal.* **49**, 381.

Joseph, D. D. & Fosdick, R. L. 1973 The free surface on a liquid between cylinders rotating at different speeds. Part I. *Arch. Rat. Mech. Anal.* **49**, 321.

Kantorovich, L. V. & Krylov, V. I. 1958 *Approximate Methods of Higher Analysis*. Interscience.

Kolpin, B. E. D., Beavers, G. S. & Joseph, D. D. 1980 Free surface on a simple fluid between cylinders undergoing torsional oscillations. IV. Oscillating rods. *J. Rheol.* **24**, 719.

TIEU, A. H. 1983 Second-order effects in complex rheological flows. Ph.D. thesis, University of Minnesota.

TROGDON, S. A. & JOSEPH, D. D. 1980 The stick–slip problem for a round jet. I. Large surface tension. *Rheol. Acta* **19**, 404.

WATSON, G. N. 1958 *A Treatise on the Theory of Bessel Functions*. Cambridge University Press.

YOO, J. Y. 1977 Fluid motion between cylinders rotating at different speeds. Ph.D. thesis, University of Minnesota.

YOO, J. Y. & JOSEPH, D. D. 1978 Stokes flow in a trench between concentric cylinders. *SIAM J. Appl. Maths* **34**, 247.